# Studies on Peroxisome Motility in the Model Fungal System *Ustilago maydis*

Submitted by Gulay Dagdas

to the University of Exeter for the degree of Doctor of Philosophy in Biological Sciences.

September 2014



I certify that all material in this thesis which is not my own work has been identified and that no material has been previously submitted and approved for the award of a degree by this or any other University.

Gulay Dagdas

**Abstract**

Peroxisomes are ubiquitous organelles found in almost all eukaryotes. They are sensitive to changes in cellular homeostasis and involved in various metabolic processes. Deficiencies in peroxisome function cause severe neurological problems. Here I report, investigation of peroxisome motility and its relation to peroxisomal functions in the fungal model system *Ustilago maydis.* Peroxisomes are mostly motile in *Ustilago maydis*. Motile peroxisomes show different motility patterns: short-range pulse type movements and long range bidirectional motility. Motility behaviour is not static as oscillating peroxisomes may start long-range motility. Here, I present evidence that long-range bidirectional peroxisome motility is an energy driven process and is essential for homogeneous distribution of peroxisomes. Similar to early endosomes and endoplasmic reticulum, microtubule motors kinesin-3 and dynein are responsible for long-range peroxisome transport. In addition to using the same molecular motors for transport, early endosomes, endoplasmic reticulum and peroxisomes have the same transport velocity. Interestingly, motile peroxisomes and endoplasmic reticulum tubules co-localize with early endosomes. Functional investigation of early endosome mutants, *Δrab5a* and *Yup1ts* has revealed a novel transport mechanism where endoplasmic reticulum and peroxisomes hitch hike on early endosomes. Additionally, I report functional characterization of an AAA-ATPase, um05592, which has high homology to human protein NP_055873. Altogether these results reveal molecular mechanism of peroxisome transport in *Ustilago maydis*. Similarities in transport machinery illustrate *Ustilago maydis* as a model system to study peroxisome function in mammalian cells.

**Table of Contents**

**List of Figures**

## List of Tables

**Acknowledgements**

I would like to thank my supervisor Gero Steinberg for his support and guidance. Many thanks to everyone in Exeter Biosciences and post graduate office that has helped me with several issues over the last five years.

I would like to acknowledge Ewa Bielska for sharing her unpublished results related to motile peroxisomes co-localizing with early endosome, which lead to the hitchhiking model eventually. I would also like to thank Nadine Pavolleck for her initial analysis on um05592 in chapter 5. I would like to thank all the members of lab 201, present and past, particularly Magdalena Martin-Urdiroz, Sreedhar Kilaru, Catherine Collins, Anna Shiel, Martin Schuster and Sofia Guimaraes for their technical and social support during my stay at Exeter.

The biggest thanks to my family, particularly to my dearest husband, Yasin Dagdas, to my amazing daughters, Emine Ayse Dagdas and Hatice Gülsüm Dagdas, for their infinite love, support and patience.

Finally, I would like to dedicate this thesis to my parents; Ayşe and Abdurrahman Gök.

**Abbreviations**

| | |
|---|---|
| Aa | amino acid |
| α _anti- | *(antibodies)* |
| ATP | adenosinetriphosphate |
| bleR | phleomycin-resistance-cassette |
| bp | base pair(s) |
| cbxR | carboxin-resistance-cassette |
| CCCP | carbonyl cyanide 3-chlorophenylhydrazone |
| CM | complete medium |
| C-terminal | carboxy-terminal |
| DIC | differential interference contrast |
| DMSO | |
| DNA | deoxyribonucleic acid |
| dNTP | deoxynucleotides |
| Dyn2 | dynein 2 from *U. maydis* |
| EE | early endosome |
| eGFP | enhanced green fluorescent protein |
| ER | endoplasmic reticulum |
| FRAP | fluorescent recovery after photo-bleaching |
| GFP | green fluorescent protein |
| h | hour |
| HDEL | endoplasmic reticulum retention signal |
| hygR | hygromycin-resistance-cassette |
| kb | kilo bases |
| Kin1 | kinesin-1 |
| Kin3 | kinesin-3 |
| LatA | Lantrucullin A |
| mCherry | monomeric Cherry fluorescent protein |
| min | minute |
| ml | millilitre |
| µl | microlitre |
| µm | micrometer |
| µM | micromolar |

| | |
|---|---|
| ms | millisecond |
| MT | microtubule |
| n | sample size |
| natR | nourseothricin-resistance-cassette |
| nar – promoter | conditional nitrate reductase promoter |
| nm | nanometre |
| N-terminal | amino-terminal |
| ORF | open reading frame |
| *otef*-promoter | promoter of the translation elongation factor 1 of *U. maydis* |
| p | probability |
| PCR | polymerase chain reaction |
| PEX | peroxin |
| PO | Peroxisome |
| rab5a | small endosomal Rab5-like GTPase |
| rpm | rounds per minute |
| RT | room temperature |
| s | second |
| sd | standard deviation |
| Tub1 | α-tubulin from *U. maydis* |
| Ts | temperature-sensitive allele |

# 1. General Introduction

## 1.1 *Ustilago maydis:* a model system to study intracellular trafficking

*Ustilago maydis* belongs to the Hemibasidiomycete smut fungi. As many other members of smut fungi, *Ustilago maydis* is an economically important maize pathogen, causing severe yield losses. It induces formation of tumors on aerial parts of maize and these galls reduce crop yields (reviewed in Brefort et al., 2009; Feldbrugge et al., 2004; Horst et al., 2010).

*Ustilago maydis* genome was sequenced in 2006. The genome is 20.5 Mb. It is relatively small compared to other plant pathogenic fungi and does not contain many repetitive elements. The genome of *Ustilago maydis* is organized in clusters and there are 23 chromosomes (Kamper et al., 2006).

### 1.1.1 The disease cycle

*Ustilago maydis* is a biotrophic pathogen and keeps its host alive during the disease cycle. In *Ustilago maydis*, pathogenicity is linked to sexual development. During infection, haploid cells from opposite mating types have to fuse to form a dikaryon hypha, which then infects plant cells (Brefort et al., 2009). The mating process is controlled by *a* and *b* mating loci. *A* mating loci encode a pheromone receptor system which enables *a* mating type haploid cells to detect the opposite mating type haploid cells. *B* loci encode a pair of homeodomain transcription factors named *bE* and *bW* (Brachmann et al., 2001; Hartmann et al., 1999; Kahmann et al., 1995; Muller et al., 2003; Quadbeck-Seeger et al., 2000; Schlesinger et al., 1997; Urban et al., 1996a; Urban et al., 1996b). *bE* and *bW* transcription factors dimerize and control sexual and pathogenic development. Dikaryotic hypha grows in a polarized manner until it reaches the plant surface. Sensing the yet unidentified plant

signal induces formation of an appressorium and an invasion hypha forms and penetrates the plant cells. Initially the fungus grows intracellularly, closely surrounded by the plant plasma membrane. After the initial stage, it is mainly found closely associated with the vascular system. 5-6 days after infection, massive fungal proliferation happens and visible tumors are formed (reviewed in Brefort et al., 2009)(Figure 1.1).

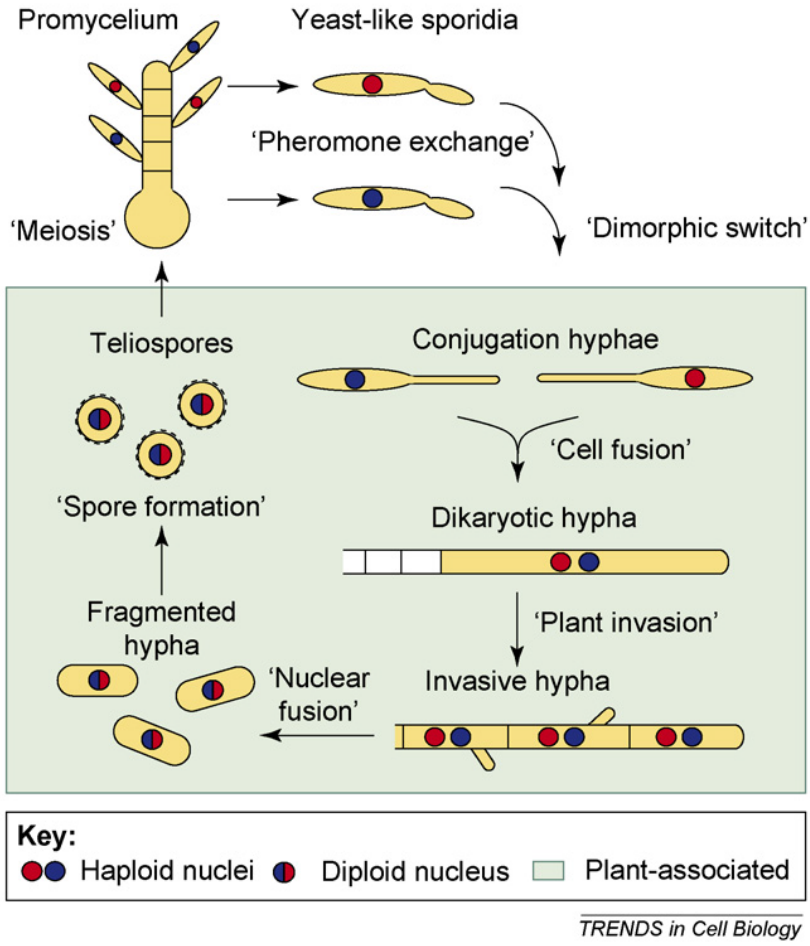


**Figure 1.1: Life cycle of *Ustilago maydis* (taken from Steinberg and Perez-Martin, 2008)** Light green area represent plant-dependent stages of *U. maydis* life cycle. Haploid cells elongate and fuse to form dikaryotic hypha which enters and invades plant tissue. Diploid spores germinate and form haploid sporidia by meiosis.

### 1.1.2 *Ustilago maydis* has distinct morphological states

During its life cycle *Ustilago maydis* undergoes a series of morphological transitions. When it is cultured in rich growth medium, it grows like budding yeast. Yeast cells have similar cellular organization to *S. cerevisiae* cells with defined microtubule organizing centres and mother-bud cell axis. When these cells perceive the presence of the opposing mating type cells, they switch from the yeast-like form to polarized growth and form a hypha (Figure 1.2). These transitions are tightly coupled to the cell cycle. When the yeast-like cells fuse to form the dikaryon hyphae, the cell cycle is arrested. This arrest is essential for infection and tightly controlled by cell cycle checkpoints (Basse et al., 2002; Djamei and Kahmann, 2012; Doehlemann et al., 2008; Garrido et al., 2004; Kahmann et al., 1995; Lanver et al., 2014; Mendoza-Mendoza et al., 2009; Spellig et al., 1994). Association between cytoskeleton and nucleus is very well characterized in the yeast-like form, which makes it ideal to study organelle motility from mother to daughter cells and *vice versa* (Steinberg and Perez-Martin, 2008). Similarly hyphal cells of *Ustilago maydis* are highly polarized and well characterized and this makes these cells ideal systems to study long-range organelle motility, which will be discussed in more detail below.

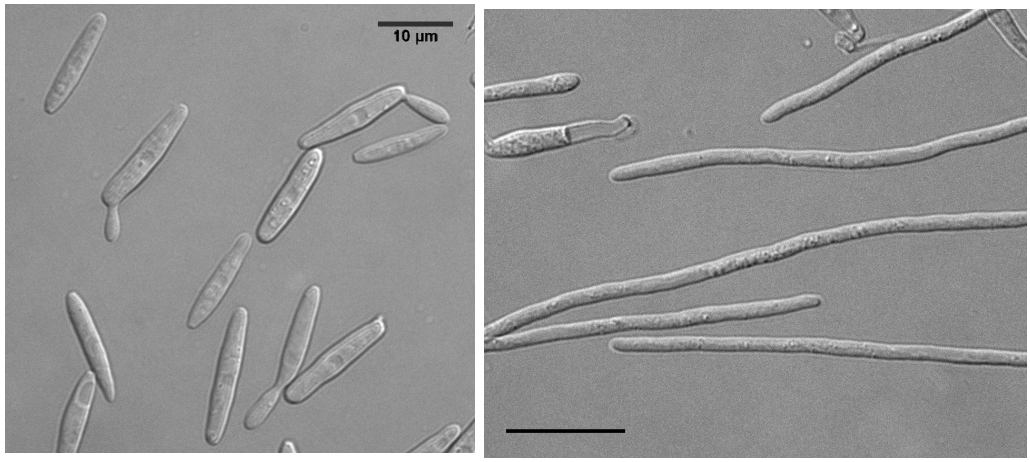


**Figure 1.2: Distinct morphological stages of *Ustilago maydis.***
Yeast-like cells and hyphal cells of *Ustilago maydis* were shown. Scale bars are 10 and 15 µm, respectively.

Although fungal cells have cell walls, phylogenetic analysis using ribosomal RNAs and protein sequences has placed fungi closer to animals than plants (Whittaker, 1969). Combined with the genetic amenability and easy handling of fungal cells, budding and fission yeast have been established as model systems to study eukaryotic cell biology. Genetic and molecular analysis of these organisms has led to fundamental discoveries in regulation of gene expression, cell cycle and cancer biology (Nurse, 2002). However, cellular processes such as closed mitosis and lack long-range organelle motility in these fungi proved that other model organisms are needed to investigate mammalian cell behaviour (Steinberg and Perez-Martin, 2008).

Unlike yeast cells *Ustilago maydis* can generate long hyphal cells. These cells have very similar properties to neuronal cells. They grow apically and material transfer to the hyphal tip requires long-range microtubule transport (Becht et al., 2006). Similar to neurons, transport to the tip is carried out by molecular motors called Kinesin 1 (Kin1) and Kinesin 3 (Kin3) and retrograde

transport is performed by dynein ATPases (Wedlich-Söldner et al., 2002a; Wedlich-Söldner et al., 2002b). Yeast cells lack both long-range motility and Kin3 motors supporting the idea that *Ustilago maydis* could be used to study mammalian neuron dynamics. Additionally similar to neuron cells, actin-based motor myosin V and kinesins cooperate to mediate cellular growth at the tip (Schuchardt et al., 2005). Dynein is responsible for organizing microtubule arrays within the hyphal cells. Without functional dynein, microtubule arrays are lost (Steinberg and Perez-Martin, 2008). Kin1 is also involved in microtubule organization in *Ustilago maydis* and there is growing evidence suggesting a similar role for Kin1 in animal cells (Steinberg et al., 1998; Steinberg et al., 2001; Straube et al., 2006) (Figure 1.3).

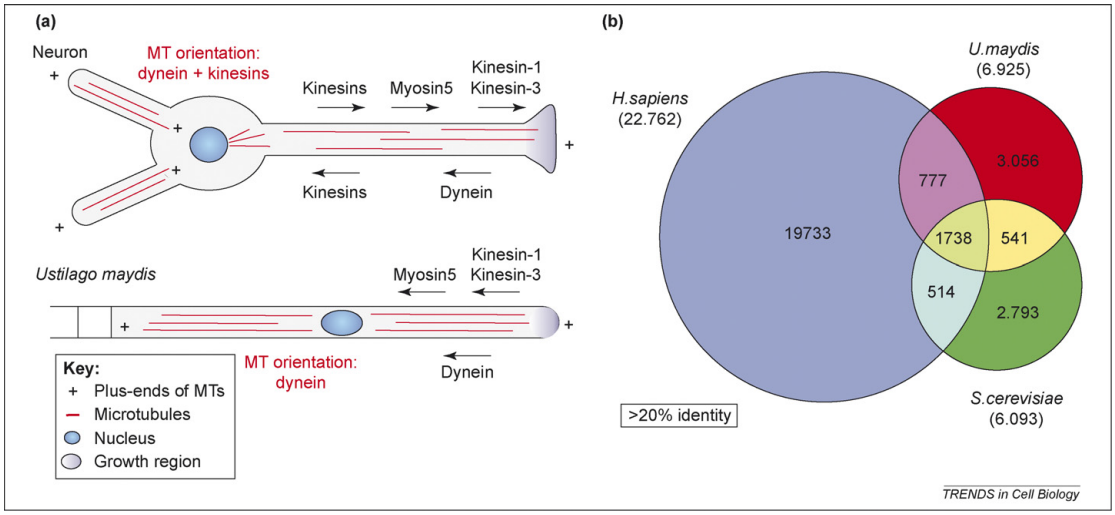


**Figure 1.3: *Ustilago maydis* is a model system to study human cell biology.**

A) Neurons and *U. maydis* hyphal cells have similar microtubule organization and motor set. B) *U. maydis* has more proteins that show >20% homology to human proteins. As seen in Venn diagrams, both budding yeast and *Ustilago* have several proteins that are conserved in human cells, but *Ustilago* has more homologous proteins than yeast (Figure taken from (Steinberg and Perez-Martin, 2008).

Ascomycete fungi have closed mitosis, i.e. the nuclear envelope and nuclear pores do not dissolve during mitosis and mitotic spindle forms within the nucleus (Heath, 1980). However in animal cells, the nuclear envelope is disassembled during interphase and is reassembled after mitosis. Similarly, *Ustilago maydis* has open mitosis where similar to animal cells dynein plays an important role in nuclear break down. Nucleoporins, especially Nup107 have very similar dynamics to animal cells, which further supports the idea of using *Ustilago maydis* as a model system to study animal cell biology (Belgareh et al., 2001; D'Angelo et al., 2006; Rabut et al., 2004; Theisen et al., 2008). Besides being biologically similar to neurons, the *Ustilago maydis* community developed several molecular tools over the years to establish *Ustilago maydis* as a model system to study cell biology (Table-1).

**Table 1.1: Molecular tools to study cell biology in *Ustilago maydis***

(adapted from Steinberg and Perez-Martin, 2008)

| | |
|---|---|
| FB1, FB2, FB6a. FB6b strains | Haploid strains with different mating loci |
| SG200 | Solopathogenic haploid strain, which does not need to fuse with the mating partner to make hyphal cells |
| AB33 | Haploid strain which carries two compatible b-alleles under nar1 inducible promoter; when shifted to inductive medium generates hyphae |
| FBD11 | Diploid solopathogenic strain |
| Ptef promoter | Constitutively active promoter |
| Potef promoter | Modified tef promoter with tetracycline responsive elements |
| Crg1 promoter | Conditional promoter. Active when cells are grown using arabinose as carbon source; inactive when cells are grown with glucose media. |
| Nar1 promoter | Nitrogen conditional promoter. Active in the presence of nitrate, inactive in the presence of ammonium |
| Tet-system | Tetracycline regulated inducible gene expression system |
| Fluorescent proteins | Several lines including cytoskeletal components and motors are already generated and functionally tested. |
| Mating assays | Cell-cell fusion assays can be done using charcoal medium |
| Synthetic pheromone | A short peptide, when added to liquid growth medium actives dimorphic switch. |

## 1.2 Intracellular trafficking

Intracellular traffic maintains proper distribution and communication of subcellular entities -ranging from proteins, RNAs, small vesicles to larger membranous organelles- within the cell (Grant and Sato, 2006). The cytoskeleton and molecular motors mediate intracellular transport. Cell cytoskeleton is composed of dynamic and motile cell elements, providing structural support to the cell and acting as trails for intracellular transport. There are two types of cytoskeletal tracks for cargo transport: actin microfilaments and microtubules. Actin filaments are formed by polymerization of GTP-bound actin monomers (G-actin) and called F-actin. Most of the intracellular transport in plants and yeast take place along F-actin. Microtubules are composed of α- and β- tubulin heterodimers. Fungi and animal cells mostly use microtubules as primary tracks for intracellular transport of cell contents (Amos and Schlieper, 2005; Vale, 2003).

### 1.2.1 Molecular motors

Motor proteins comprise of head region and tail region; the head region interacts with the cytoskeletal track and hydrolyses ATP, the tail region binds cargo. Cargo movement is accomplished by a conformational change in the head of the motor as a result of ATP hydrolysis (Goodson et al., 1997; Vale, 1992; Vale, 1999). There are three major groups of molecular motors to mediate intracellular traffic: myosins, kinesins and dynein (Hackney, 1996).

#### 1.2.1.1 Myosins

Myosins are-actin based molecular motors, which are implicated to act usually in short-range transport of intracellular cargoes. Majority of the myosins moves to plus ends of actin filaments (Bearer et al., 1993; Reedy, 1993). In *S. cerevisae* MyoV is the major motor maintaining vesicle and organelle transport in the cell. There are two types of MyoV: i) Myo2p and ii) Myo4p. Myo4p has roles in mRNA transport and inheritance of cortical ER (Estrada et al., 2003). Myo2p is involved in movement of many cargoes such as vacuoles, peroxisomes, secretory vesicles and mitochondria (Ali et al., 2002; Hoepfner et al., 2001; Reck-Peterson et al., 2000). Plant myosins carry peroxisomes, mitochondria, ER, chloroplasts, vacuole and plastids (Boevink et al., 1998; Higaki et al., 2006; Liebe and Menzel, 1995; Sparkes, 2011; Sparkes et al., 2009; Van Gestel et al., 2002; Wada et al., 2003). In filamentous fungi, MyoV is involved in pathogenesis related processes including dimorphic switch and host cell invasion (Oberholzer et al., 2002; Weber et al., 2003; Woo et al., 2003). In mammalian cells, MyosinV has a role in transport of several organelles including melanosomes, phagosomes, smooth ER, endocytic and recycling vesicles (Krendel and Mooseker, 2005; Langford, 2002).

#### 1.2.1.2 Kinesins

Kinesin molecular motors, also called as Kinesin superfamily proteins (KIFs), comprise the largest molecular motor family with 14 families and more than 45 genes encoded in mammalian genome. Most of kinesins move toward plus ends of microtubules while some move to minus ends. (Beushausen et al., 1993; McCart et al., 2003; Miki et al., 2003). In mammals, kinesins support

many transport processes in neurons. Conventional kinesins, Kin1 and Kin3 family motors carry the essential synaptic compounds including synaptic vesicle precursors containing synaptotagmin, Rab3A, synatubulin, syntaxin and mitochondria and mRNA in axons (Diefenbach et al., 2002; Kanai et al., 2004; Kanai et al., 2000; Su et al., 2004; Tanaka et al., 1998). Kin3/unc-104 - based transport in *Drosophila melanogaster* is important in dendrite morphogenesis and synapsis formation (Kern et al., 2013). Failure of Kin1 and Kin3 function in neuronal cells is linked to some neurodegenerative disease such as Charcot-Marie-Tooth type 2A disease and hereditary spastic paraplegia (Reid et al., 2002; Zhao et al., 2001). In plants, most of the kinesins function during cell division by organizing cytoskeletal structures (Goto and Asada, 2007; Müller et al., 2006; Preuss et al., 2003). A few have roles in transport and position the cell organelles such as mitochondria, Golgi body, and chloroplast (Lee et al., 2001; Suetsugu et al., 2010; Van Gestel et al., 2002; Wei et al., 2009). In fungal cells, the role of kinesins varies among species due to different cell morphologies. In *S. cerevisae,* six kinesins were identified and they have role in organizing microtubule dynamics during mitosis (Vale, 2003). In *Saccharomyces pompe*, Kinesin 14 Klp2, a minus end directed kinesin, was reported to mediate sliding of microtubules along each other. This helps to maintain polarity of interphase microtubules for cells to grow longitudinally (Carazo-Salas et al., 2005). In *Ustilago maydis*, *Aspergillus nidulans* and *Neurospora crassa,* Kin1, Kin3 and Kin7 motors function in membrane traffic including transport of early endosomes, peroxisomes, mitochondria, secretory vesicles and mRNA along microtubules to support hyphal tip growth (Egan et al., 2012a; Fuchs and Westermann,

2005; Seiler et al., 1997; Wedlich-Söldner et al., 2002b; Zekert and Fischer, 2009). Failure of kinesin activity leads deficiencies in hyphal growth (Lenz et al., 2006; Seiler et al., 1997).

#### 1.2.1.3 Dynein

Cytoplasmic dynein is a large molecular motor complex, which travels towards minus microtubule end in fungal and animal cells (Alberti-Segui et al., 2001; Cho and Vale, 2012; Goldstein and Vale, 1991; Lenz et al., 2006; Sheetz et al., 1986). Plant cells do not encode dynein, minus end traffic is carried out by kinesins and myosins (King, 2002). Dynein transports membrane bound organelles, proteins and RNA complexes such as Golgi vesicles, lysosomes, peroxisomes, endosomes, ribonucleoprotein granules in mice, Drosophila and Xenopous oocytes (Harada et al., 1998; Harrell et al., 2004; Kural et al., 2005; Ling et al., 2004). In neuronal cells, dynein mediates long distance retrograde movement of organelles and vesicles along axons towards cell body (Pfister, 1999; Schnapp and Reese, 1989). Deficiencies in dynein-mediated motility leads to neurological disorders (Sivagurunathan et al., 2012; Vallee et al., 2000; Yamada et al., 2008). Herpes viruses are carried along axons to the nucleus by dynein in neurons to establish the infection (Diefenbach et al., 2008). Lissencephaly is a neurological disorder which is linked to a mutation in dynein regulator protein, Lis1 (Hirotsune, 2008). In this disease, brain development is retarded as neuron cell migration failed (Wynshaw-Boris, 2007). Dynein function impairment is also proposed to have a role in the formation of intracellular bodies, which appear during some

neurodegenerative conditions such as Huntington's disease, Parkinson's disease (Tran and Miller, 1999).

In budding yeast, dynein has roles in nuclear migration to the neck during mitosis by mediating sliding of astral microtubules (Yeh et al., 2000). In fission yeast, dynein is involved in nuclear migration during meiosis, telomere clustering and nuclear fusion (Marsh and Rose, 1997; Miki et al., 2002; Yamamoto et al., 1999). In filamentous fungi, dynein also function in nuclear transport in addition to carrying other organelles and vesicles including vacuoles, endosomes, ER and peroxisomes (Egan et al., 2012b; Seiler et al., 1999; Wedlich-Söldner et al., 2002a; Wedlich-Söldner et al., 2002b). If dynein-based transport of organelles and vesicles fails, hyphal growth is disrupted and cells have aberrant morphology (Egan et al., 2012a; Fischer et al., 2008; Steinberg, 2000; Suelmann and Fischer, 2000; Xiang and Fischer, 2004; Xiang and Plamann, 2003; Xiang et al., 1995; Yamamoto and Hiraoka, 2003; Zhang et al., 2010).

#### 1.2.1.4 Motor-Cargo Recognition

Motor cargo attachment may occur in three ways: i) direct linkage of motor to cargo lipid membrane or a trans-membrane protein, ii) linkage of motor to cargo via an adaptor protein and iii) linkage of motor to its cargo via a protein complex (Hirokawa and Takemura, 2005; Kardon and Vale, 2009; Mimori-Kiyosue and Tsukita, 2003; Schlager and Hoogenraad, 2009; Simmchen et al., 2012; Vale, 2003; Wozniak and Allan, 2006; Xiang and Plamann, 2003).

A well known example of direct interaction is the one between plekstrin homology (PH) and phosphatidylinositol 4,5-bisphosphate (PtdIns(4,5)$P_2$)

lipids. KIF1A/Unc-104 kinesin binds and transport synaptic vesicles through PH to PtdIns(4,5)$P_2$ binding (Klopfenstein et al., 2002; Klopfenstein and Vale, 2004).

Melanosome movement in pigment cells represents adaptor protein involvement in motor cargo interaction. Rab27a GTPase binds to melanosome membrane and recruits melanophillin, a Rab GTPase binding protein. Melanophillin binding to myoV links the motor to the cargo, melanosomes (Bridgman, 2004; Langford, 2002; Wu et al., 2002).

DENN/MADD is a Rab-GEF that can bind to stalk regions of Kin3 motors, KIF1A and KIF1B, together with Rab3-GTP. These interactions with KIF1A and KIF1B mediate transport of Rab3-GTP carrying vesicles by Kin3 in axons (Niwa et al., 2008). Cargo binding and unloading are regulated by GTP hydrolysis as DENN/MADD cannot bind to Rab3-GDP and thus number of transported vesicles is reduced (Hirokawa et al., 2009; Tanaka et al., 2001).

Dynein interact with several adaptor proteins to enable transport of a wide range of cargoes in the cell. One of the best-known adaptors is called the dynactin multisubunit protein complex, which consists of several proteins including $p150^{Glued}$, ARP1 and dynamitin. Dynactin facilitates many processes such as targeting dynein to particular locations within the cell, helping dynein to bind its cargo and regulating dynein motor activity. p150 subunit of dynactin binds to Sec23, which is a Rab GTPase protein. This association enables dynein to move ER vesicles to Golgi (Kardon and Vale, 2009; Melkonian et al., 2007; Moore et al., 2008; Ozaki et al., 2011; Plamann et al., 1994; Schuster et al., 2011a; Skop and White, 1998; Tai et al., 2002; Valetti et al., 1999). Lis1, NudE and NudEL proteins are known as ubiquitous cofactors of

dynein (Kardon and Vale, 2009). In fungi, Lis1 and NudE have role in dynein based nuclear binding by mediating dynein positioning to the plus ends of microtubules (Lenz et al., 2006; Xiang, 2003; Yamada et al., 2008; Zhang et al., 2010). Bicadual D (BicD) is another cofactor of dynein, which is only found in metazoans. In fruit fly, BicD recognizes mRNA cargo receptor Egalitarian and drives dynein–based transport of mRNA molecules (Dienstbier et al., 2009). In mammalian cells BicD is reported to recruit Golgi to dynein-dynactin complex by binding to Rab6GTP-bound vesicles (Hoogenraad et al., 2001).

## 1.3 Peroxisomes

### 1.3.1 Peroxisome structure and function

Peroxisomes are ubiquitous organelles found in most eukaryotic cells. They are usually spherical in shape and their diameters range from 0.1 μm to 1.0 μm (Titorenko and Rachubinski, 2001). Peroxisomes are single membrane organelles. They don't have their own DNA or protein synthesis machinery. Typically they contain at least one hydrogen peroxide producing-oxidase and catalase to break down the hydrogen peroxide (Lazarow and Fujiki, 1985; Subramani, 1996). Mainly due to the catalase enzymes, they have a granular, sometimes even crystalline matrix. This is often used as a diagnostic tool for peroxisome identification (Schrader and Fahimi, 2008; Smith and Aitchison, 2013).

Peroxisomes are involved in maintaining cellular homeostasis. They are highly adaptable organelles and can change shape, size, distribution and content according to changing environmental conditions. They perform many activities related to lipid metabolism and detoxification. In most eukaryotic

cells their main function is to carry out oxidative reactions related to lipid β-oxidation and hydrogen peroxide degradation. However they also have very specific roles in different organism such as glycosomes of *Leishmania* and Trypanasomes, which do not seem to have the hallmark enzyme catalase but contain glycolytic enzymes (reviewed in Smith and Aitchison, 2009; Smith and Aitchison, 2013; Titorenko and Mullen, 2006; Titorenko and Rachubinski, 2001; Titorenko and Rachubinski, 2004). In fungi, peroxisomes contribute to methanol metabolism and penicillin biosynthesis. General and specific functions of peroxisomes are given in Table 1.2.

**Table 1.2: Metabolic functions of peroxisomes** (adapted from Smith and Aitchison, 2013).

| Functions of Peroxisomes | Plants | Fungi | Protozoa | Animals |
|---|---|---|---|---|
| Biosynthesis | | | | |
| Bile acids | | | | ✔ |
| Hormonal Signaling molecules | ✔ | | | ✔ |
| Polyunsaturated fatty acids | | | | ✔ |
| Plasmalogens | | | ✔ | ✔ |
| Pyrimidines | | | ✔ | ✔ |
| Purines | | | | ✔ |
| Antibiotics (penicillin) | | ✔ | | |
| Toxins for plant pathogenesis | | ✔ | | |
| Lysine | | ✔ | | |
| Biotine | ✔ | ✔ | | |
| Secondary metabolites Degradation | ✔ | ✔ | | |
| Prostoglandin | | | | ✔ |
| Aminoacids | | ✔ | | ✔ |
| Polyamine | ✔ | ✔ | | ✔ |
| Hydrogen peroxide | ✔ | ✔ | ✔ | ✔ |
| Fatty acid | ✔ | ✔ | ✔ | ✔ |
| Purine | ✔ | | ✔ | ✔ |
| Superoxide | ✔ | | ✔ | ✔ |
| Glycerol | | | ✔ | |
| Glucose | | | ✔ | |
| Methanol | | ✔ | | |
| Glyoxylate cycle | ✔ | ✔ | | |
| Photorespiration | ✔ | | | |
| Other | | | | |
| Cellular integrity (Woronin b.) | | ✔ | | |
| Firefly luciferase | | | | ✔ |
| Antiviral innate immunity | | | | ✔ |
| Hydrogen peroxide signaling in hypothalamic neurons | | | | ✔ |

Since peroxisomes lack their own protein synthesis machinery, peroxisomal proteins are synthesized on free polysomes at cytosol. These proteins are then imported to either peroxisomal membrane or matrix via special transporters. Matrix proteins are targeted posttranslationally via the C-terminal PTS1 and PTS2 signals. PTS1 is found in most matrix proteins and is a short sequence composed of (Ser/Ala/Cys)(Lys/Arg/His)(Leu/Met/Ile)(Brocard and Hartig, 2006a). PTS2 is rare and found in N-terminus of some matrix proteins. Its sequence is (Arg/Lys) (Leu/Val/Ile) ($Xaa_5$) (His/Glu)(Leu/Arg) (where Xaa is any aminoacids)(Mukai and Fujiki, 2006). Peroxisomal membrane proteins (PMPs) have membrane target signals (mPTS). They are sorted to peroxisomes directly from cytosol via their mPTS1 or indirectly from ER via their mPTS2 (reviewed in Titorenko and Rachubinski, 2004). Whether into membrane or matrix, all proteins are recognized by their receptors, which mediate the transport. These receptors and many other proteins that take role in biogenesis, division, inheritance, distribution and protein import of peroxisomes are collectively called peroxins. Peroxins are well-conserved proteins and are encoded by *PEX* genes. So far, more than 30 *PEX* genes are identified in yeast and mammalian cells. Roles of peroxins are summarized in Table 1.3.

### 1.3.2 Peroxisome biogenesis

The origin of peroxisomes has been debatable for many years. Current data suggests that there are basically two ways to generate a peroxisome: peroxisomes can either form *de novo* by fusion of pre-peroxisomal vesicles that are originating from ER (Haan et al., 2006; Heiland and Erdmann, 2005;

Hoepfner et al., 2005) or by division of pre-existing peroxisomes (Fagarasanu et al., 2007; Lazarow and Fujiki, 1985; Mullen and Trelease, 2006). *De novo* generation of peroxisomes is slower but enables formation of peroxisomes that are fully functional and does not have any toxic aggregates. However peroxisome formation by fission is quicker but requires pre-existing peroxisomes (Smith and Aitchison, 2009).

**Table 1.3: Functions of peroxins** (Adapted from (Smith and Aitchison, 2013).

| Peroxin | Function |
|---|---|
| **Targeting of matrix proteins** | |
| PEX7 | PTS2 cargo |
| PEX20 | PTS2 cargo |
| PEX21-PEX18 | PTS2 cargo |
| PEX5 | PTS1 and PTS2 cargo |
| **Matrix protein transport** | |
| PEX5-PEX14 | Cargo translocating channel |
| PEX13-PEX17-PEX14-PEX33 | Receptor docking complex |
| PEX8 | Importomer assembly |
| PEX4 | Receptor export |
| PEX22 | PEX4 anchor |
| PEX2-PEX10-PEX12 | Receptor export |
| PEX1-PEX6 | Receptor recycling |
| PEX15-PEX26 | Membrane receptor for PEX1 and PEX6 |
| **Targeting of peroxisomal membrane proteins (PMPs)** | |
| PEX3 | Receptor docking |
| PEX19 | Soluble chaperone and receptor |
| **Peroxisome biogenesis** | |
| PEX3-PEX19 | *De novo* generation of peroxisomes |
| PEX25 | *De novo* generation of peroxisomes |
| PEX16 | Recruits PMPs from ER |
| PEX1-PEX6 | Mediates fusion of preperoxisomal vesicles |
| PEX23-PEX30 | Regulate *de novo* generation of peroxisomes |
| **Fission** | |
| PEX11-PEX25 | Membrane elongation and remodeling |
| PEX27 | Negative regulator of fission |
| PEX34 | Positive regulator of fission |
| **Regulation of peroxisome biogenesis** | |
| PEX24-PEX28-PEX29-PEX23- | Form a complex that mediates the |

| | |
|---|---|
| PEX30-PEX32 | contact with ER subdomains |
| PEX31 | Contains a dysferlin domain involved in ER contact regulation |
| | |

*De novo* formation of peroxisomes happens via heterotypic fusion of pre-peroxisomal vesicles that are budding from ER (Hoepfner et al., 2005; Motley et al., 1994; Tabak et al., 2006; Titorenko et al., 1997). These vesicles have different protein complements and there are sorting mechanisms to make sure that mature peroxisomes contain all the required materials. Fission is mainly controlled by PEX11 family members, which tubulate the membrane. PEX11 also recruits Dynamin-like proteins that mediate the scission at the constricted membrane regions (Delille et al., 2010). Selection of biogenesis mechanism most likely depends on the level of cellular stress and environmental conditions. It is likely that oxidative stress and accumulation of ROS will induce *de novo* formation, whereas lipids will induce peroxisome fission since they need to be metabolized quickly (Loson et al., 2013).

### 1.3.3 Peroxisome dynamics

Changes in environmental conditions and cellular physiology affect peroxisome size, distribution and shape. There are various reports showing dynamic regulation of peroxisome size and shape in response to lipid accumulation, tissue specialization and cellular aging. The number of peroxisomes was increased when additional lipid was provided to cultured cells. This is achieved at transcriptional level. Fatty acid transcription factors induce expression of *PEX* genes that activate peroxisome proliferation

(Issemann et al., 1992; Lalwani et al., 1985; Smith et al., 2000; Smith et al., 2002).

### 1.3.4 Peroxisomal diseases

Mutations in *PEX* proteins are linked to severe genetic neurological diseases, which are collectively called Peroxisome Biogenesis Disorders (PBDs) (Clayton et al., 1988; Shimozawa et al., 2005; Wanders, 2014). So far 13 *PEX* proteins including *PEX*1, *PEX*3, *PEX6*, *PEX*16 and *PEX*19 are associated with PBDs. Mutant cells have either no peroxisome at all or aberrant peroxisomes with varying size and number (Mast et al., 2011). These diseases include Zellweger syndrome, neonatal adrenoleukodystrophy, infantal refsum disease and rhizomelic chondrodysplasia punctate. Patients suffer from insufficient brain development, failure in liver functions as well as physical disabilities (reviewed in Wanders, 2014).

Besides *PEX* genes, some peroxisomal enzymes are also associated with diseases which are called single peroxisomal enzyme deficiencies (PEDs). PEDs are related to failure of particular peroxisome function such as X-linked adrenoleukody strophy (X-ALD). X-ALD results from a defect in the peroxisomal beta-oxidation process that leads to the accumulation of very-long-chain fatty acids. Patients suffer from behavioural, cognitive and neurological setbacks (reviewed in Islinger et al., 2012).

### 1.3.5 Peroxisomal interactions with other organelles

Although still heavily debated, the Endoplasmic reticulum seems to play a key role in *de novo* synthesis of peroxisomes (Geuze et al., 2003; Haan et al., 2006; Hoepfner et al., 2005; Mullen et al., 1999; Titorenko et al., 1997). A set of peroxisomal membrane proteins called as group I PMPs (*PEX*2, *PEX*3, *PEX*13 *PEX*16 and *PEX*19) are synthesized on cytosolic polyribosomes and are targeted to the Endoplasmic reticulum (Geuze et al., 2003; Haan et al., 2006; Hoepfner et al., 2005; Kim et al., 2006; Titorenko and Rachubinski, 1998). These proteins localize to specific regions in the endoplasmic reticulum membrane and form pre-peroxisomal vesicles (PPVs). PPVs grow into mature peroxisomes by importing matrix proteins and fusing with other PPVs as in yeast (Titorenko et al., 2000; Titorenko and Rachubinski, 2000; van der Zand et al., 2006). Endoplasmic reticulum also provides lipid constituent for expanding peroxisomes. Interestingly, recent evidence suggests the ER might play a role in division of peroxisomes in plant cells (Barton et al., 2013).

Peroxisomes and mitochondria have common features in their biogenesis and function. Both organelles have roles in lipid metabolism. Some fatty acid metabolism products of peroxisomes such as acetyl Co-A and propionyl Co-A are further degraded to $CO_2$ and $H_2O$ in mitochondria (Schrader and Yoon, 2007). Peroxisome and mitochondria are involved in generation and degradation of reactive oxygen species (Jezek and Hlavata, 2005; Moldovan and Moldovan, 2004; Schrader and Fahimi, 2006). High morphological plasticity in both organelles suggests common mechanism in division. In mammalian cells, Fis1 is targeted to peroxisome and mitochondria membrane and acts as a receptor for DLP1, a dynamin like GTPase protein, which

mediates fission of peroxisomes and mitochondria (Koch et al., 2004; Koch et al., 2005; Stojanovski et al., 2004; Yoon et al., 2003).

Peroxisomes and lipid bodies (lipid droplets) are involved in lipid homeostasis. Physical contacts between peroxisomes and lipid bodies promote lipid breakage in lipid bodies in yeast (Binns et al., 2006).

### 1.3.6 Peroxisomes and Plant Pathogenicity

Lipid storage and metabolism of the pathogen is very critical during plant infection. Fatty acid β-oxidation is required for morphological transition of pathogen to invade the host (Wang et al., 2007). *PEX*6-deleted mutant of *Colletotrichum leganerium*, where import of matrix proteins was impaired, is not able to infect host plant (Kimura et al., 2001). Similarly, abolishment of PTS1 import pathway by deletion of *PEX*5 and PTS2 import pathway by deletion of *PEX*7 lead to defective fungal growth and extensive reduction in pathogenicity (Wang et al., 2013). *PEX*13, a peroxisomal biogenesis protein, has also a role in the processes of plant infection (Fujihara et al., 2010). A peroxisomal multifunctional beta-oxidation enzyme (mfe) of *Ustilago maydis* is dispensable for early stages of plant infection but essential for subsequent stages including proliferation on host cells and tumor production (Klose and Kronstad, 2006; Kretschmer et al., 2012).

### 1.3.7 Peroxisomal motility

Intracellular peroxisome movements are important for morphology and spatial organization of peroxisomes in the cell. In mammalian cells peroxisomes are associated with microtubules and moved by dynein and kinesin motors (Rapp

et al., 1996; Schrader et al., 1996; Thiemann et al., 2000; Wiemer et al., 1997). Dynactin and Lis1 regulate dynein-driven peroxisome motility (Egan et al., 2012b). Some peroxisomes are moving directionally and fast whereas, most peroxisomes are moving slowly like oscillation (Schrader et al., 2003).

In human cells microtubules and minus end motor Dynein have role in early stages of peroxisome biogenesis. Transport of membrane elements from ER to pre-peroxisomal vesicles occurs along microtubules. However, pharmacological assays suggest that protein import into peroxisomal matrix is independent from microtubules (Brocard et al., 2005). *PEX*14 is a peroxisome membrane protein, which interacts with *PEX*5 and *PEX*19 and has roles in protein import and degradation of peroxisomes (pexophagy). *PEX*14 binds tubulin directly and this binding competes with *PEX*5. It has been proposed that when the cell starves *PEX*14-tubulin binding is favoured and peroxisomes are transported for degradation. So, peroxisome motility serves for pexophagy (Bharti et al., 2011). In *Drosophila melanogaster*, dynein and Kin1 act in cooperation for efficient transport of peroxisomes in the cell (Kural et al., 2005).

In *S. cerevisiae,* peroxisomes align with actin filaments and peroxisome movement is mediated by Myo2p. Segregation of peroxisomes between mother and bud cells is managed by actin-based transport of peroxisomes (Hoepfner et al., 2001). A peroxisome membrane protein inp1p (inheritance of peroxisomes protein 1) acts as an anchor between peroxisomes and cell cortex. Inp1p function ensures half of peroxisomes retains in the mother cell (Fagarasanu et al., 2005b). Inp2p, acts as a Myo2p receptor and regulates transport of peroxisomes from mother cells to bud cells (Fagarasanu et al.,

2006). In *Yarrowa lipolytica PEX*3, peroxisome biogenesis factor, acts as Myo2p during peroxisome inheritance (Chang et al., 2009).

Interestingly, in fission yeast peroxisome motility is found to be independent from cytoskeleton. Mitochondrial dynamics mediate peroxisomal movements (Jourdain et al., 2008). Fission yeast peroxisomes are aligned with microtubules but do not move along them.

Recent findings in *Aspergilus nidulans* showed that peroxisome motility in yeast and filamentous fungi has different mechanisms. In *A. nidulans*, dynein and Kin3 transport peroxisomes bidirectionally on microtubules as in animal cells. Peroxisome transport ensures that there are adequate peroxisomes in the growing hyphal tip (Egan et al., 2012b).

As in yeast cells, peroxisome motility in plant cells is also acto-myosin-dependent (Jedd and Chua, 2002).

### 1.4 Aim of the current study

This study attempts to characterize peroxisome motility in *Ustilago maydis*.

First objective of the study was to analyse peroxisome movements quantitatively and reveal underlying mechanism in *U. maydis* cells. To this end,,

1) I quantified velocity, run length and frequency of GFP-SKL signals
2) I tested cytoskeleton and molecular motors using molecular and cell biological techniques

Second objective of the study was to investigate motor cargo interaction in peroxisome movement. To do this,,

1) I analysed other cargoes of the same motor carrying peroxisomes.
2) I investigated interaction of peroxisome with those cargoes using molecular and cell biological methods.

Third objective of the study was to address potential roles of peroxisome transport. Previous studies propose that peroxisome motility mediates spatial organization of the peroxisomes, fusion and fission events and communication between each other and other organelles in the cell (Bonekamp et al., 2012; Liu et al., 2009; Schrader et al., 2003). Quantitative imaging of peroxisome motility revealed interesting patterns and dynamics between peroxisomes and other organelles. I discussed potential roles of these patterns.

Fourth objective of this study was to characterize um05592, an *U. maydis* protein with unknown function. This protein was detected in comparative genomic search and showed high similarity to a human protein with unknown

function (Münsterkötter and Steinberg, 2007). To characterize function of this protein,

1. I generated a um05592-GFP fusion to analyse subcellular localization and distribution of this protein.
2. I generated *a* um05592 deletion strain and fatty acid utilization in this strain.
3. I did plant infection assays with this deletion strain.

## 2. General Methods

### 2.1 Chemicals, Solutions, Buffers and Media

All chemicals used in this study were purchased from Merck (Haar, Germany), Invitrogen (Paisley, UK), Roth (Karlsruhe, Germany), Duchefa Biochemie (Haarlem, Netherlands), Prolabo (Dublin, Ireland), Fisher Scientific (Loughborough, UK), Fluka and Sigma (Hamburg, Germany, and Poole, UK), unless stated otherwise.

Restriction endonucleases and Phusion DNA Polymerase were obtained from New England Biolabs (Herts, UK). Manufacturer's protocols were applied to set reactions.

For preparation of standard buffers and media, standart lab protocols available in lab manuals (Hanahan, 1985; Guthrie and Fink, 1991; Sambrook and Russell, 2001) were followed. The list of solutions and media is given below with final concentration of the ingredients and in an alphabetical order.

**Alkaline lysis solution:** 1% SDS (w/v), 0.2 M NaOH

**CM (complete) medium:** 0.25% casaminoacids (w/v), 0.1% (w/v) yeast extract, 1% (v/v) vitamin solution (Holliday, 1974), 6.25% (v/v) salt solution (Holliday, 1974), 0.05% (w/v) DNA from herring sperm, 0.15% (w/v) $NH_4NO_3$

**DNA wash buffer:** 50 mM NaCl, 10 mM Tris-HCl pH 7.5, 2.5 mM EDTA, 50% (v/v) ethanol

**dYT-glycerol:** 1.6% (w/v) tryptone, 1% (w/v) yeast extract, 0.5% (w/v) NaCl, 69.6% (v/v) glycerol

**dYT medium:** 1.6% (w/v) tryptone, 1% (w/v) yeast extract, 0.5% (w/v) NaCl

**Neutralization solution:** 0.9 M sodium acetate pH 4.8, 0.5 M NaCl

**NM (nitrate minimal) medium:** 0.3% (w/v) $KNO_3$, 6.25% (v/v) salt solution (Holliday, 1974)

**NSY-glycerol:** 0.8% (w/v) nutrient broth, 0.1% (w/v) yeast extract, 0.5% (w/v) sucrose, 69.6% (v/v) glycerol

**PBS buffer:** 137 mM NaCl, 2.7 mM KCl, 4.3 mM $Na_2HPO_4*7H_2O$, 1.4 mM $KH_2PO_4$

**Reg (regeneration) agar:** 1% (w/v) yeast extract, 2% (w/v) peptone, 2% (w/v) sucrose, 18.22% (w/v) sorbitol, 1.5% (w/v) agar

**Salt solution** (Holliday, 1974): 16% (w/v) $KH_2PO_4$, 4% (w/v) $Na_2SO_4$, 8% (w/v) KCl, 4.08% (w/v) $MgSO_4*7H_2O$, 1.32% (w/v) $CaCl_2*2H_2O$, 8% (v/v) Trace elements

**SCS buffer:** 20 mM Na-citrate pH 5.8, 1 M sorbitol

**Sc-Ura medium:** 0.17% (w/v) yeast nitrogen base without amino acids, 0.5% (w/v) ammonium sulphate, 0.5% (w/v) casein hydrolysate, 0.002% (w/v) adenine, 2% (w/v) glucose

**STC buffer:** 10 mM Tris-HCl pH 7.5, 100 mM $CaCl_2$, 1 M sorbitol

**TE buffer pH 8.0:** 10 mM Tris, 1 mM EDTA

**Trace elements** (Holliday, 1974): 0.06% (w/v) $H_3BO_3$, 0.14% (w/v) $MnCl*4H_2O$, 0.4% (w/v) $ZnCl_2$, 0.4% (w/v) $Na_2MoO_4*2H_2O$, 0.1% (w/v) $FeCl_3*6H_2O$, 0.04% (w/v) $CuSO_4*5H_2O$

**Vitamin solution** (Holliday, 1974): 0.1% (w/v) thiamine HCl, 0.05% (w/v) riboflavin, 0.05% (w/v) pyridoxine HCl, 0.2% (w/v) D-pantothenic acid hemicalcium salt, 0.05% (w/v) 4-aminobenzoic acid, 0.2% (w/v) nicotinic acid, 0.2% (w/v) choline chloride, 1% (w/v) myo-Inositol

**Yeast lysis buffer:** 2% (v/v) Trition X-100, 1% (w/v) SDS, 100 mM NaCl, 1 mM EDTA, 10 mM Tris

**$YEPS_{light}$ medium:** 1% (w/v) yeast extract, 0.4% (w/v) peptone, 0.4% (w/v) sucrose

**YPD medium:** 1% (w/v) yeast extract, 2% (w/v) peptone, 2% (w/v) D-glucose

Agar media were obtained by adding 2% (final concentration; CM, Sc-Ura) or 1.3% (final concentration; dYT) of agar.

### 2.2 Growth and Maintenance of microbial material

#### 2.2.1 Cultivation of *E. coli*

All *E. coli* strains were grown in dYT liquid or agar medium (Sambrook and Russell, 2001) containing Ampicillin (100µg/ml) at 37 °C. Liquid cultures were shaked at 200 rpm. Cultures were mixed with dYT-Glycerol medium at 1:1 ratio and stored at -80 °C.

#### 2.2.2 Cultivation of *Ustilago maydis*

All *U. maydis* strains, apart from Dyn2 temperature-sensitive strain, were grown in CM-G liquid or agarose medium at 28°C unless otherwise stated. Liquid cultures were shaked at 200 rpm. Dyn2ts and control cells were grown at 22°C and transferred into 32°C incubator. Selective CM-G agar media contained phleomycin (40µg/ml), carboxine (2µg/ml), hygromycin B (200µg/ml) or ClonNAT(150µg/ml). *Ustilago* strains were stored at -80°C as glycerol stocks mixing with NSY-Glycerol medium at 1:1 ratio.

### 2.2.3 Measurement of optical density

Overnight *Ustilago maydis* cells were measured at 600 nm ($OD_{600}$) in a Spekol 1500 photometer (Analytik Jena, Germany) to determine cell density. Uninoculated medium was used as a reference solution.

## 2.3 Molecular biological methods

Standard molecular techniques were applied as described in (Sambrook and Russell, 2001). Plasmids were obtained by using yeast recombination system (Kitazono, 2009). Briefly, gene fragments with 30bp overlaps were amplified and transformed into *S. cerevisae* strain DS94 (Tang et al., 1996) along with linearized yeast-*E. coli* shuttle vector (Schuster et al, 2011). Plasmids were isolated from positive yeast colonies and transformed into *E. coli* cells. Positive bacteria colonies were selected on antibiotic containing medium. Isolated plasmids were tested by endonuclease digestion. Positive plasmids were linearized and transformed into *Ustilago maydis* protoplasts.

### 2.3.1 Standard PCR

All the gene products with 30 bp overhangs were amplified by standard PCR using Phusion ® high fidelity polymerase (NEB, UK). Manufacturer's protocol was followed as below:

| Component: | Volume(25µl): |
|---|---|
| Template(gDNA) | 0.5µl |
| Phusion enzyme | 0.5µl |
| Forward primer (10µM) | 1µl |
| Reverse primer (10µM) | 1µl |
| dNTPs(10mM) | 2.5µl |
| Phusion HF buffer(5X) | 5µl |
| $dH_2O$ | 14.5µl |

PCR conditons:

| | | |
|---|---|---|
| Step 1 | 98°C | 30 sec |
| Step 2 | 98°C | 10 sec |
| Step 3 | Tm(55-70°C) | 20 sec |
| Step 4 | 72°C | 15 sec per kb |
| | | 35 cyles of step2-4 |
| Step 5 | 72°C | 10 min |
| Step 6 | 10°C | ∞ |

### 2.3.2 Colony screening PCR

Yeast colonies were screened to find positive transformants by using DreamTaq Green PCR Master Mix (Fermentas). This solution already contains Dreamtaq DNA polymerase, DreamTaq Green buffer, $MgCl_2$ and dNTPs. PCR protocol is:

| Component: Volume(20µl): | |
|---|---|
| Template (yeast colony; picked by pipette tip ) | - |
| DreamTaq Green Master Mix | 10µl |
| Forward primer (10µM) | 1µl |
| Reverse primer (10µM) | 1µl |
| $dH_2O$ | 8µl |

PCR conditons:

| | | |
|---|---|---|
| Step 1 | 95°C | 3 min |
| Step 2 | 95°C | 30 sec |
| Step 3 | Tm (55-70°C) | 30 sec |
| Step 4 | 72°C | 1 min per kb |
| | | 35 cyles of step2-4 |
| Step 5 | 72°C | 10 min |
| Step 6 | 10°C | ∞ |

### 2.3.3 Purification of PCR products

PCR products were loaded onto agarose gel (0.8%) and excised by using razor blade. Each gel slice was mixed with 1 ml of 6M Sodium Iodide and incubated at 55 °C until the gel dissolve completely. 50 µl of 10% silica bead solution (w/v; in 3M sodium iodide) was added to bind DNA to the beads and incubated at 55 °C for 5 min. The mixture was centrifuged at 13300 rpm for 1

min. Pellet was washed by 500 µl of DNA wash buffer by three times. Next, 15 µl $dH_2O$ was added to the pellet and incubated at 55 °C for 5 min to elute DNA. Followed by 1 min spin, supernatant containing purified DNA is taken into a sterile tube.

### *2.3.4 S. cerevisiae* transformation

Homologous recombination in yeast was done as described in (Schuster et al., 2011a). Briefly, *S. cerevisae* strain (MAT$\alpha$, *ura3-52*, *trp1-1*, *leu2-3*, *his3-111*, and *lys2-801*; (Raymond et al., 1999)) was grown in 3 ml YPD containing tube at 30 °C overnight shaking at 200 rpm. 2 ml cell culture was inoculated into 50 ml YPD containing flask and incubated at 30 °C for 5 h shaking at 200 rpm. Cells were spun down for 5 min at 2200 rpm (centrifuge; Heraeus Biofuge Stratos, Germany, rotor Heraeus #3047). The pellet was gently washed by 10 µl of $dH_2O$ and spun for 5 min at 2200 rpm. Then, cells were resuspended in 300 µl of $dH_2O$. 50 µl of cells was mixed with 50 µl of 2 µg/µl salmon sperm DNA solution (in $dH_2O$;Sigma). 2 µl of linearized vector and 2-4 µl of each PCR product were added to the cell mixture followed by addition of 32 µl of 1M lithium iodide (in $dH_2O$; Sigma) and 240 µl PEG 4000 (w/v in $dH_2O$; Prolabo). The mixture was gently pipetted and incubated at 30°C for 30 min. Next, it was transferred to 45°C water bath for heat shock and incubated for 15 min followed by centrifugation at 2000 rpm for 2 min. The pellet was resuspended in 200 µl $dH_2O$ and spread onto two Sc-Ura plates with 1:1 and 1:10 dilutions. Transformation plates were incubated at 30 °C for 2-3 days.

### *2.3.5 E. coli* transformation

*E. coli* strain DH5α (Hanahan, 1983) was used for all cloning and plasmid generation purposes. For *E. coli* transformation, 50 µl chemically competent cells were mixed with 6-8 µl isolated yeast plasmid and allowed to thaw on ice for 20 min. Heat shock was applied at 42 °C water bath for 45 s followed by 5 min incubation on ice. Next, 200 µl of dYT was added and reaction tubes were incubated at 37°C shaking at 200 rpm. Cells were spread onto ampicillin containing dYT agar plates and incubated at 37°C overnight.

### *2.3.6 Ustilago maydis* transformation

*Ustilago* protoplasts were prepared as described in (Schulz et al., 1990). Briefly, *Ustilago* cells were grown in 50 ml YEPS medium until $OD_{600}$ reached 0.6-0.8. Cell culture was spun at 3000 rpm for 10 min and pellet was resuspended in 25 ml of SCS followed by another spin at 3000 rpm for 10 min. Next, Lysing enzyme (Sigma, USA) was added to pellet and reaction tube was allowed to incubate at RT for 10-15 min until %30-40 of cells became rounded (assessed by microscope observation). After lysing step, 10 ml of ice cold SCS was added and cells were spun at 2400 rpm for 10 min at 4 °C. Washing with SCS was repeated two more times. Then, cells were washed with 10 ml of ice cold STC followed by centrifugation at 2400 rpm for 10 min at 4 °C. Finally, pellet was gently resuspended in 500 µl of STC and 50 µl aliquot was used for each transformation.

To transform *Ustilago* cells, 50 µl of *Ustilago* protoplasts, 4 µl of linearized vector and 1 µl of Heparin (1mg/ml) were mixed and incubated on ice for 30 min. Next, 500 µl of 40% PEG solution (w/v in STC) was added and mixed by

gentle pipetting followed by incubation on ice for 15 min. Reg agar plates with antibiotic containing bottom layer and only reg agar containing upper layer were prepared and 20% of transformation reaction was spread onto one plate and 80% of reaction was spread onto another plate. Plates were incubated at 28 °C for 3-6 days. *Ustilago* colonies were streaked onto CM-agar plates containing selective antibiotics. Then positive strains were verified by microscopy and or Western and/or Southern blotting.

### 2.3.7 Plasmid isolation from *S. cerevisiae*

Positive yeast colonies were inoculated into 15 ml Sc-ura containing flasks and grown at 30 °C overnight shaking at 200 rpm. Cells were harvested by spinning at 1500 rpm for 5 min at RT. Cell pellet was resuspended in 500 µl $dH_2O$ and transferred into 1.5 ml eppendorf tubes followed by 2 min spin at 13300 rpm. Supernatant was discarded and cells were resuspended in residual water. Next, 200 µl of yeast lysis buffer and 200 µl of phenol:chloroform:isoamylalcohol (25:24:1) were added to cells. After the addition of 0.3 g acid washed glass beads (425-600 µm), tubes were allowed to vibrate for 10 min on IKA Vibrax VXR (IKA-Werke, Germany). 200 µl of TE was added into tubes followed by 5 min spin at 13300 rpm. The aqueous phase was transferred into a new tube and mixed with $1/10^{th}$ volume of 3M sodium acetate (pH 5.5) and 1 ml of 96% ethanol followed by incubation at -20 °C for 15 min. Then, the tubes were spun at 13300 rpm for 5 min and the pellet was resuspended in 400 µl TE buffer (pH 8.0) and 4 µl RNAse A (10 mg/ml). Tubes were incubated at 37 °C until the pellets were dissolved completely. Next, 10 µl of 4M ammonium acetate and 1 ml of 96 % ethanol

(v/v) were added to the cells and mixed by pipetting. Tubes were centrifuged at 13300 rpm for 2 min. Pellet was washed in 70% ethanol for two times and allowed to dry at RT. Air-dried pellet was dissolved in 20 µl of $dH_2O$.

### 2.3.8 Plasmid isolation from *E. coli*

Plasmids were isolated from positive *E. coli* colonies by using alkaline lysis method (Birnboim, 1983). Briefly, each colony was inoculated into 3 ml dYT-ampicillin medium and grown at 37 °C overnight. Cells were briefly centrifuged in eppendorf tube and pellet was resuspended in 150 µl TE buffer (pH 8.0) along with 5 µl RNAse (10mg/ml). Next, 150 µl alkaline lysis solution was added and tube was mixed by inverting followed by 5 min incubation at -20 °C. Then, 500 µl of neutralization solution was added to mixture, tube was inverted to mix and incubated at -20 °C for 10 min. Tube was spun at 13300 for 10 min and supernatant was transferred to a new tube. 750 µl of isopropanol was added and mixture was vortexed followed by 5 min centrifugation at 13300 rpm. 500 µl of 70% ethanol was added to the pellet ,after brief vortexing and it was spun at 13300 rpm for 5 min. Then, the pellet was allowed to dry and resuspended in 15-20 µl $dH_2O$.

### 2.3.9 Restriction enzyme digestion

Restriction endonucleases were used to verify plasmids and linearize plasmid of interest before *Ustilago* transformation. A sample of digestion protocol is as below:

| Component: | Volume(10µl): |
|---|---|
| Plasmid DNA | 0.5µl |
| Restriction endonuclease | 0.5µl |
| NEB buffer | 1µl |
| $dH_2O$ | 8.2µl |

To verify plasmids by digestion pattern, reaction was incubated at 37 °C for 45 min and run on agarose gel (0.8%). To linearize plasmids for transformation, larger digestion reaction (50-100 µl; 2h incubation) was set and linearized plasmid was cleaned (See purification of PCR products).

**2.4 Cell biological methods and image analysis**

Light microscopy was performed as described in (Schuster et al. 2011a). Briefly, cell culture was placed on a thin 2% agar cushion and covered by coverslip followed by observation on a IX81 motorized inverted microscope (Olympus, Hamburg, Germany). Fluorescently labelled proteins were excited by using VS-LMS4 Laser-Merge-System consisting of solid state lasers (488 nm and 561 nm, Visitron System, Munich, Germany). A Dualview Microimager (Photometrics) with filter sets that consist of excitation dual-line beam splitter (z491/561; Chroma, Rockingham, VT), an ET-Bandpass 525/50 (Chroma), and a BrightLine HC 617/73 (Semrock, Rochester, NY). was used to colocalize fluorescent signals. Images were captured by using a Charged-Coupled device, Photometric CoolSNAP HQ2 (Roper Scientific, Germany). Whole imaging system was operated by software package MetaMorph (Molecular Devices, Downingtown, USA) which was also used to do measurements and process images.

## 2.5 Materials and Methods for Chapter 3

**Oleic acid induction:** Oleic acid solution (Merck Millipore, Darmstad, Germany) was kindly provided by Prof Michael Schrader (Bonekamp et al., 2012). *Ustilago maydis* cells were grown in liquid CM-glucose media overnight and transferred into NM minimal media supplemented with 0.5 % oleic acid (v/v) and 0.5 % tergitol (v/v; NP-40, Sigma, St. Louis, USA).

**Imaging and tracking peroxisome motility:** GFP SKL signals were observed by using 488 nm laser with 20% power output at 100 ms exposure time. mCherry SKL signals were obtained by using 561 nm laser with 50% power output. 100-frame or 200-frame movies were acquired. To track peroxisome movements, movies were projected into kymographs. Velocity and runlength were measured on kymographs. All events with displacement>0.5 µm and velocity> 0.5 µm/sec were assigned as long-range motility events. The frequency was calculated by total number of long-range motility events divided by total observation time.

**Inhibitor studies:** *Ustilago maydis* cells were grown in liquid CM-glucose media overnight to $OD_{600}$ 0.6 and incubated with either 30 µM benomyl (stock: 10 mM in Dimethyl sulfoxide (DMSO); Fluka,USA) or 10 µM Latrunculin A (stock: 20 mM in DMSO: Enzo Life Sciences,USA) for 30 min. Cells were treated with the same amount of the solvent DMSO as control. In ATP depletion assay, which was performed to reduce ATP level in the cell, *U. maydis* culture was incubated with 100 µM of carbonyl cyanide m-chlorophenylhydrazone (CCCP) (Sigma-Aldrich) for 8 min. The same amount of DMSO was used as a solvent control.

**Calculation of Peroxisome density:** In order to find number of peroxisomes per unit area ($\mu m^3$), the total number of peroxisomes was counted and divided by cell volume. Peroxisome count was done on GFPSKL expressing cells processed by maximum projection. Cell volume was calculated with the formula $v = 4/3\pi ab^2$ by assuming that cells are in prolate ellipsoid shape (Maeda and Thompson, 1986). Values of a and b were measured by using Metamorph (Molecular Devices, Downingtown, PA).

**Plasmids and strains:** $po^H$ChSKL: this plasmid contains mCherry SKL fusion protein under the control of otef promoter (Spellig et al., 1996), Tnos sequence and hyromycin resistance cassette. $po^C$GFPSKL (Steinberg and Schuster, 2011): this plasmid contains GFP-SKL fusion protein under the control of otef promoter, Tnos sequence and carboxin resistance cassette. $Po^H$GFPSKL was obtained by replacing the carboxin resistance cassette in $po^C$GFPSKL with the hygromycin resistance cassette. Hygromycin was amplified by using pSL+Hyg plasmid and $GD17_F$ and $GD18_R$ primers.
FB2GFPSKL was generated by cutting $po^C$GFPSKL by BglI and inserting into succinate dehydrogenase locus (cbx) (Keon et al., 1991) of FB2 cells; FB2_GFP-SKL_GFP-Tubulinα was generated by ectopic insertion of GFP_tubulin::nat vector (Isabel Schuchardt and Gero Steinberg, unpublished) ,cut by AlwNI, into FB2GFPSKL cells. To obtain AB33_GFP-Tubα_mCherry-SKL, $po^H$mCherrySKL plasmid was linearized with EcoRV and ectopically integrated into AB33 GT genome. To obtain AB33_LifeAct-GFP_ChSKL; $po^H$mCherrySKL vector was cut by EcoRV and inserted into AB33LifeActGFP cells (Schuster et al., 2012) ectopically. AB5_*Dyn2ts*-GSKL was obtained by transforming AB5Dyn2ts cells (kindly provided by M. Feldbrugge) by linearized $po^H$GFPSKL ectopically. To generate AB33_*ΔKin1*_GSKL and AB33_*ΔKin3*_GSKL; $po^H$GFPSKL was linearized by BglI and transformed into AB33_Δ*Kin1* cells and AB33_Δ*Kin3* cells (Schuchardt et al., 2005) ectopically.

**Table 2.1 Strains used in Chapter 3**

| Strain | Genotype | Reference |
|---|---|---|
| FB2GSKL | a2b2 otef-GFP-SKL,cbx | Chapter 3 |
| FB2GSKLGT | a2b2 Potef-GFP-SKL, cbx/ Potef GFP-Tub,nat | Chapter 3 |
| AB33GSKL | a2 Pnar-bW2 Pnar-bE1, ble/ Potef GFP-SKL-cbx | Steinberg and Schuster, 2011 |
| AB33LifeAct-GFP | a2 Pnar-bW2 Pnar-bE1, ble/ Potef-Lifeact-GFP, cbx | Schuster et al., 2012 |
| AB33GTChSKL | a2 Pnar-bW2 Pnar-bE1, ble/Potef GFP-tub-cbx/Potef-mCherry-SKL,hyg | Chapter 3 |
| AB33LifeAct-GFPChSKL | a2 Pnar-bW2 Pnar-bE1, ble/ Potef Lifeact-GFP-cbx/ Potef-mCherry-SKL,hyg | Chapter 3 |
| AB5*Dyn2ts*-GSKL | a1 Pnar-bW2bE1 Dyn2ts, hyg | Chapter 3 |
| AB33*ΔKin1*GSKL | a2 Pnar-bW2 Pnar-bE1, ble *Δ*kin1, hyg / Potef-gfp-skl, cbx | Chapter 3 |
| AB33*ΔKin3*GSKL | a2 Pnar-bW2 Pnar-bE1, ble *Δ*kin3, hyg / Potef-gfp-skl, cbx | Chapter 3 |

*a*, *b*, mating type loci; P, promoter; -, fusion; *hyg*R, hygromycin resistance; *ble*R, phleomycin resistance; *nat*R, nourseothricin resistance; *cbx*R, carboxin resistance; ts, temperature-sensitive allele; Δ, deletion; /, ectopically integrated; *otef*, constitutive promoter; *nar*, conditional nitrate reductase promoter; *E1*, *W2*, genes of the *b* mating-type locus; *egfp*, enhanced green fluorescent protein; *mCherry*, monomeric Cherry; GT, gfp-tubulin; *dyn2*: C-terminal half of the dynein heavy chain; *kin1*, kinesin-1; *kin3*, kinesin-3

## 2.6 Materials and methods for Chapter 4

**Imaging and tracking organelle motility:** rab5GFP and GFPHDEL signals were observed by using 488 nm laser with 50% power output at 100 ms exposure time. 50- or 100-frame movies were acquired. Colocalization analysis was done by using Dual-View Micro imager; the 488 nm laser at 20% output power, the 561 nm laser at 50% output power with exposure time of 150 ms.

**Photobleaching:** FRAP (Fluorescent Recovery After Photobleaching) was applied as reported before (Schuster et al., 2011a). Briefly, 405 nm/60 mW iodade laser at 100% laser power was applied on region of interest followed by acquisition of image series.

**Protein extraction and immunodetection by Western Blotting**: Western blotting protocol was followed as previously described (Bielska et al., 2014). To analyse the expression level of Kin3 by Western Blotting, cell extracts of the FB1*Yup1ts*Kin3GFP strain grown as 200 ml culture at 32 °C and a control strain FB1*Yup1ts*Kin3GFP grown at 22 °C were obtained by disruption of $LN_2$-frozen *Ustilago* cells grown to OD600 0.9-1.2 in a mixer mill MM200 (Retsch) at frequency 30/s for 2.5 min. Milling step was repeated. Cell extracts were thawed on ice and resuspended in 0.1-0.5 ml of 50 mM Hepes, 50 mM KCl, 1 mM EGTA, 1 mM $MgCl_2$, pH 7.0 complemented with protease inhibitor (Roche Complete Mini #11836153001). Sample tubes were centrifuged at 50,000 g for 30 minutes at 4 °C. Bradford assay was performed to determine concentrations of soluble fractions (Bradford, 1976). From each sample, 30 ug of inoculum was loaded on 8% SDS-polyacrylamide gels and the gel was transferred onto nitrocellulose membrane (GE Healthcare, United Kingdom) for 55 min at 190 mA in a semi-dry blot chamber (Fastblot, Analytik Jena, Germany). The membrane was blocked for an hour with 5% non-fat milk in TBS-1% Tween-20. Next, the blot was incubated with anti-GFP mouse IgG monoclonal antibodies in a 1:5000 dilution (Roche, #11814460001) overnight at 4°C followed by incubation with HRP-conjugated anti-mouse IgG in a 1:4000 dilution (Promega #W402B). As a loading protein control, the blot was

stripped and re-probed with mouse anti-$\alpha$ tubulin antibodies in a 1:4000 dilution (Oncogene Science, Cambridge, MA) followed by HRP-conjugated anti-mouse IgG in a 1:4000 dilution. Blot development was done by using EC Plus Western Blotting Detection system, according to the manufacturer's instructions (GE Healthcare #RPN2132).

**Plasmids and strains used in the chapter:** AB33Kin3G_ChSKL; the strain was generated by cutting po$^{C}$mCherrySKL plasmid by EcoRV and inserting into AB33Kin3GFP (Schuster et al., 2011b). AB33Kin3G_ChHDEL; the strain was generated by ectopic insertion of po$^{C}$mCherry HDEL linearized with AlwNI into AB33Kin3GFP cells. FB1ERGFP_Chrab5 (S. Kilaru, unpublished); strain was generated by inserting po$^{N}$mCherryrab5 vector,linearized by SapI, into FB1ERGFP cells (Wedlich-Söldner et al., 2002a) ectopically. AB33Chrab5_GSKL (E. Bielska, unpublished); strain was generated by ectopic integration of po$^{H}$GFPSKL ,cut by AgeI, into AB33Chrab5a genome. AB33Grab5_ChSKL: po$^{H}$mCherrySKL vector was linearized with EcoRV and integrated into AB33Grab5 cells (Schuster et al., 2011c) ectopically. AB33Eca1G_Chrab5 (S. Kilaru, unpublished); Strain was generated by inserting po$^{N}$mCherryrab5, cut with SapI, into AB33Eca1GFP cells ectopically. AB33*ΔKin3*_ERGFP (I. Schuchardt, unpublished); strain was generated by inserting linearized po$^{C}$GFPHDEL into AB33_*Δkin3* (Schuchardt et al., 2005) ectopically. FB1*Yup1ts*_Grab5_ChSKL; po$^{H}$mCherrySKL vector was cut by EcoRV and integrated into FB1yup1tsGFPrab5 cells (D. Aßmann, unpublished) ectopically. FB1*Yup1ts*_Chrab5_GHDEL; po$^{N}$mCherryrab5 and po$^{C}$GFPHDEL plasmids were linearized and co-integrated into FB1yup1ts cells (Wedlich-Soldner unpublished). FB1*Yup1ts*_Kin3G (D. Aßmann, unpublished); Strain was generated by insertion of po$^{C}$Kin3GFP plasmid into FB1Yup1ts cells. AB33*Δrab5*_Yup1G; Yup1GFP vector was linearized and transformed AB33_*Δrab5* (Anne Raßbach and Gero Fink, unpublished) ectopically. AB33*Δrab5*_GSKL; po$^{C}$GFPSKL vector was cut by BglI and transformed AB33_*Δrab5* ectopically.

**Table 2.2 Strains used in Chapter 4**

| Strain | Genotype | Reference |
|---|---|---|
| AB33Grab5 | a2 Pnar-bW2 Pnar-bE1, ble /Potef-GFP-rab5-1, cbx | Schuster et al., 2011b |
| AB33GSKL | a2 Pnar-bW2 Pnar-bE1, ble/ Potef GFP-SKL-cbx | (Steinberg and Schuster, 2011) |
| AB33EG | a2 Pnar-bW2 Pnar-bE1, ble / Potef-GFP-HDEL, cbx | Wehlich-Soldner, 2002a, MBoC |
| AB33Eca1GFP | a2 Pnar-bW2 Pnar-bE1, ble/ Potef-eca1-GFP, cbx | Wehlich-Soldner, 2002a, |
| AB33Kin3GChrab5 | a2 Pnar-bW2 Pnar-bE1, ble, Pkin3-kin3-gfp, hyg/ Potef-mCherry-Rab5a, nat | Schuster et al., 2011b |
| AB33Kin3GChSKL | a2 Pnar-bW2 Pnar-bE1, ble, Pkin3-kin3-gfp, hyg/ Potef-mCherry-SKL, cbx | Chapter 4 |
| AB33Kin3GChHDEL | a2 Pnar-bW2 Pnar-bE1, ble, Pkin3-kin3-gfp, hyg/ Potef-mCherry-HDEL, cbx | Chapter 4 |
| FB1ERGChrab5 | a1b1/ Potef-GFP-HDEL, cbx / Potef-mCherry-rab5a, nat | Chapter 4 |
| AB33Chrab5GSKL | a2 Pnar-bW2 Pnar-bE1, ble/ Potef-mCherry-Rab5.1, nat/ Potef-GFP-SKL, hyg | Chapter 4 |
| AB33Grab5ChSKL | a2 Pnar-bW2 Pnar-bE1, ble / Potef-GFP-rab5, cbx/ Potef-mCherry-SKL, hyg | Chapter 4 |
| AB33Eca1GChrab5 | a2 Pnar-bW2 Pnar-bE1, ble/Potef-Eca1-GFP, cbx/ Potef-mCherry-rab5a, nat | Chapter 4 |
| AB33*Δkin3*Grab5 | a2 Pnar-bW2 Pnar-bE1, ble /Dkin3,nat / Potef-GFP-rab5a, cbx | Schuster et al., 2011b |
| AB33*Δkin3*ERGFP | a2 Pnar-bW2 Pnar-bE1, ble /Dkin3,hyg / Potef-GFP-HDEL, cbx | Chapter 4 |
| FB1*Yup1ts*Grab5 | a1b1 yup1ts / Potef-GFP-rab5a, cbx | |
| FB1*Yup1ts*Grab5ChSKL | a1b1 yup1ts / Potef-GFP-rab5a, cbx/Potef-mCherry-SKL, hyg | Chapter 4 |
| FB1*Yup1ts*Chrab5GHDEL | a1b1 yup1ts / Potef-mCherry-rab5a, nat/ Potef-GFP-HDEL, cbx | Chapter 4 |
| FB1*Yup1ts*Kin3G | a1b1 yup1ts / PKin3-Kin3-GFP, cbx | Chapter 4 |
| AB33*Δrab5*Yup1G | a2 Pnar-bW2 Pnar-bE1, ble Drab5_1::nat / Potef--yup1-sgfp, cbx | Chapter 4 |
| AB33*Δrab5*_GSKL | a2 Pnar-bW2 Pnar-bE1, ble Drab5_1::nat / Potef-GFP-SKL, cbx | Chapter 4 |

*a*, *b*, mating type loci; P, promoter; -, fusion; *hyg*R, hygromycin resistance; *ble*R, phleomycin resistance; *nat*R, nourseothricin resistance; *cbx*R, carboxin resistance; ts, temperature-sensitive allele; Δ, deletion; /, ectopically integrated; *otef*, constitutive promoter; *nar*, conditional nitrate reductase promoter; *E1*, *W2*, genes of the *b* mating-type locus; *egfp*, enhanced green fluorescent protein; *mCherry*, monomeric Cherry; *kin3*, kinesin-3

## 2.7 Materials and methods for Chapter 5

### Plasmids and strains used in the chapter:

po$^{C}$um05592GFP: this plasmid contains um05592 GFP fusion under the control of otef promoter. For otef promoter, $GD3_F$ and $GD4_R$ primers were used. For um05592 $GD5_F$ and $GD6_R$ were used. For GFP amplification $GD7_F$ and $GD8_R$ were used. AB33um05592G_ChSKL; Strain was generated by cutting po$^{C}$um05592GFP plasmid by *Bgl*I and integrating ectopically into AB33mCherrySKL cells. FB2*Δum05592* (S.Mitchell unpublished); Strain was generated by insertion of pCRIITOPO_*Δ*um05592 vector (D. Aßmann unpublished), linearized with *BamH*I+*Pst*I, into FB2 cells. SG200*Δum05592* (N. Pawolleck unpublished); Strain was generated by inserting pCRIITOPO_*Δ*um05592 vector cut by *BamH*I+*Pst*I into FSG200 cells.

**Table 2.3 Strains used in Chapter 5**

| Strain | Genotype | Reference |
|---|---|---|
| AB33GSKL | a2 Pnar-bW2 Pnar-bE1, ble/ Potef GFP-SKL-cbx | Chapter 3 |
| FB2GSKL | a2b2 /Potef-egfp-SKL, cbx | Chapter 3 |
| FB2GSKLGT | a2b2 GFP SKL, cbx/ GFP tub, nat | Chapter 3 |
| AB33*ΔKin3*GSKL | a2 Pnar-bW2 Pnar-bE1, ble Dkin3::hyg / Potef-gfp-skl, cbx | Chapter 3 |
| AB33um05592GChSKL | a2 Pnar-bW2 Pnar-bE1,ble/otef cherry SKL,Hyg/ otef um05592GFP,cbx | Chapter 5 |
| FB2 | a2b2 | wild type |
| FB2*Δum05592* | a2b2 *Δ*um05592::nat | Chapter 5 |
| SG200 | a1 mfa2 bW2 bE, ble | Bolker et al, 1995 |
| SG200*Δum05592* | a1 mfa2 bW2 bE1, ble *Dum5592::nat* | Chapter 5 |

*a*, *b*, mating type loci; P, promoter; -, fusion; *hyg*R, hygromycin resistance; *ble*R, phleomycin resistance; *nat*R, nourseothricin resistance; *cbx*R, carboxin resistance; ts, temperature-sensitive allele; Δ, deletion; /, ectopically integrated; *otef*, constitutive promoter; *nar*, conditional nitrate reductase promoter; *E1*, *W2*, genes of the *b* mating-type locus; *egfp*, enhanced green fluorescent protein; *mCherry*, monomeric Cherry; GT, gfp-tubulin; *kin3*, kinesin-3

## Table 2.4 Primers used in this thesis

| Primer | Sequence 5' → 3' |
|---|---|
| GD3 | GACGATAGAGGTACTCAAGGTGCCACCCTAGCAAATATGTCAACTCTC |
| GD4 | ATGATCAGTATTAGTCGGAGGTAGTCGTGGGTCAATTGACGCTTAGG |
| GD5 | GGGATGGTACTCAAAAGGGTGATCCAGCAAATATGTCAGACGACTCTGCTTC |
| GD6 | GTAACACATACATCAGAGTCGGGCAGCTAGGTCGTTCAAAACTCATAGC |
| GD7 | ATTCTCACCAGTGTCGTTCAAAACTCATAG CCACACCACACGGCCACTGT |
| GD8 | CCTGCTAGCAAGCCGCTTGTCTGCAGAAGCCCGTGGCGCA TGGATGCAC |
| GD9 | TGGTAACAACTCGTTCAACTGATACTTTTCAGTCTATCTAGTGG GAACTT |
| GD10 | GTCCAAGAGGCGAGCTGACGTACGGACGAAGTTGCCAC CAGCGTGGGTCC |
| GD17 | TATTTGAGAAGATGCGGCCAGCAAAACTAACTGAAGCTTGCATGCCTGC |
| GD18 | TACAAGTCGAAGCTTTAAAGCGGCCGCCCGGCTGCAGATCGTTCAAAC |

## 3. General Aspects of Peroxisome Motility

### 3.1 Introduction

Peroxisomes are ubiquitous organelles found in almost all eukaryotes. These organelles show high plasticity changing their size, shape and number according to cellular and environmental stimuli (Huber et al., 1999; Schrader et al., 2003). Peroxisomes associate with the cytoskeleton and molecular motors for spatiotemporal organization in the cell. In mammalian cells, peroxisomes move along microtubules by cooperation of kinesin and dynein motors (Huber et al., 1999; Rapp et al., 1996; Schrader et al., 2000; Wiemer et al., 1997). In yeast cells, peroxisomes are transported by Myo2 on actin filaments (Fagarasanu et al., 2006; Fagarasanu et al., 2005a; Hoepfner et al., 2001). In a filamentous fungi, *Aspergillus nidulans*, dynein and Kin3 are involved in bidirectional peroxisome motility (Egan et al., 2012b). Although, peroxisome motility is well studied in yeast and mammalian cells, a comprehensive analysis of peroxisome movements and underlying mechanism is still missing in filamentous fungi.

The aim of the work described in this chapter is to analyse peroxisome motility in *Ustilago maydis*. In order to visualize peroxisomes, I took advantage of peroxisome targeting signal I (PTS1), a universal tripeptide present at C terminal end of the majority of peroxisome matrix proteins (Gould et al., 1989). In this study, green fluorescence protein (GFP) was tagged with SKL sequence (PTS1 peptide) at its C terminus to visualize peroxisomes in *Ustilago maydis* cells. Peroxisomes have key role in lipid metabolism and peroxisome proliferation is induced when lipid content is increased (Valenciano et al., 1996). The localization of the GFP-SKL signal in

peroxisomes was confirmed by metabolic function applying fatty acids to the growth media (Brocard and Hartig, 2006b; Jourdain et al., 2008). Here, I confirmed that GFP SKL signals are peroxisomal signals by quantifying peroxisome proliferation upon fatty acid intake. Following verification of GFP-SKL import into peroxisomes, I designated motility events with run-length>0.5 µm and velocity> 0.5 µm/s as long-range motility and quantified motility parameters including frequency, run length and velocity of peroxisomes. After quantification of peroxisome motility, I then undertook some pharmacological assays prior to *in vivo* investigation of the cytoskeletal elements and molecular motors involved in the long-range peroxisome transport. Drug assays provided information on whether peroxisome motility is active or passive, and if active, what are the potential cytoskeletal tracks that peroxisomes are transported along. In order to confirm the results of the drug assays, both peroxisomes and either of the cytoskeletal tracks were labelled with fluorescent tags in the same cell and analysed by dual view imaging. Finally, the molecular motors having role in peroxisome motility were investigated.

I performed experimental studies on both yeast-like and hyphal cell forms of *Ustilago maydis.* Each cell type offers different advantages; for example in medium budded yeast cells, microtubule (MT) orientation is well established in which plus ends of tubules are present at cell poles whereas minus ends of tubules are present at neck and nucleus regions of the cell (Fink and Steinberg, 2006). Such cells serve as a useful tool to determine the direction of movement and the motors involved in intracellular transport. Moreover, small size and fast growth of the yeast cells make it easy to handle and

analyze quantitatively. By contrast, hyphal cells resemble neuronal cells with respect to microtubule orientation and common transport mechanisms (Steinberg and Perez-Martin, 2008). I thus used hyphal cells of *Ustilago maydis* as a model cell for neuronal organelle dynamics and intracellular transport.

## 3.2 Results

### 3.2.1 GFP-SKL is imported into peroxisomes

I set out to demonstrate that GFP-SKL can be used as peroxisome marker in *Ustilago maydis*. GFP was tagged with SKL tripeptide as the majority of peroxisomal matrix proteins have SKL as recognition signal (Brocard and Hartig, 2006b; Gould et al., 1989). The GFP-SKL fusion protein was expressed in FB2GSKL (See table 3.1 for all strains used in this chapter) cells and investigated using epifluorescence microscopy. GFP-SKL localized to "dot-like" structures in the cell (Figure 3.1). Their shape and distribution is reminiscent of peroxisomes in other systems (Egan et al., 2012b; Gronemeyer et al., 2013; Hynes et al., 2008; Kim et al., 2006) suggesting that SKL signal is targeted to peroxisomes in *Ustilago maydis*. To verify this conclusion, cells were grown in the presence of 0.5 % oleic acid (v/v), a long chain fatty acid, as sole carbon source. In budding and fission yeasts, the metabolism of oleic acid induces peroxisome proliferation and increases peroxisome number (Jourdain et al., 2008; Veenhuis et al., 1987). Consistent with this, in *Ustilago maydis* incubation with oleic acid increased the number of GFP-SKL positive structures (Figure 3.1). To quantify this effect, the number of GFP-SKL signals per cell volume was estimated (see 3.2 Materials and Methods). This analysis revealed that 0.42±0.02 peroxisomes per $\mu m^3$ are present in the cells grown in glucose containing medium whereas the number increased to 1.45 ± 0.14

peroxisomes per μm$^3$ for the cells grown in the presence of oleic acid (Figure 3.1, significant increase at P<0.0001,Student's *t-test*). Altogether, these

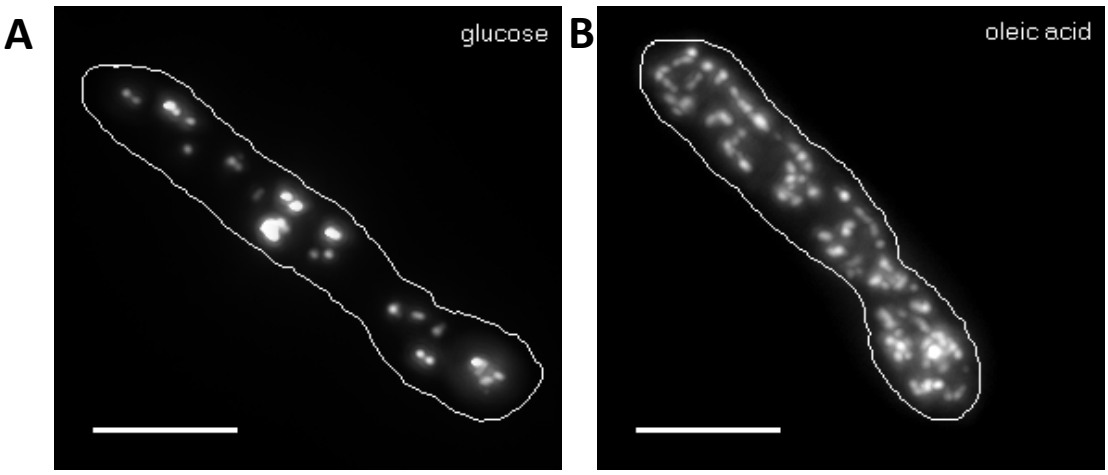


results strongly suggest that GFP-SKL is imported to peroxisomes in *U. maydis*.

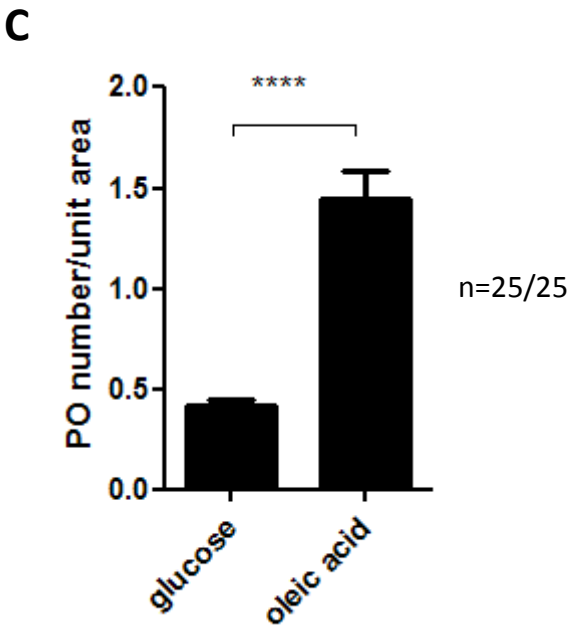


**Figure 3.1 GFP-SKL as a marker protein for peroxisomes in *U. maydis.***
Strain FB2GSKL was cultured in liquid CM-glucose medium overnight and shifted to liquid minimal medium NM supplemented with either glucose 1% (w/v) or oleic acid 0.5% (v/v). Followed by 4 hours incubation, cell cultures were examined. (A and B) GFP-SKL signals in cells grown in the presence of glucose and oleic acid. The number of fluorescent dots is increased in response to oleic acid induction. Scale bars = 5 μm. (C) Bar chart showing the average number of GFP-SKL signals in the presence of glucose and oleic acid. Mean values ± standard error of the mean is given; sampled size "n" is indicated. Triple asterisk indicates statistical difference at P<0.0001, Student t-test.

### 3.2.2 Analysis of peroxisome motility

#### 3.2.2.1 Peroxisomes switch between two motility states

After having verified that GFP SKL positive dots are most likely peroxisomes, I set out to investigate cellular dynamics of the organelles. To this end, series of fluorescent images were acquired in FB2GSKL cells. Obtained video sequences were processed and analysed by Metamorph software (see General Materials and Methods). Based on these data, I identified two types of peroxisome motility; (1) a short-range movement that appeared un-directed and (2) long-range movement that appeared bidirectional with linear displacement (Figure 3.2). Observations showed that almost all peroxisomes changed their positions over time (Figure 3.2). During short-range movement, peroxisomes freeze or oscillate whereby they remain almost stationary or change their positions over short distances ($x<0.5$ μm). In the long-range motility, peroxisomes can move long distances ($x>0.5$ μm) with directed manner. Individual tracks for each peroxisome indicated that motility types are interchangeable; a peroxisome moves in long-range and then changes to short range state (Figure 3.2). Occasionally, this directed motility enabled the organelles to travel in and out of the growing daughter cell (Figure 3.2).

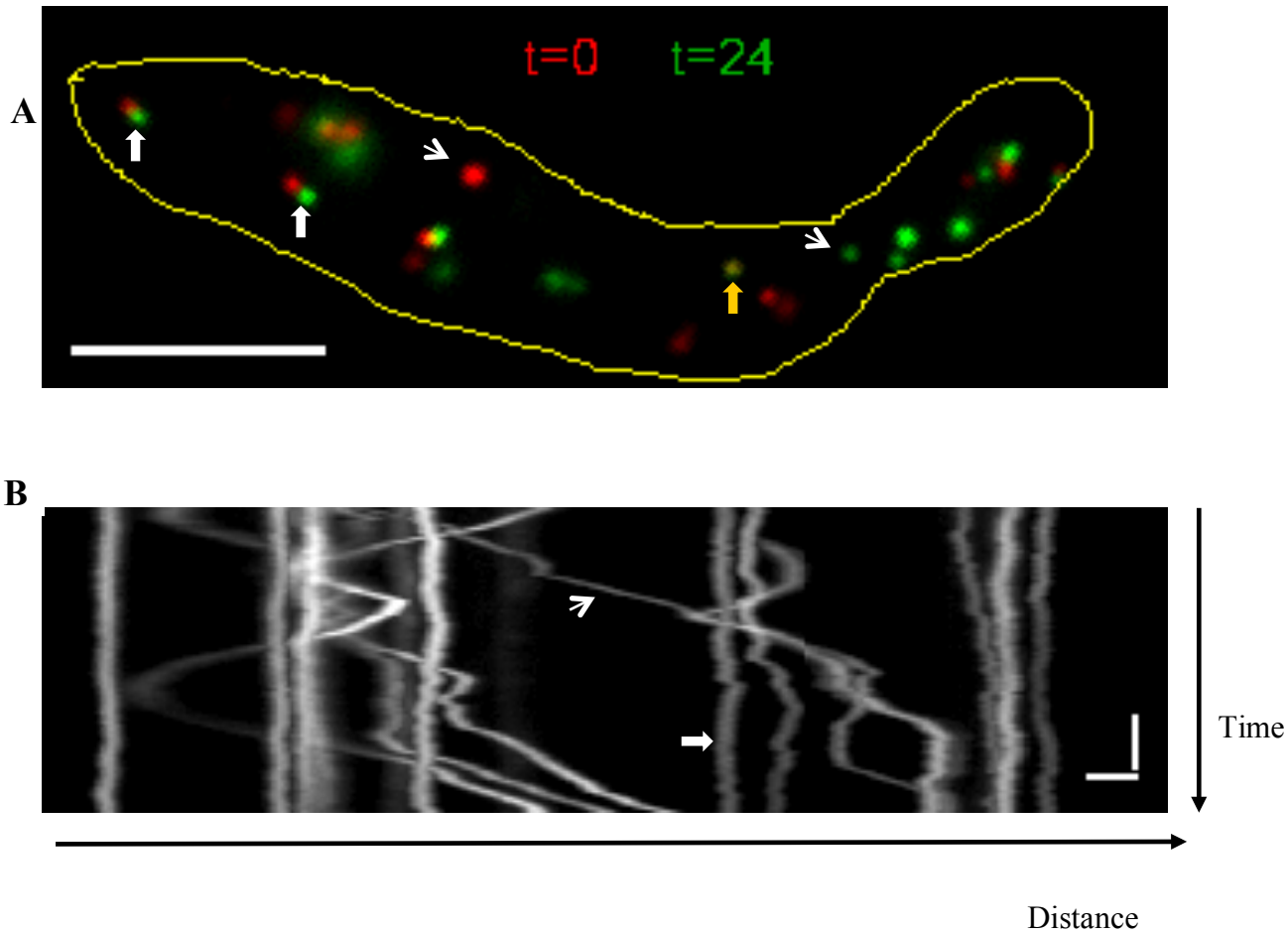


**Figure3.2. Two types of peroxisome motility in *U. maydis*.**
(A) Motility of peroxisomes was observed in the strain FB2eGSKL. First plane (t=0, red) and the last plane (t=24 s, green) of the image series were merged to show relative positions of each peroxisome after 24 s. White thick arrows indicate peroxisomes displace in short distance whereas thin arrow shows peroxisomes displace in long distance within 24 s. Yellow arrow shows a stationary peroxisome that does not displace in detectable distance. Bar=5 μm. (B). Kymograph showing peroxisome motility in the cell shown in (A). Long-range movement is shown with a thin arrow and short-range peroxisome tracks were pointed by thick arrow. Scale bars= 1 μm /2 s.

### 3.2.2.2 Quantitative analysis of long-range peroxisome motility

In yeast-like cells, 73 medium budded yeast-like cells expressing GFP-SKL were analysed quantitatively for peroxisomal movements. Peroxisomes travelled with mean velocity of 1.93±0.03 μm/s (488 events). Average run length of peroxisomes was calculated as 2.40±0.08 μm (503 events). The frequency of peroxisome motility was 0.38±0.04 (73 cells; 20 sec of total observation time) in yeast-like cells.

In hyphal cells, 42 cells were analysed for motility parameters. Average peroxisome velocity was 2.08±0.05 μm/s (156 events) and average run length was 3.85±0.35 μm (155 events). Finally, the frequency of the peroxisome movement was 0.59 events/sec. (42 cells; 20 sec of total observation time) in hyphal cells.

Motility parameters of two cell types are summarized in the Table 3.1. A comparison of these motility parameters revealed that the average velocity of peroxisome movement is not significantly different between cell types (*Student*'s t-test, P=0.1584, Figure 3.3). However, the average run length and the average frequency of peroxisome movement in hyphal cells were found to be significantly different than those of yeast like cells (Figure 3.4 and Figure 3.5, with kymographs provided for qualitative assessment).

**Table 3.1** Quantitative analysis of long-range peroxisome motility

| **CELL TYPE** | **velocity(μm/s)** | **run length(μm)** | **frequency(events/s)** |
|---|---|---|---|
| yeast | 1.93±0.03 n= 488 | 2.40±0.08 n= 503 | 0.38±0.04 n=73 |
| hyphae | 2.08±0.05 n= 156 | 3.85±0.35 n= 155 | 0.59±0.06 n=42 |

Thus, analysis of peroxisome motility revealed that peroxisomes are motile organelles. Different motility behaviours in yeast-like and hyphal cells suggest that peroxisome motility depends on cell types.

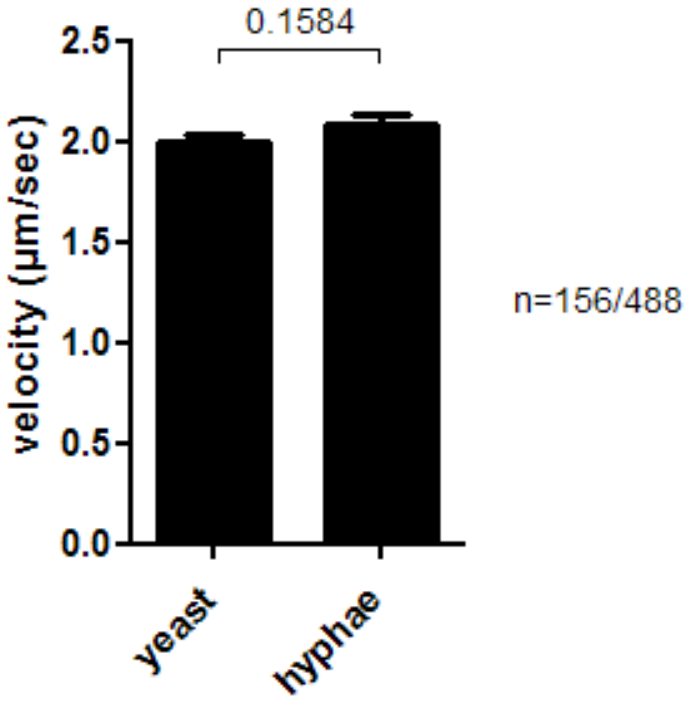


**Figure 3.3 Velocity of peroxisome motility in yeast-like and hyphal cells.**
Peroxisome motility in AB33GSKL cells. Bar chart showing average peroxisome velocity in yeast and hyphal cells. Mean values ± standard error of the mean is given; sampled size "n" is indicated. No significant difference was found between two cell types (P=0.1584, Student t-test).

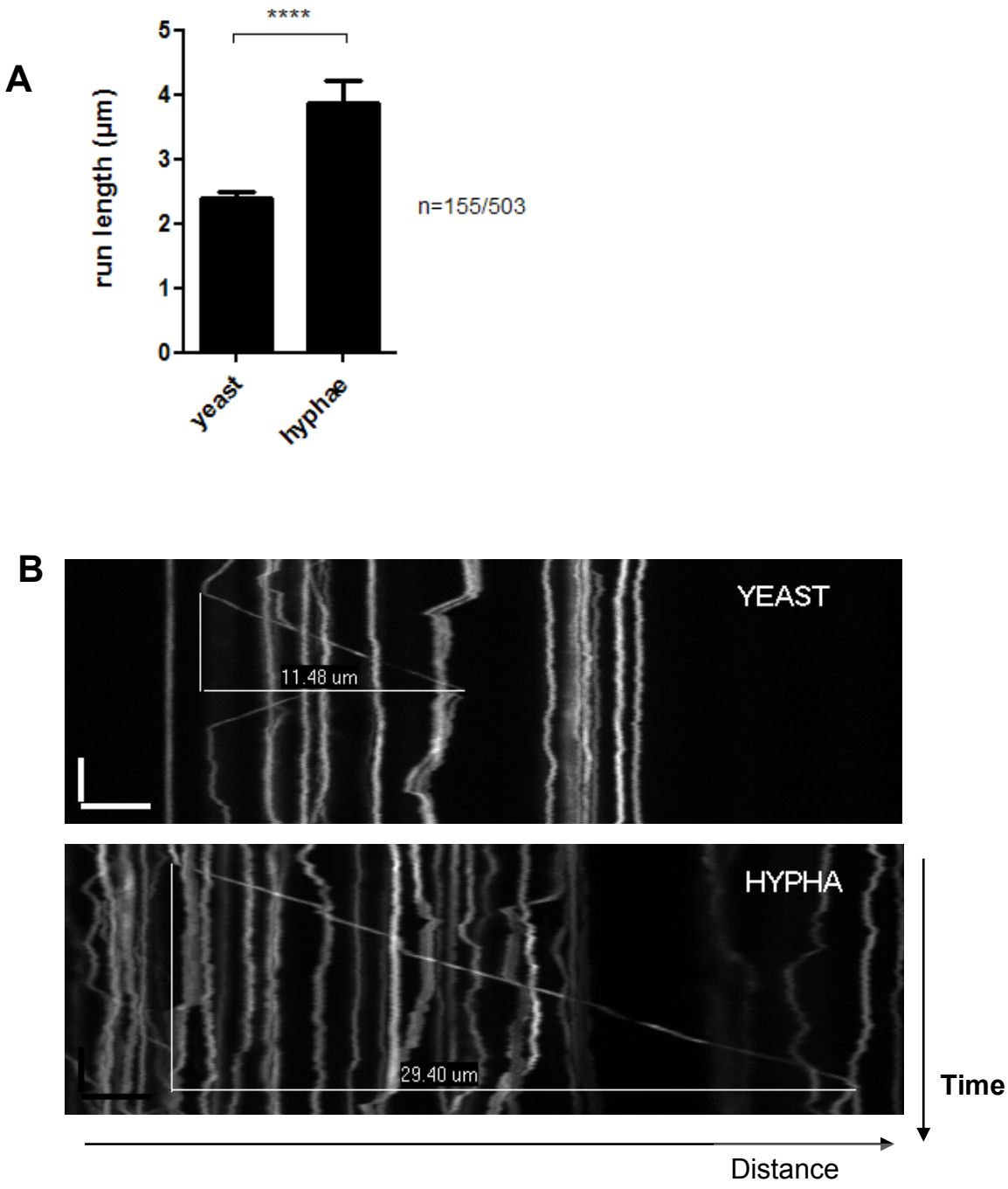


**Figure 3.4 Run length of peroxisomes in yeast-like and hyphal cells.**
(A) Peroxisome motility in AB33GSKL cells. Bar chart showing average run length of mobile peroxisome in yeast-like and hyphal cells. Mean values±standard error of the mean is given, sample size "n" is indicated. Quadruple asterisk indicates statistical significance at P<0.0001. (B) Kymographs showing two representative peroxisome runs in yeast-like and hyphal cells. Scale bars= 3µm/3s

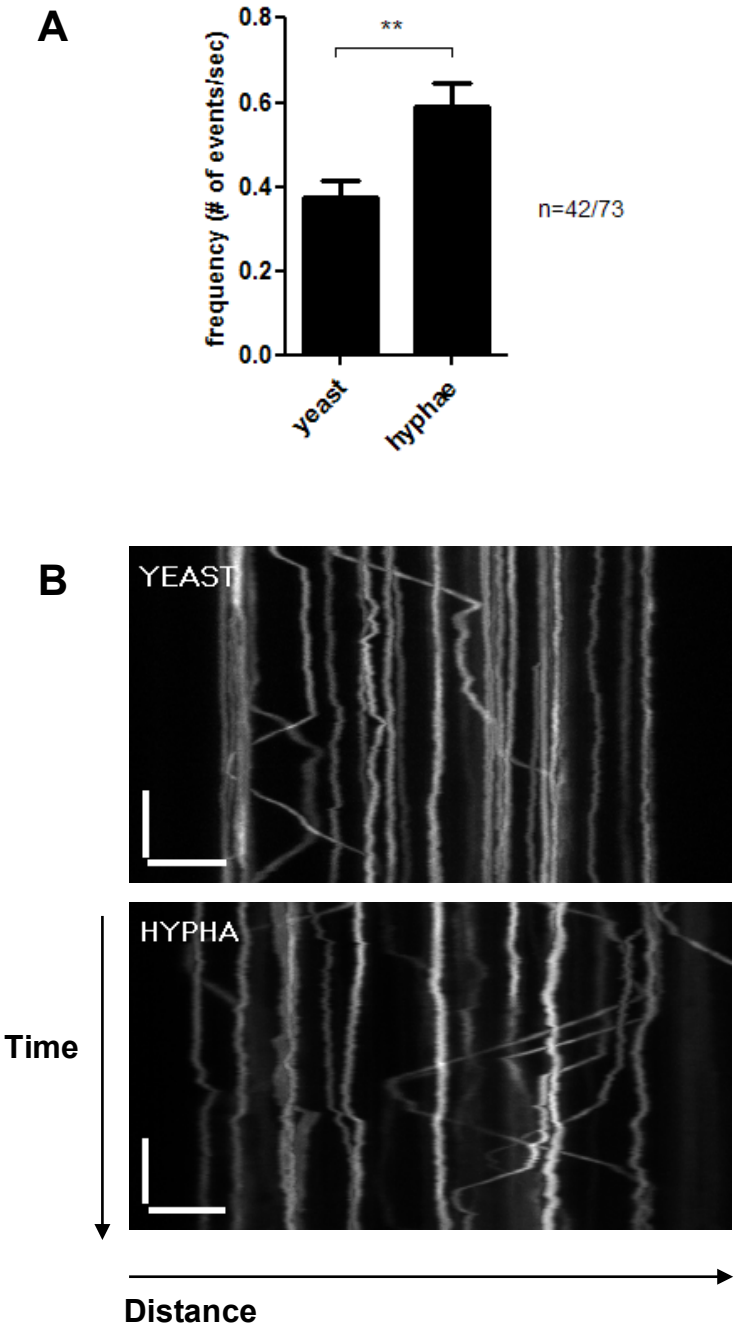


**Figure 3.5 Frequency of peroxisome motility in yeast-like and hyphal cells.**

(A) Peroxisome motility in AB33GSKL cells. Bar chart showing the average frequency of peroxisome motility in yeast-like and hyphal cells. Mean values± standard error of the mean is given, sample size "n" is indicated. Double asterisk indicates statistical difference at P=0.0029. (B) Kymographs showing peroxisome motility in yeast-like and hyphal cells. Scale bars=3µm/4s .

### 3.2.3 Long-range peroxisome motility is an active process

The directed peroxisome motility described above suggested that motility of peroxisomes is an energy-driven process along the fibres of the cytoskeleton. To support this idea, cells were treated with carbonyl cyanide 3-chlorophenyl hydrozone (CCCP). This drug has an inhibitory effect on respiration chain reversibly (Hirose et al., 1974) and was previously used to reduce ATP levels in *U. maydis* (Lehmler et al., 1997; Wedlich-Söldner et al., 2000). When CCCP was applied to FB2GSKL cells, long-range peroxisome motility ceased, whereas the solvent control di-methyl sulfoxide (DMSO) showed no obvious inhibitory effect on long-range motility of peroxisomes (Figure 3.6). This data demonstrate that peroxisome motility is an energy-dependent process.

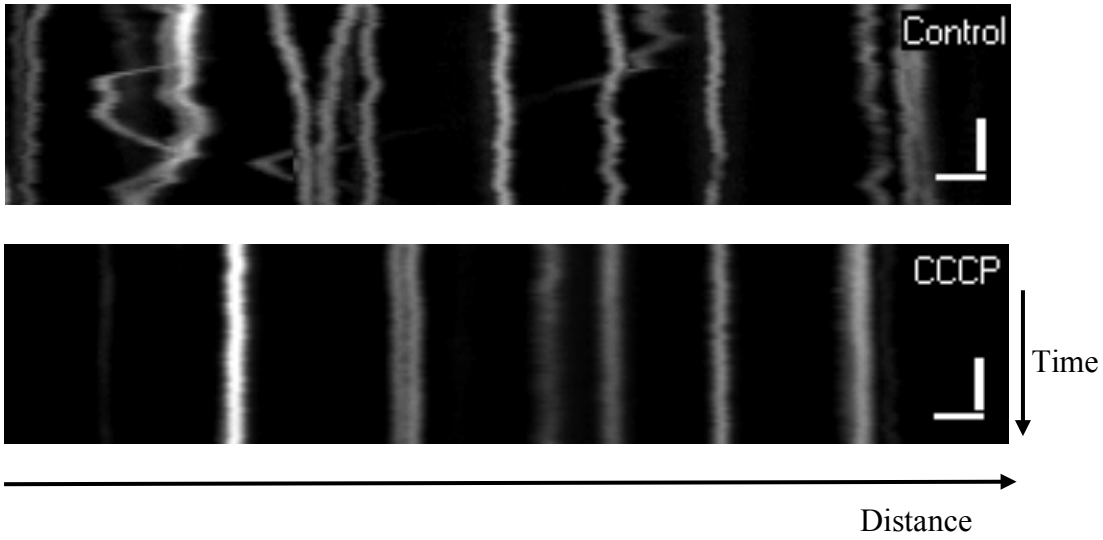


**Figure 3.6 Peroxisome motility in response to CCCP treatment**
FB2GFPSKL cells were cultured in liquid CM-glucose medium and treated with 100μM CCCP for 8 min (See 3.2 Materials and Methods). Kymographs to show peroxisome motility in DMSO-treated (Control) and CCCP-treated (CCCP) cells. In control cells, both long- and short-range peroxisome motility events were observed. In CCCP cells, long-range motility is absent only stationary peroxisomes are observed. Scale bars= 1μm/2 s.

Next, I tested if long-range peroxisome motility occurs along microtubules (MTs) or filamentous actin (F-actin). To this end, cells were treated with two inhibitors of the cytoskeleton: Benomyl, a MT depolymerisation agent (Jung et al., 1992) and Latrunculin A (Lat-A), an actin polymerisation inhibitor (Spector et al., 1989). Both drugs effectively disrupt respective cytoskeletal elements in *Ustilago maydis* (Fuchs et al., 2005). Indeed, treatment of FB2GTGSKL cells with 30µM Benomyl destroyed MTs within 30 min (Figure 3.7). Incubation of AB33LifeactGFP cells with 10µM Lat-A also destroyed actin network within 30 min (Figure 3.8).

After disruption of MT polymerization, long-range peroxisome motility was abolished. In contrast, disruption of F-actin assembly by Lat-A treatment showed no obvious effect on long-range peroxisome motility (Figure 3.9). Quantitative analysis of long-range motility confirmed absence of motility in benomyl-treated cells (Figure 3.10 and Figure 3.11, $P<0.0001$, for yeast-like and hyphal cells, Student t-test). However, the average frequency of long-range peroxisome motility was not affected in Lat-A treated cells (Figure 3.10 and Figure 3.11, $P=0.6679$ for yeast-like cells, $P=0.1645$ for hyphal cells, Student t-test).

Taken together, these results indicate that long-range motility of peroxisomes depends on microtubules, but not on actin.

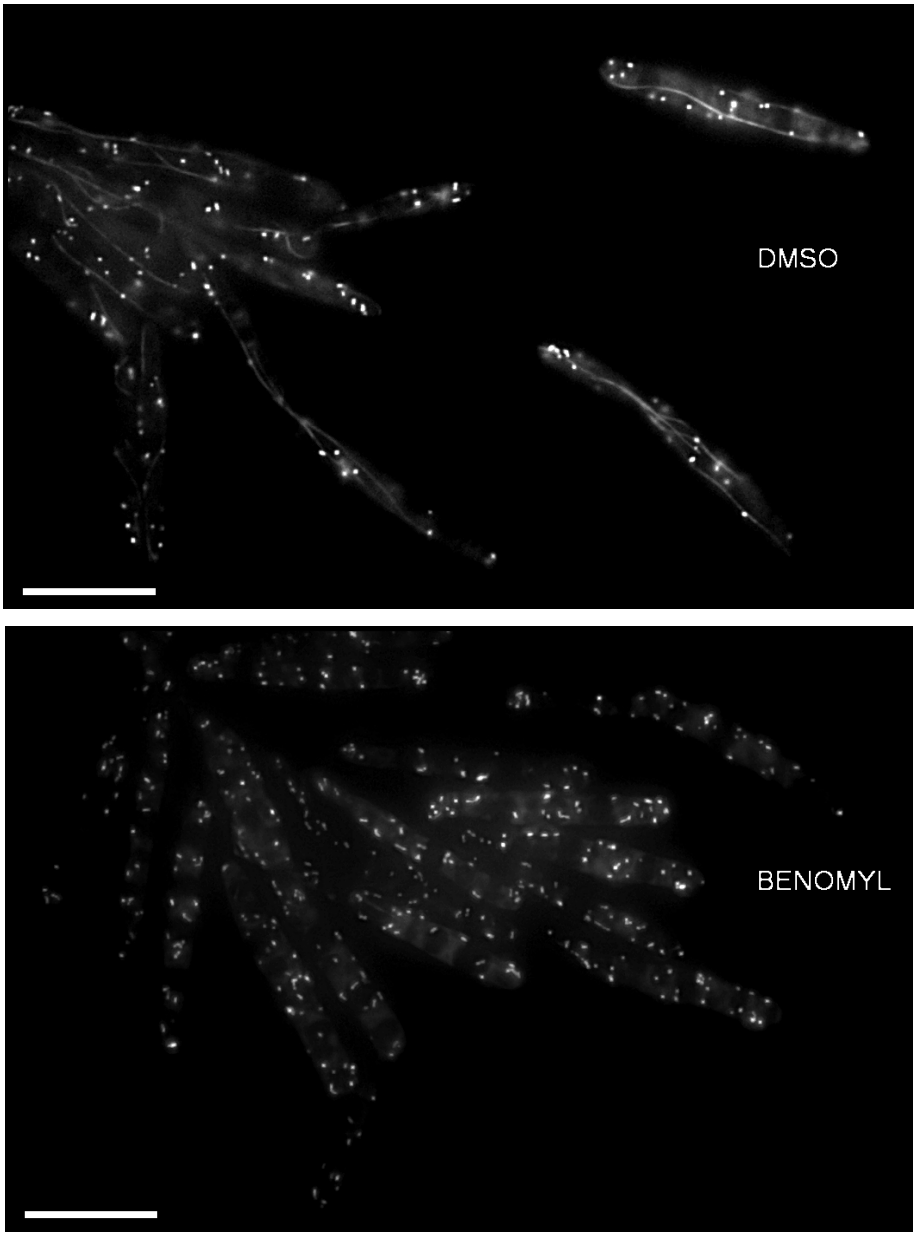


**Figure 3.7 Benomyl treatment distrupts MT assembly**
FB2GTGSKL cells were treated with Benomyl and DMSO as control. After 30 min incubation, MTs disappeared in the presence of Benomyl whereas DMSO treatment showed no effect. Scale bars= 10μm.

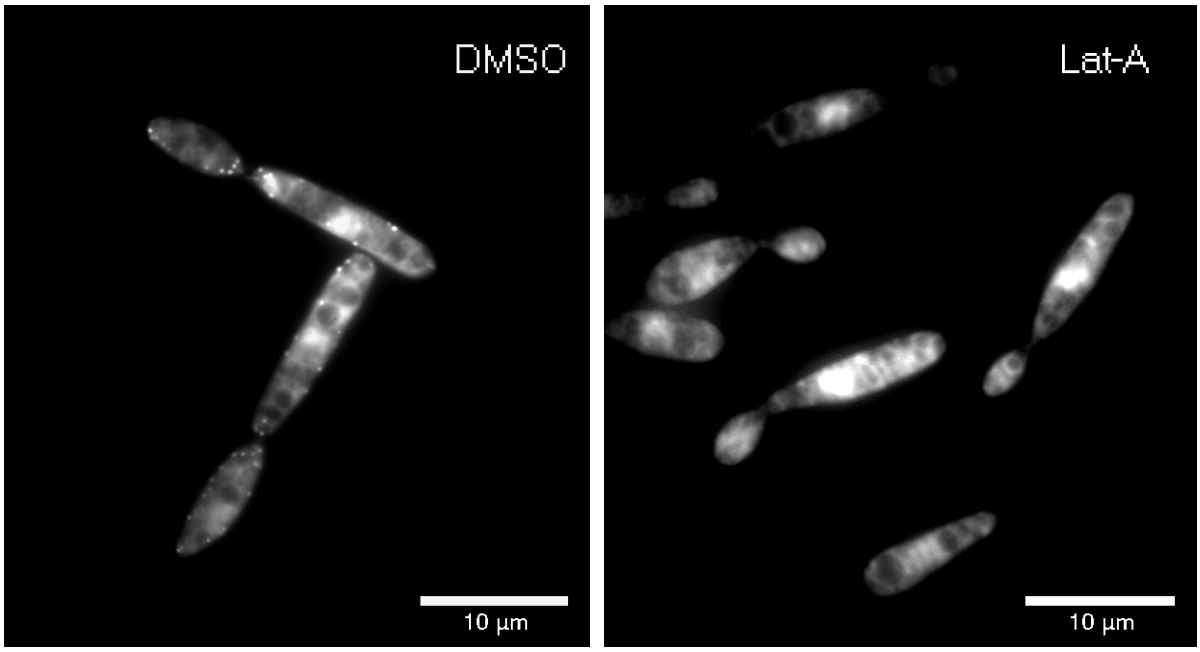


**Figure 3.8 Lat-A treatment distrupts actin structures**
AB33Life-actGFP cells were treated with Lat-A and DMSO. After 30 min incubation, actin patches disappeared in the presence of Lat-A; while DMSO treatment showed no effect. Scale=10µm.

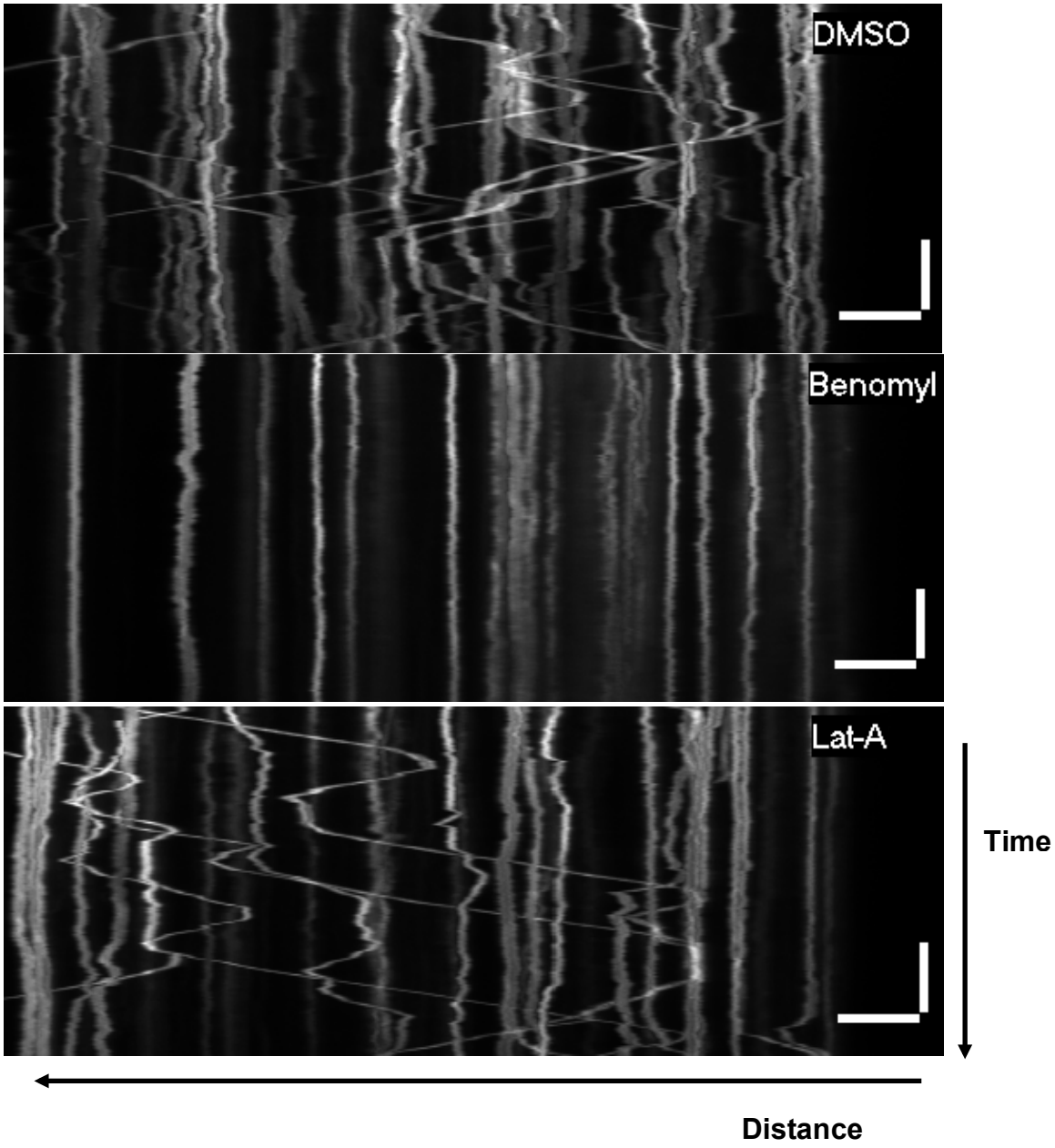


**Figure 3.9 Long-range peroxisome motility is abolished in the presence of Benomyl**

Hyphal cells of AB33GSKL were incubated with DMSO, Benomyl and Lat-A for 30 min. Kymographs show short and long-range peroxisome motility in DMSO- and Lat-A-treated cells, whereas long range motility is abolished in Benomyl-treated cells. Scale bars=3µm/ 6s

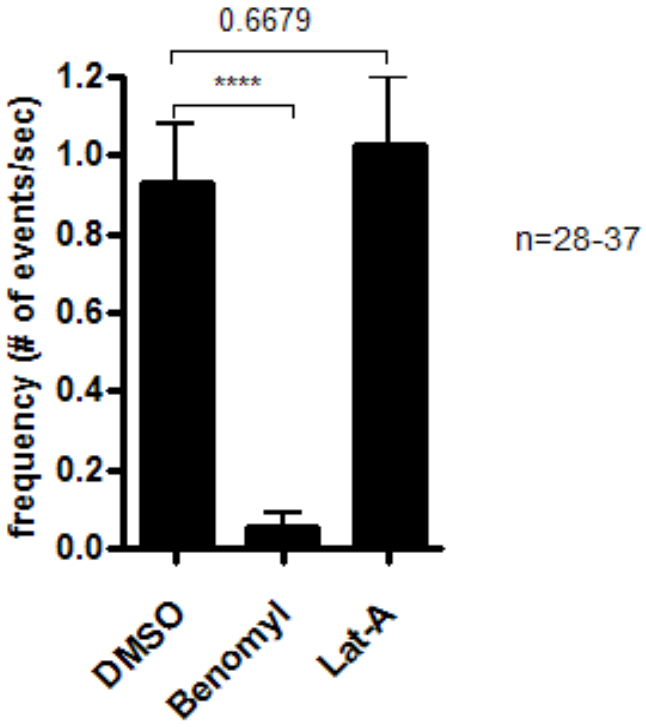


**Figure 3.10 Frequency of peroxisome motility in yeast-like cells in response to drug treatments.**
Bar chart showing frequency of peroxisome motility in DMSO, Benomyl and Lat-A treated yeast-like cells of strain AB33GSKL. Mean values ± standard error of the mean is given. Sample sizes are n(DMSO)=28, n(Benomyl)=36 and n(Lat-A)=37. Quadruple asterisk indicates significant statistical difference between Benomyl- and DMSO-treated cells at P<0.0001, Student t-test. No significant difference found between DMSO and Lat-A treated cells P =0.6679, Student t-test.

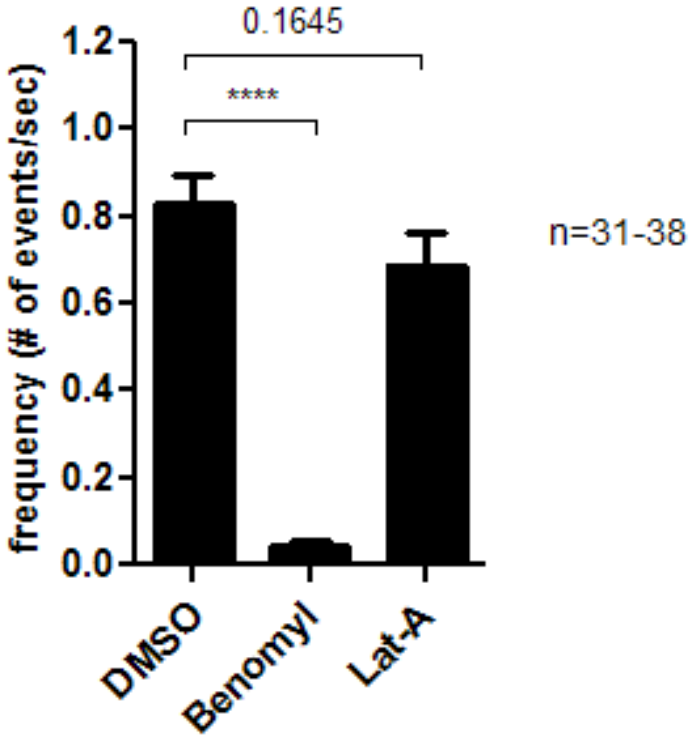


**Figure 3.11 Frequency of peroxisome motility in hyphal cells in response to drug treatments.**

Bar chart showing frequency of peroxisome motility in DMSO, Benomyl and Lat-A-treated hyphal cells of strain AB33GSKL. Mean values ± standard error of the mean is given. Sample sizes are n(DMSO)=31, n(Benomyl)=36 and n(Lat-A)=38. Quadruple asterisk indicates statistical difference between DMSO- and Benomyl-treated cells at $P<0.0001$, Student t-test. No significant difference found between DMSO- and Lat-A-treated cells $P = 0.1645$, Student t-test.

### 3.2.4 Peroxisomes associate with microtubules but not actin

Pharmacological studies in previous section suggest that peroxisome motility is mediated by MTs. To further support these results, I set out to co-visualize peroxisomes and microtubules in yeast-like cells. To this end, I generated strain FB2_GSKL_GT, which co-expressed GFPSKL and GFPαtubulin. Despite both labelled with GFP, peroxisomes and MTs could be distinguished reliably (Figure 3.12). Co-observation of both fusion proteins in yeast-like cells revealed that most peroxisomes co-localizing with MTs (52.9±2.4%, n=755; Figure 3.14). Next I generated strain AB33_GT_ChSKL, which co-expressed mCherrySKL fusion protein and GFPαtubulin. Co-observation of both fusion proteins, revealed that 96.2±1.2% (n=198) of all long-range motility occurs along MTs. This motility was often bi-directional (Fig. 3.12). In contrast, no significant co-localization was observed between peroxisomes and actin structures in yeast-like cells when mCherrySKL-labelled peroxisomes were co-observed with Lifeact-GFP (Figure 3.13). Along with inhibitor studies, these data suggest that peroxisomes associate with and move along MTs in *U. maydis*.

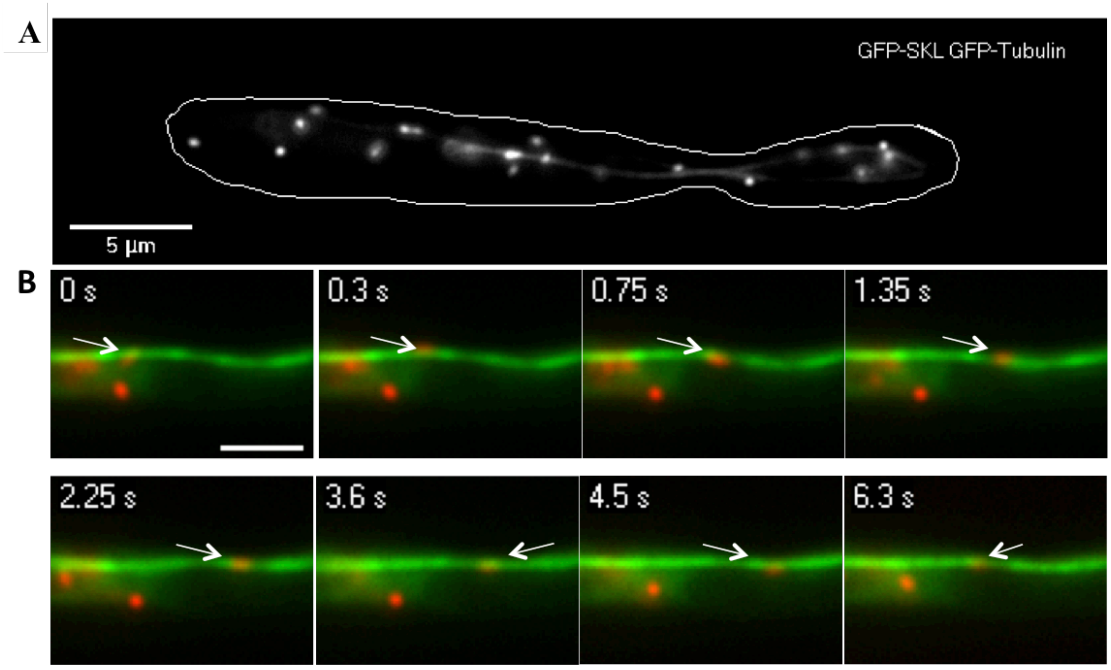


**Figure 3.12 Peroxisomes associate with MTs in *U. maydis*.**
**(A)** In cells of strain FB2GSKLGT, most GFP-SKL labelled peroxisomes localize to MTs (arrowheads) Scale bar=5 µm **(B)** Image series of mCherry-SKL labelled peroxisomes(red) on GFP-α-tubulin labelled MTs (green). Each panel indicates position of the peroxisome at elapsed time given. Moving peroxisome is marked by an white arrow and the direction of the arrow changes with the direction of the movement. Scale bar=2 µm.

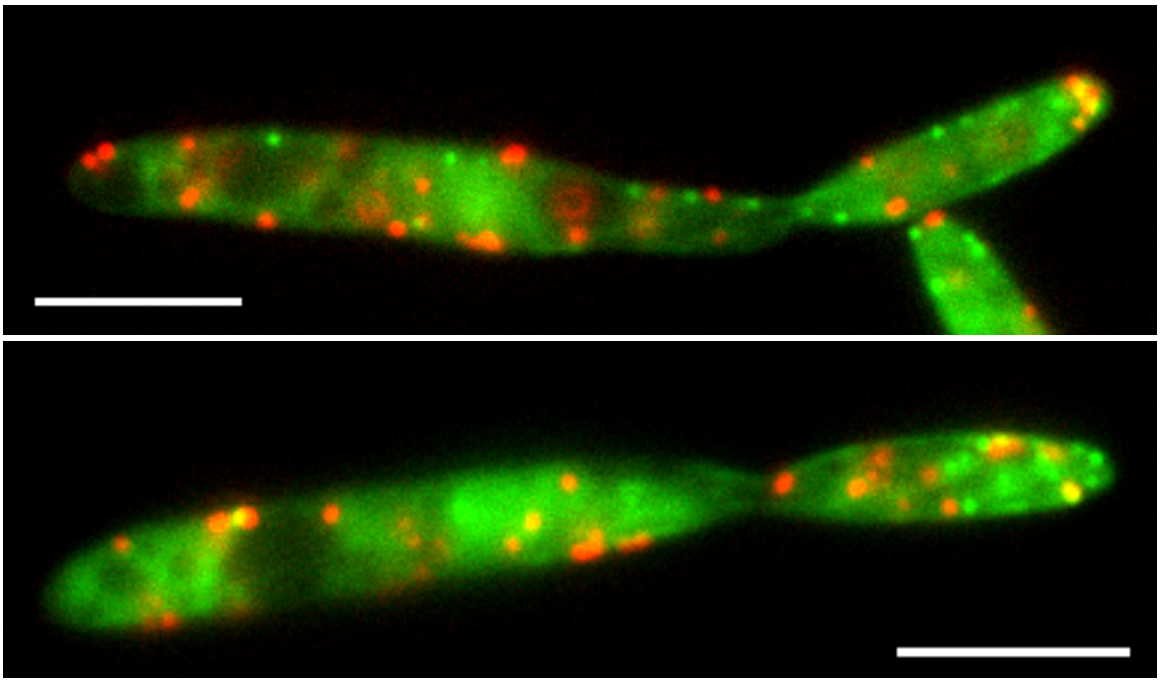

**Figure 3.13 Peroxisome and actin co-localization in *U.maydis*.**
Co-observation of GFP-LifeAct (green) and mCherrySKL-labelled peroxisomes (red) in strain AB33LifeActGFPmChSKL. The overlay images show that there may not be obvious co-localization between actin structures and peroxisomes. Scale bars=5μm.

### 3.2.5 Dynein, Kin1 and Kin3 mediate peroxisome transport

The results provided so far suggested that long-range peroxisome motility is an energy and MT-dependent process. Previous studies have demonstrated that two kinesin motors, Kin1 and Kin3, and cytoplasmic dynein use the tubulin cytoskeleton to support membrane trafficking in *Ustilago maydis* (Lenz et al., 2006; Schuchardt et al., 2005; Schuster et al., 2011b; Schuster et al., 2012). Therefore, these motors were good candidates for being the transport machinery that moves peroxisomes in *Ustilago maydis*.

Firstly, I investigated the potential role of dynein in peroxisome motility. I made use of a temperature-sensitive allele of *dyn2* (Wedlich-Söldner et al., 2002a), which encoded the C-terminal half of the dynein heavy chain (Straube et al., 2001) and generated strain AB5_*Dyn2ts*-GSKL. In cells of the temperature-sensitive mutant strain, peroxisomal motility was normal at permissive temperature (22 °C), but largely abolished when the cells are grown at restrictive temperature (32 °C, Figure 3.14 and 3.15; $P<0.0001$, *Student*'s t-test). This result strongly argues that dynein supports long-range minus-end-directed motility of peroxisomes in *Ustilago maydis*.

I next set out to identify the plus-end directed motor involved in peroxisome motility. In *Ustilago maydis*, plus end membrane trafficking appears to be mediated by only two kinesins; Kin1 and Kin3 (Schuchardt et al., 2005). Therefore I examined GFP-SKL labelled peroxisomes in null mutants of both kinesins (AB33Δ*Kin1G*SKL and AB33Δ*Kin3*GSKL). Surprisingly, in yeast-like cells of both mutants long-range peroxisome motility was almost abolished (Figure 3.17). Frequency of peroxisome movement was significantly reduced ($P<0.0001$; Student t-test; Figure 3.16). The inhibition of peroxisome motility

was also found in hyphal cells of both mutants (Figure 3.17). Thus, both Kin1 and Kin3 are involved in plus-end directed motility of peroxisomes in *Ustilago maydis*. In conclusion, my studies demonstrate that peroxisomes in *Ustilago maydis* undergo long-range motility. Long-range motility happens along the MT cytoskeleton and is mediated by dynein, Kin1 and Kin3.

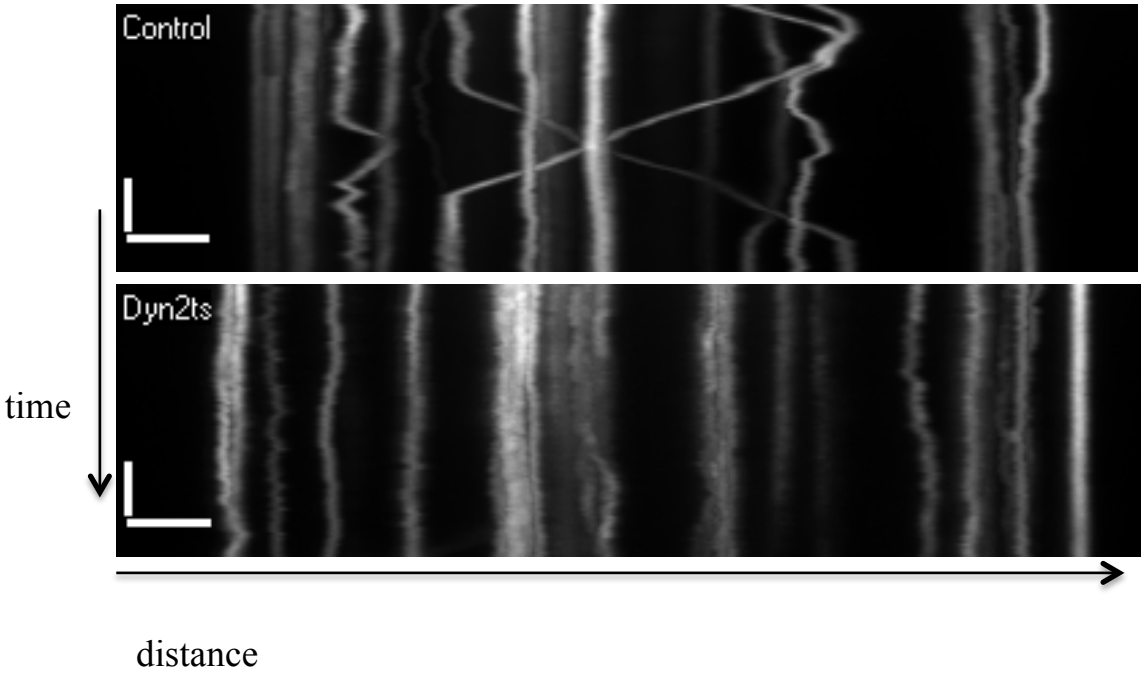


**Figure 3.14 Peroxisome motility in temperature-sensitive dynein mutant of *U. maydis*.**
Yeast-like cells of strain AB5*Dyn2*$^{ts}$GSKL were incubated at permissive (22 °C) and restrictive (32 °C) temperatures for 3 hours. Kymographs of *Dyn2ts* cells at permissive (22 °C) and restrictive temperature (32 °C). Long-range motility is largely abolished, when dynein function is inactivated at restrictive conditions. ° Scale bars=2µm/ 2s.

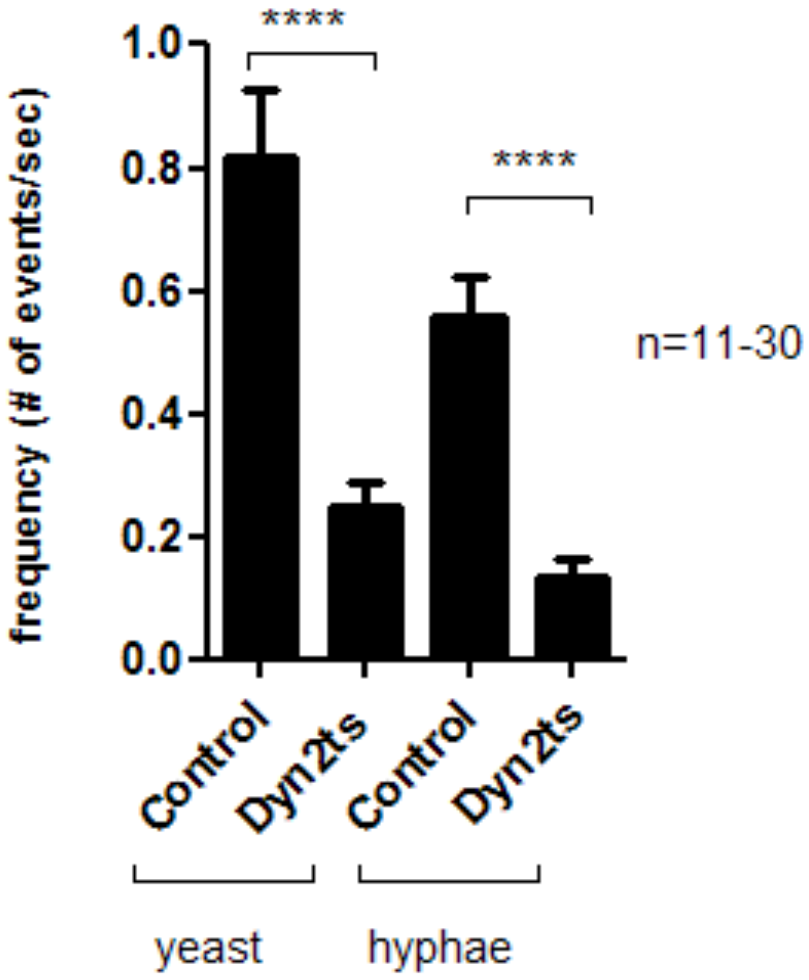


**Figure 3.15 Frequency of peroxisome motility in temperature-sensitive dynein mutant of *U. maydis*.**

Bar chart showing frequency of long-range peroxisome motility at two different temperature conditions in yeast-like and hyphal cells. Mean values ± standard error of the mean is given; sampled size are n(yeast, 22 °C)= 30, n(yeast, 32 °C)=14, n(hypha, 22 °C)=25 and n(hypha, 32 °C)= 11 Quadruple asterisk indicates statistical difference at $P<0.0001$, Student t-test.

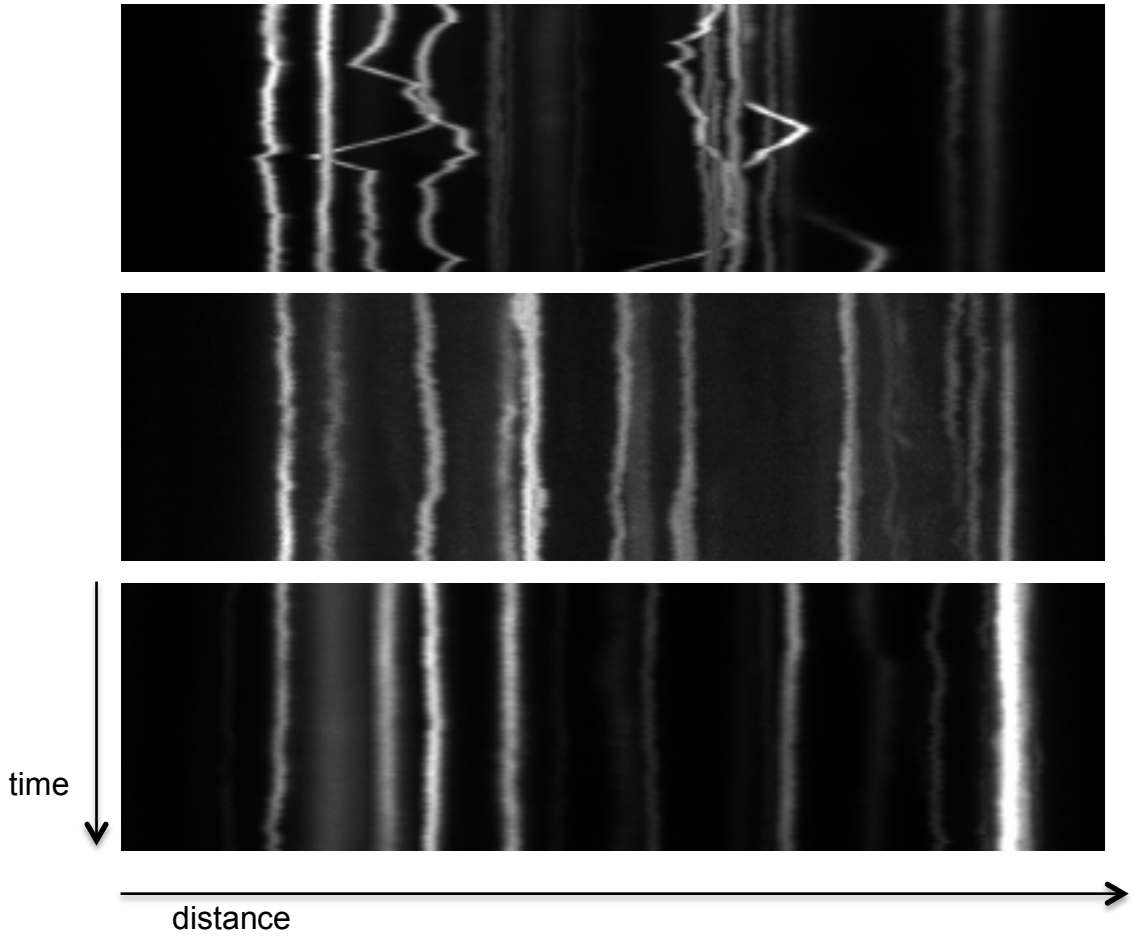


**Figure 3.16 Peroxisome motility in null mutants of *Kin1* and *Kin3***

Kymographs showing the dynamic behaviour of GFP-SKL labelled peroxisomes in AB33GSKL (Control)(A), AB33*ΔKin1*GSKL (Kin1KO)(B), AB33*ΔKin3*GSKL (Kin3KO)(C). No long-range motility of peroxisomes are observed in mutant strains . Scale bars= 2 μm/2s.

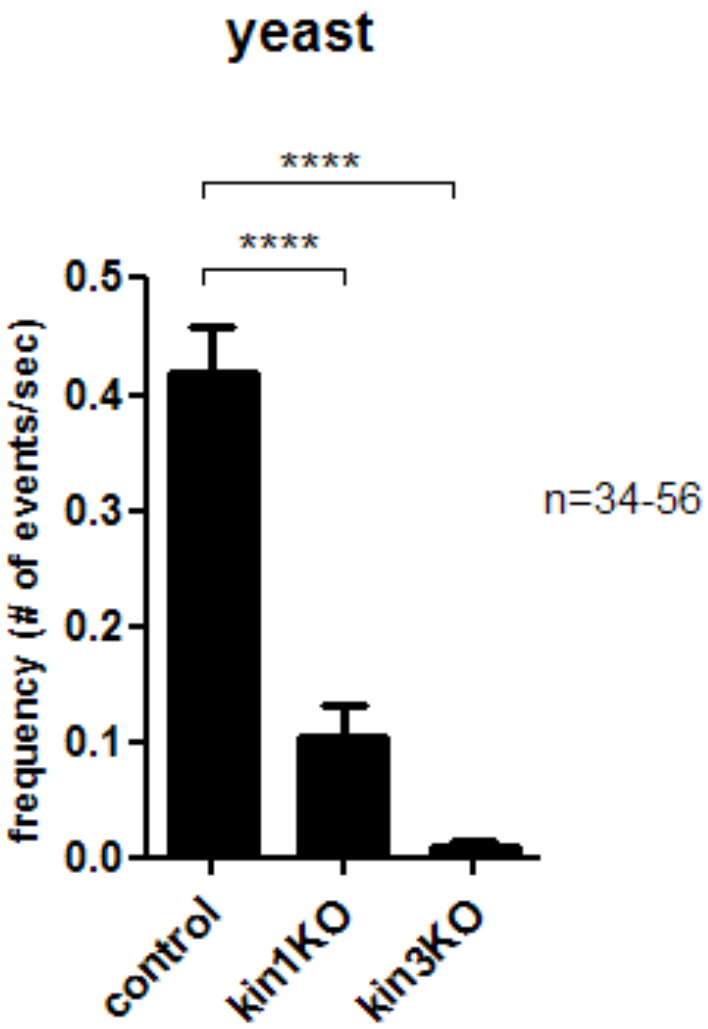


**Figure 3.17 Frequency of peroxisome motility in *Kin1* and *Kin3* knockout yeast-like cells**

Bar chart showing frequency of long-range peroxisome motility in both *ΔKin1* and *ΔKin3* yeast-like cells. Quadruple asterisks indicate significant difference to control cells at P <0.0001 Student t-test. Mean values ± standard error of the mean is given; sampled sizes are n(control)= 56, n(Kin1KO)= 34 and n(kin3KO)= 39.

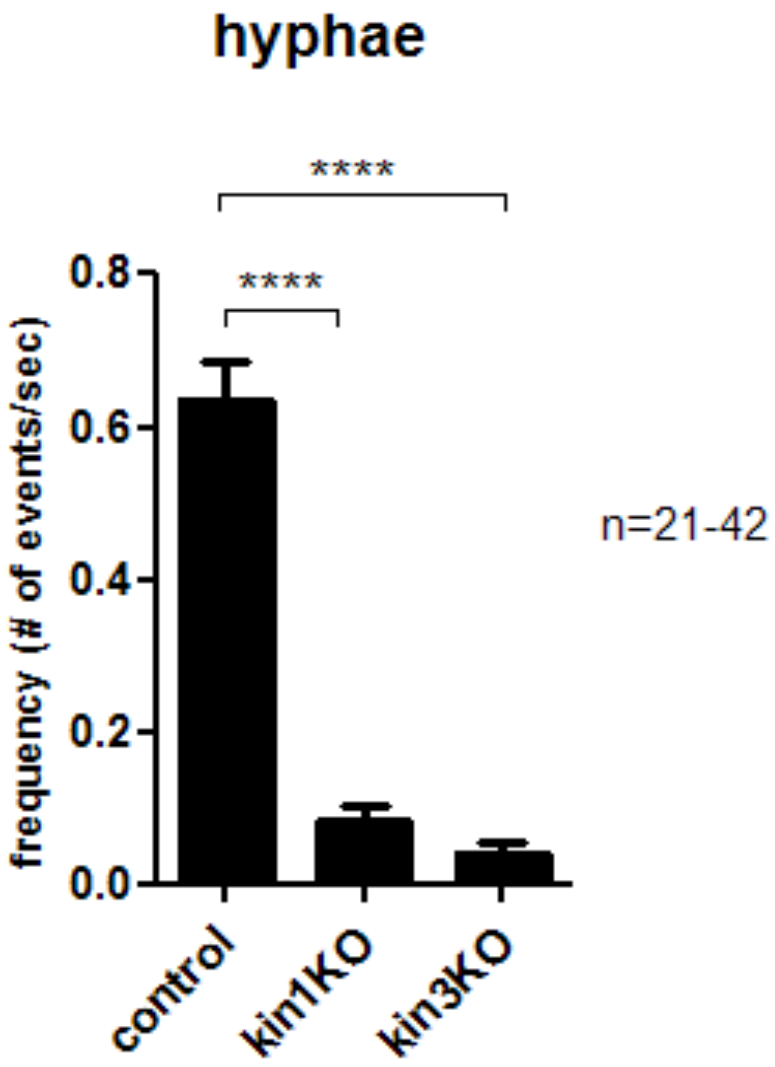


**Figure 3.18 Frequency of peroxisome motility in *Kin1* and *Kin3* knockout hyphal cells**

Bar chart showing frequency of long-range peroxisome motility in both *ΔKin1* and *ΔKin3* hyphal cells. Quadruple asterisks indicate significant difference to control cells at P <0.0001 Student t-test. Mean values ± standard error of the mean is given; sampled size are n(control)= 42, n(Kin1KO)= 33 and n(Kin3KO)= 21.

### 3.3 Discussion

Peroxisome motility was investigated to explore characteristics and underlying mechanism of peroxisome movements. GFP-SKL signals were imported into rounded “spot-like” structures dispersed within the cytoplasm of *Ustilago maydis* cells (Steinberg and Schuster, 2011)(this chapter). This appearance is consistence with peroxisome morphology described in other organisms (Chang et al., 2007; Fagarasanu et al., 2006; Kim et al., 2006). Peroxisomes proliferate when fatty acid intake increased in the cell (Jourdain et al., 2008). To test localization of GFP-SKL, cells were grown in oleic acid-containing media and the number of GFP-SKL spots was increased. This result confirmed that GFP-SKL signals are located at peroxisomes.

Image streams of GFPSKL signals showed that peroxisomes are motile organelles. Evaluation of GFP-SKL signals suggested that there are basically two different types of movements observed: i) short-range and ii) long-range directed movement, as exemplified in kymographs obtained from stacks. In short-range motility, some peroxisomes displace in very short distances (<0.5 µm) and some are almost stationary. In long-range movements, linear displacements (>0.5 µm) take place, organelles move in anterograde and retrograde directions. This behaviour was previously reported in yeast, plant and mammalian cells and categorized into three types; i) no movement/arrest ii) short-range/ brownian/oscillation and iii) long-range/saltations (Huber et al., 1999; Rapp et al., 1996; Schrader et al., 2000). I also recognized non-mobile peroxisomes. However, in this study, first two types of peroxisome motility were merged into one category, as short-range motility, for the sake of simplicity.

I next focused on long-range peroxisomal motility events. As peroxisome dynamics and functions may vary according to cell types (Kunze et al., 2006; Reumann and Weber, 2006; van der Klei et al., 2006), both yeast-like and hyphal cells of *Ustilago maydis* were investigated to calculate velocity, run length and frequency of peroxisome motility. Average velocity of long-range peroxisome motility was not statistically different between both cell types. This result suggests that same machinery transports peroxisome in yeast-like and hyphae cells. However the average run length was significantly higher in hyphal cells as compared with yeast cells. Likewise, the frequency of peroxisome motility was also significantly higher in hyphal cells than yeast-like cells. This difference reflects that peroxisome movements may vary in different cell types (Jedd and Chua, 2002).

CCCP treatment has been used to test active events by depleting ATP levels in the cell reversibly in *Ustilago maydis* studies (Becht et al., 2006; Fuchs and Westermann, 2005; Lehmler et al., 1997; Schuster et al., 2011b). As a result of CCCP treatment, long-range peroxisome movements were abolished. This suggested that long-range peroxisome movements are ATP dependent processes. Drug treatments to destroy microtubules (MTs) and actin filaments formation by using Benomyl and Lantrucullin A, respectively, showed that peroxisomes are transported along MTs but not along actin cables. This confirmed that MTs provide tracks for membrane trafficking including transport of early endosomes and nuclear pores in *Ustilago maydis* (Steinberg et al., 2012; Wedlich-Söldner et al., 2002b). Furthermore, I supported this data by visualizing GFP-tubulin GFP-SKL expressing cells. I found that approximately half of the peroxisomes are located on MTs. Among the ones that are on MTs,

both short and long range of peroxisome motility can be observed. The ones that are not on microtubules were only oscillating in short range. Colocalization studies explicitly showed that peroxisomes are moving along the MTs. However there was not a distinctive colocalization between actin cables or patches and peroxisomes observed apart from a few nonspecific overlaps. For visualization of actin, I used a small peptide, LifeAct, which can bind both actin patches and filaments (Berepiki et al., 2010). However, I failed to visualize actin filaments properly. It might be due to difficulty of dual view settings. On the other hand, assays with MTs led more convincing results. So, MTs are the main tracks for peroxisome transport in *Ustilago maydis*. Taken together, these data are consistent with studies on fungi and animal cells where peroxisomes are transported along MTs (Egan et al., 2012b; Kural et al., 2005; Schrader, 2001; Wiemer et al., 1997).

In order to find out the molecular motors operating long-range peroxisome movements, GFP-SKL was visualized in temperature-sensitive mutant of dynein2 (*Dyn2*$^{ts}$) and deletion mutants of Kin1 (Δ*kin1*) and Kin3 (Δ*kin3*). Dynein is the minus end motor and it was previously reported that it has roles in the transport of endoplasmic reticulum, nucleus, nuclear pores and early endosomes in *Ustilago maydis* (Lenz et al., 2006; Steinberg et al., 2012; Straube et al., 2001; Wedlich-Söldner et al., 2002a). Since it is an essential protein in *Ustilago maydis*, temperature sensive mutant of Dynein (*dyn2ts)* was used to study its role in peroxisome motility. Quantitative analysis showed that peroxisome motility is significantly reduced in *dyn2ts* at restrictive temperatures. Therefore, in addition to the organelles previously reported; it is shown here that dynein is also responsible for the peroxisome transport in

*Ustilago maydis*. In *A. nidulans*, *D. melanogaster* and mammalian cells, dynein plays a role in peroxisome transport as well (Egan et al., 2012b; Kural et al., 2005; Schrader et al., 2000). Kin1 is a plus end motor, which has roles in transport of nuclear pores, transport of Dynein to the MT plus ends, secretion of chitin synthase and organization of MTs (Lenz et al., 2006; Schuster et al., 2012; Steinberg et al., 2012). Kin3 is another plus end motor, which has roles in transport of early endosomes, secretory vesicles and polysomes in *Ustilago maydis* (Higuchi et al., 2014; Lenz et al., 2006; Schuchardt et al., 2005; Wedlich-Söldner et al., 2002b). Peroxisome motility is investigated in Δ*kin1* and Δ*kin3* cells to find out potential plus end motor for peroxisome transport. Quantitative analysis of kymographs showed that in the absence of either motor proteins frequency of peroxisome motility was significantly reduced, which implies that both plus end motors have a role in peroxisome motility. This result is consistent with the recent findings in *A. nidulans* study where contribution of Dynein, Kin1 and Kin3 to peroxisome motility was reported (Egan et al., 2012b).

In order to find out which motor protein is the main plus end motor, a series of experiments were designed based on Kin1 and Kin3 rigor mutants (Straube et al., 2006). These mutants contain kinesin alleles, which encode motor proteins with mutated ATPase site. They are expressed under inducible promoters which enable conditional expression of the mutated motor in arabinose media. The rigor motor mutants are able to bind to cargo and track but unable to walk due to “rigorous” binding to the track (Bottin et al., 1996; Schuster et al., 2011a; Wedlich-Söldner et al., 2002b). On attempt to analyse peroxisome motility in Kin1 and Kin3 rigor expressed conditions, I failed to get

convincing results since aberrant morphology of peroxisomes were observed in arabinose medium with compared to the control cells. Another option to discriminate between plus end motors was to do co-localization between each one of the motors and peroxisomes. I failed to get dual image of Kin1GFP strain with mCherry-SKL expression properly, since Kin1GFP produced strong cytoplasmic background, which made Kin1GFP molecules undetectable as previously reported (Straube et al., 2006). Co-localization study between Kin3 and peroxisome was studied and discussed in detail in the next Chapter (see Chapter 4). In the previous studies, Kin1 was reported to affect early endosome, mRNP and peroxisome transport indirectly due to its role in Dynein transport to plus ends of microtubules (Baumann et al., 2012; Egan et al., 2012b; Lenz et al., 2006; Schuster et al., 2011a). Therefore, it is most likely that Kin3 is the plus end motor to transport peroxisomes; whereas Kin1 might contribute to peroxisome motility indirectly by transporting dynein to plus ends of microtubules.

## 4. Organelle Hitchhiking on Early Endosomes

### 4.1 Introduction

Molecular motors -kinesin, dynein and myosin- drive transport of various organelles, vesicles and protein complexes. Some molecular motors work as “multitasking proteins” as they are able to carry more than one type of cargo. Linking the motor to its cargo occurs via direct or indirect interactions (Akhmanova and Hammer, 2010; Hammer and Sellers, 2012). Binding of Kin3 motor to $PI_{4,5}P$ lipid domain of the endosome membranes via its PH domain is an example for direct interaction between motor-cargo (Klopfenstein et al., 2002; Klopfenstein and Vale, 2004). In the indirect interaction, there are adaptor proteins or protein complexes that provide link between motor and cargo. A well-known example is the Dynactin complex of the Dynein motor, which is composed of different subunits enabling dynein to bind different type of cargos (Holleran et al., 1998; Kardon and Vale, 2009; Karki and Holzbaur, 1999; McKenney et al., 2014; Schroer, 2004). Another group of proteins, which are assisting the interaction between motors and cargoes, are small rab-GTPases. For example, Rab27 binds to myosin-V and this binding promotes melonosome transport (Araki et al., 2000; Bahadoran et al., 2001; Hume et al., 2001; Strom et al., 2002).

Recent reports suggest that ‘hitchhiking on moving organelles’ is another mean of motor-driven transport. mRNAs are targeted to cortical endoplasmic reticulum (cER) and co-transported with cER by cytoskeleton-based motors in different organisms (Aronov et al., 2007; Trautwein et al., 2004). Co-trafficking of early endosomes and ribonucleoproteins (mRNPs) were observed in *Ustilago maydis.* mRNPs contain mRNAs and RNA bining protein

Rrm4. It is proposed that Rrm4 binds to early endosomes and they are co-transported by dynein and Kinesin3 (Baumann et al., 2012). Similarly, ribosomes associate to moving early endosomes through Rrm4. This association contributes to spatio-temporal organization of translation machinery in the cell (Higuchi et al., 2014).

The work in this chapter attempts to investigate associations between motile Early Endosomes (EEs), Peroxisomes (POs) and Endoplasmic Reticulum (ER). All three organelles share the same transport machinery in *Ustilago maydis* (Higuchi et al., 2014; Schuster et al., 2011b; Wedlich-Söldner et al., 2002a; Wedlich-Söldner et al., 2002b)(see Chapter3 for peroxisomes). EEs were visualized by fluorescent tagging of rab5 protein, which is a small GTP binding protein localized on membranes of EEs (Fuchs et al., 2005). ER was observed with the use of HDEL-retrieval signal fused to a reporter that is known as an ER retention signal (Wedlich-Söldner et al., 2002b). Alternatively, Eca-1-GFP was also used as an ER marker (Adamikova et al., 2004). PO visualization and observation were explained in detail in the previous chapter (See Chapter 3). Although early endosome and endoplasmic reticulum transport machinery were reported before in *Ustilago maydis* ((Higuchi et al., 2014; Schuster et al., 2011b; Schuster et al., 2011c; Wedlich-Söldner et al., 2002a; Wedlich-Söldner et al., 2002b), motility parameters and machinery of all three organelles were investigated in detail in this chapter. My aim was to be able to analyse all three organelles under the same experimental conditions.

Firstly, I observed and compared motility behaviours of three organelles by using quantitative and statistical methods. Next, I verified involvement of Kin3

in the transport of the organelles by analysing *ΔKin3* mutant strains. In addition to mutant studies, co-localization analysis between the motor and cargoes were done. I, then, carried out co-localization studies between EEs and the other two organelles to find out if there is any association between them. In addition to the co-localization data, I investigated and presented genetic evidence for the role of EEs in the motility of these organelles in conditions where EE motility was abolished.

## 4.2 Results

### 4.2.1 Subcellular Localization and motility of Early Endosomes(EEs), Peroxisomes(POs) and Endoplasmic Reticulum(ER)

I set out to demonstrate subcellular localization and respective motility behaviours of EEs, ER and POs in *Ustilago maydis* yeast-like cells.

In GFP-Rab5a expressing cells, EEs were observed as dot-like vesicles, which seem as decorating microtubules (Figure 4.1). Tracking moving endosomes indicated that EEs move rapidly in bidirectional manner, i.e. switching from anterograde to retrograde motility and *vice versa* (Figure 4.4)(Wedlich-Söldner et al., 2002b).

POs were observed as spherical organelles, which are scattered within the cell. Tracking PO signals showed that a few POs move over long distances and most POs move slowly within short distances in *Ustilago maydis* cells (Figure 4.2)(See Chapter 3).

ER, marked by GFP-HDEL has a cortical network consisting of interconnected tubules and ER network is evenly distributed in the mother and bud cell cortex (Figure 4.3) (Wedlich-Söldner et al., 2002a). Tracks from video sequence showed that ER tubules are extending out of network and connected to another part of the network by a rapid directional movement (Figure 4.5).

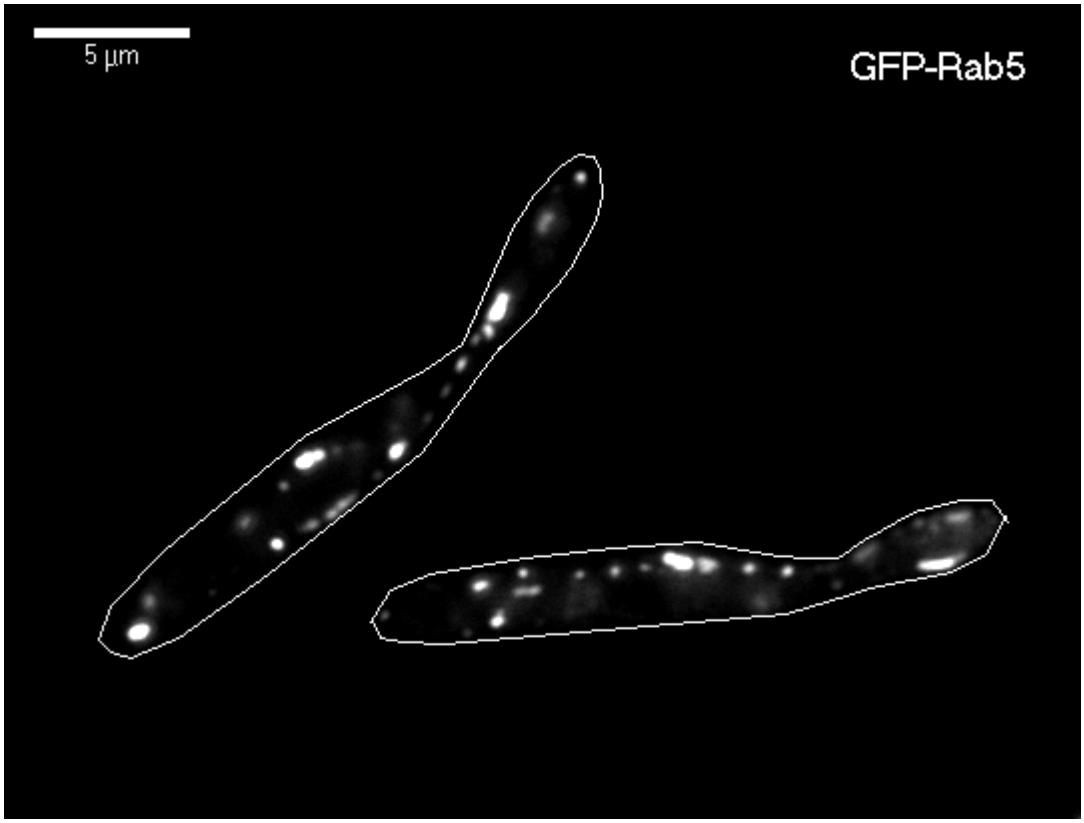


**Figure 4.1 Early endosomes (EEs) in *U. maydis* yeast-like cells.**
AB33GRab5a strain was examined to analyse organization of EEs in yeast-like cells. GFPrab5a signals were observed as spherical organelles scattered along cytoplasm within the cell. Scale bar=5µm.

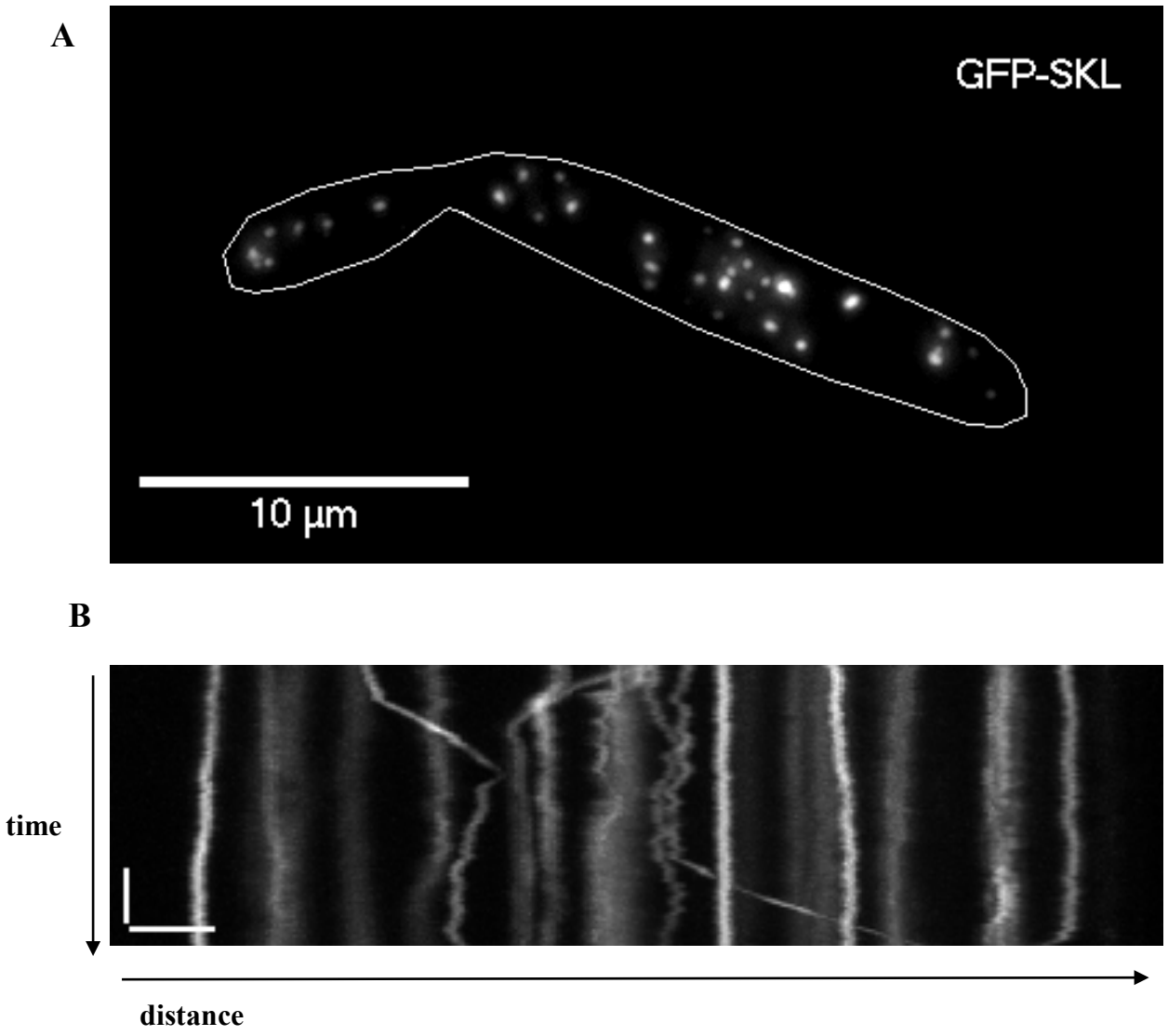


**Figure 4.2 PO spatial organization and movement in *U. maydis* yeast-like cells.**
**A)** AB33GSKL yeast-like cell showing PO localization and distribution. POs are observed as rounded organelles dispersed along cytoplasm of the cell. Scale bar=10 µm**. B**) Kymograph showing short and long range PO movements. Scale bars= 2µm/ 2s

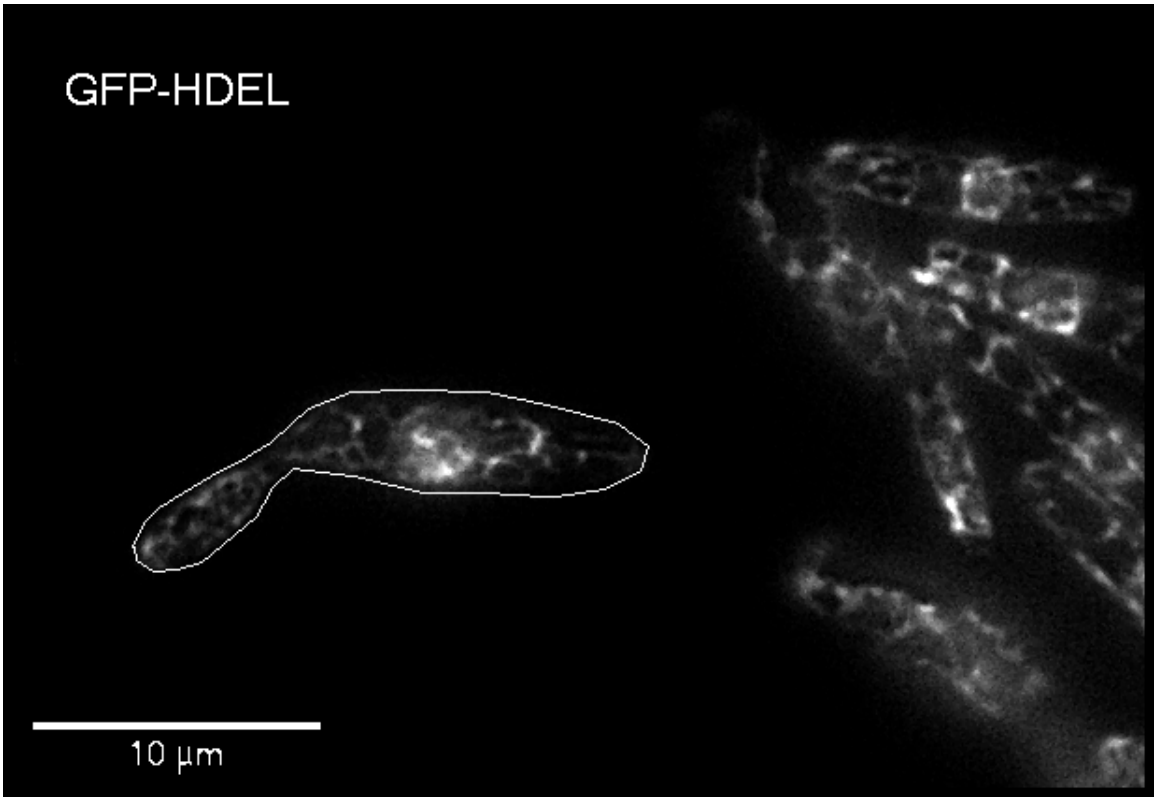


**Figure 4.3 ER cortical network in *U. maydis* yeast-like cells.**
AB33GHDEL cells were examined by epifluorescence microscopy to analyse ER cortical network. ER forms a cortical network composed of interconnected tubules in both mother and bud cells. Scale bar=10µm

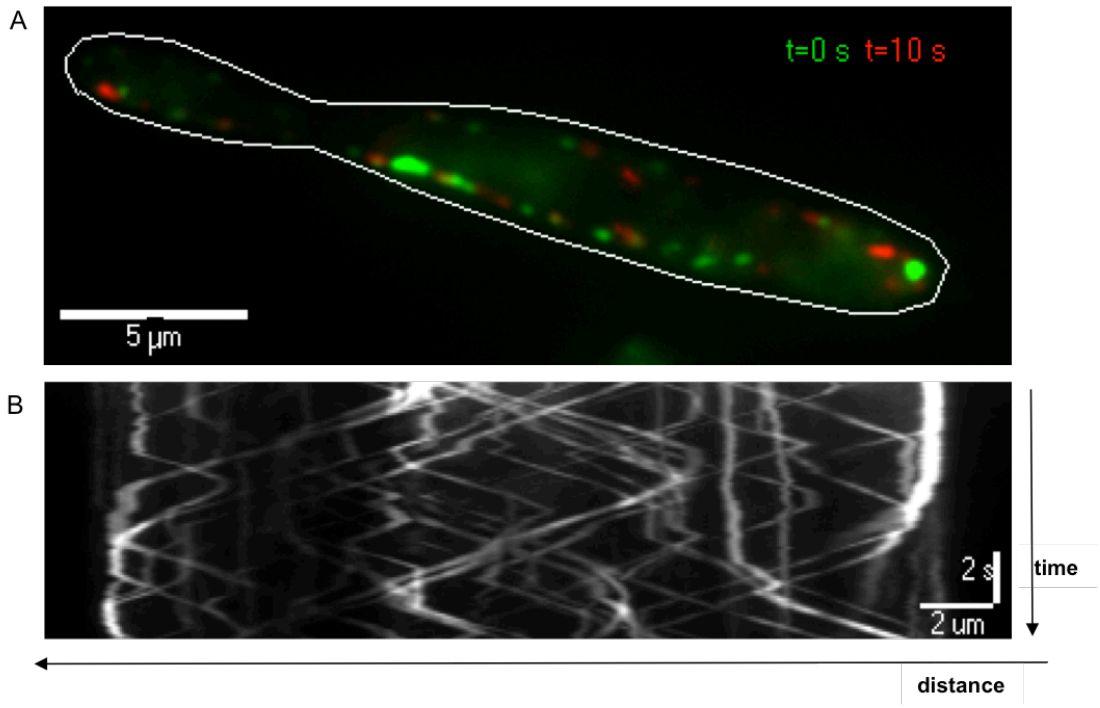


**Figure 4.4 Motility of EEs in *U. maydis* cells.**
(A)Motility of EEs was observed in the strain AB33Grab5a. First plane (t=0, green) and the last plane (t=24s, red) of the image series were merged to show distribution of EEs in 10 second-stream. All EEs rapidly relocate in the cytoplasm within 10s. Scale bar=5 µm. (B) Kymograph showing EE motility of the cell in (A), Rapid bidirectional movement of EEs was observed. Scale bars =2µm/2s.

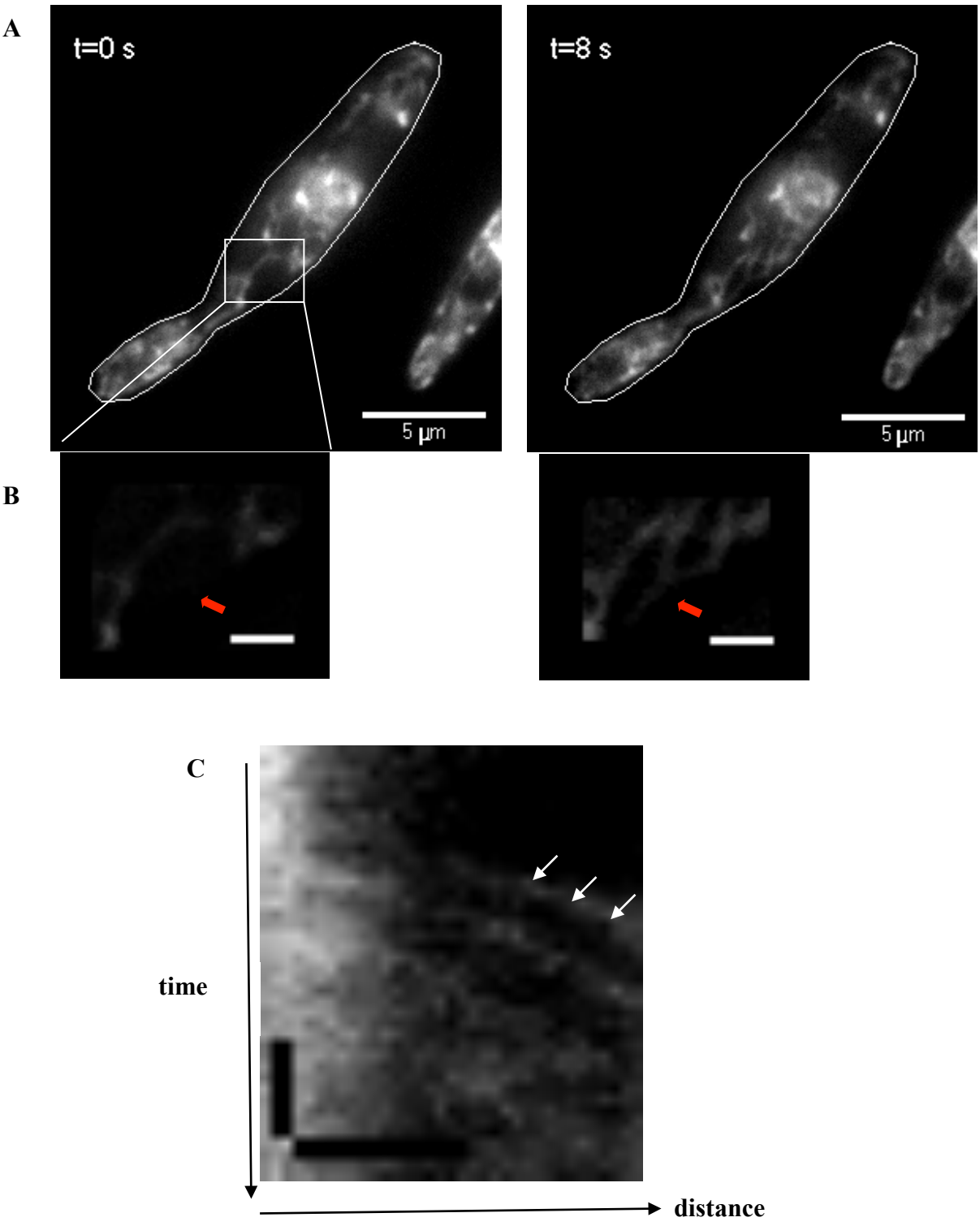


**Figure 4.5 ER tubule movement in *U. maydis* yeast-like cells.**
AB33Eca1G cells were analysed to explore ER tubule motility. GFP signals from two time points show redistribution of ER after 8s(A). Scale bar=5µm. Red arrows (in square insets) indicate ER tubule movement within 8s(B). Scale bar=1µm. Kymograph(C) showing the track of ER tubule movement (white arrows) within 8s. Scale bars= 1µm /1s.

### 4.2.2 Quantitative analysis of EE, PO and ER movements revealed common and distinct features in motility of organelles

In order to compare motility characteristics of three organelles; AB33GE, AB33GRab5a and AB33GSKL strains were examined to analyse motility parameters: (i) velocity, (ii) run length and (iii) frequency of anterograde motility.

Average velocity of ER tubule motility was 2.11±1.12 μm/s (n=35). Average velocity for EE motility was 2.07±0.03 μm/s (n=250) and for PO motility was 2.09±0.10 μm/s (n=36). Mean velocities of three organelles were not statistically different than each other ($P_{ER,PO}$= 0.7358; $P_{PO,EE}$= 0.9219; $P_{EE,ER}$= 0.7293, Student t-test, Figure 4.6). Average run-length of ER tubule motility was 1.96±0.14 μm (n=35). Average displacement for EE motility was 7.70±0.32 μm (n=44) and for PO motility was 2.93±0.34 μm (n=36). Mean run lengths of the three organelles were significantly different than each other ($P_{ER,PO}$=0.0118; $P_{PO,EE}$<0.0001; $P_{EE,ER}$<0.0001, Student t-test, Figure 4.7). Average frequency of ER tubule motility was 0.28±0.04 events/s (n=25). Average frequency for EE motility was 1.47±0.06 (n=32) and for PO motility was 0.33±0.05 (n=30). The average frequencies of ER and PO motilities are not significantly different than each other ($P_{ER,PO}$=0.4536, Student t-test). However the average frequency of EE motility is significantly different than the average frequencies of ER and PO motility ($P_{PO,EE}$<0.0001; $P_{EE,ER}$<0.0001, Student t-test, Figure 4.8).

These data –revealing varying run-length and frequency in transport- show that these organelles display different motility dynamics in the cell. However,

indifference in average velocities indicates that the same molecular motors may be operating the transport of these organelles.

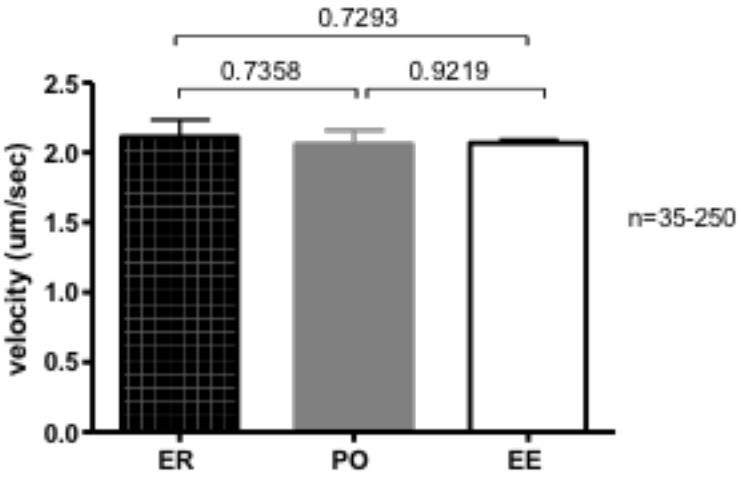


**Figure 4.6 Average velocities of ER, PO and EE movements in yeast-like cells.**
Bar chart showing that average velocities of ER, PO and EE are not significantly different than each other (P values are indicated above bars, Student t test). Mean values ± standard error of the mean is given; sample sizes are n(ER)=35, n(PO)=36 and n(EE)=250.

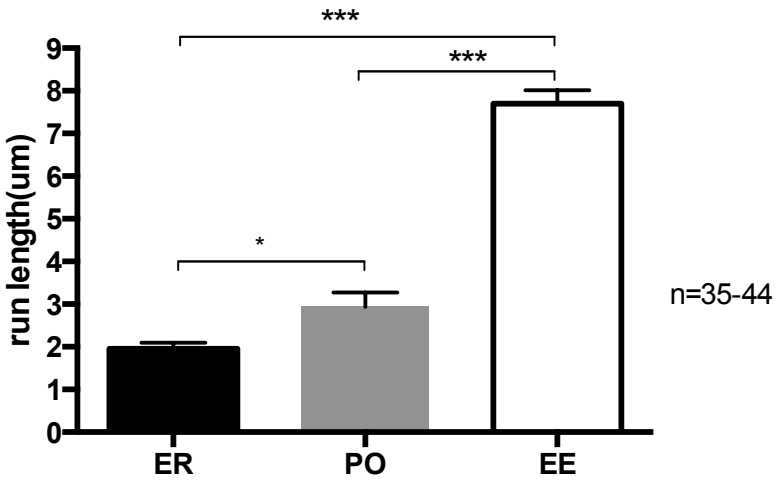


**Figure 4.7 Average run lengths of ER, PO and EE movements in yeast-like cells**

Bar chart showing average run lengths of ER, PO and EE movements. Mean values ± standard error of the mean is given; sample sizes are n(ER)=35, n(PO)=36 and n(EE)=44. Triple asterisk indicates statistical difference at P<0.0001, Student t-test. Single asterisk indicates statistical difference at P< 0.05, Student t-test.

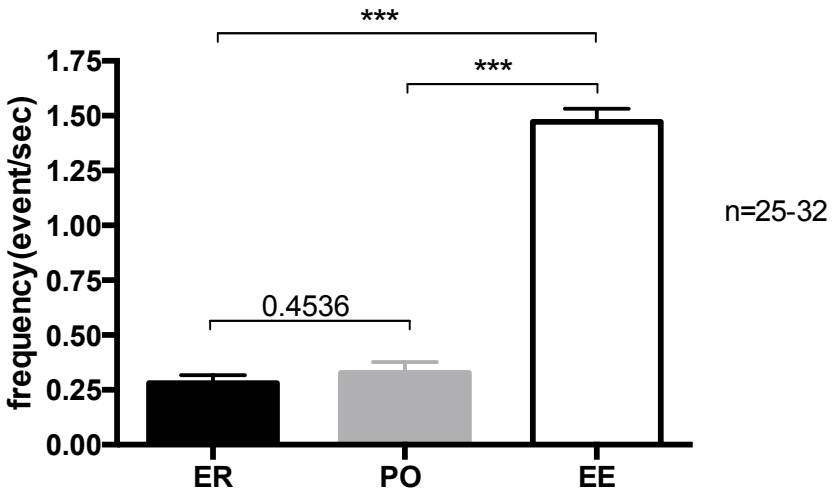


**Figure 4.8 Comparison of average frequencies of ER, PO and EE movements.**

Bar chart showing average frequency of ER, PO and EE motilities. Mean values ± standard error of the mean is given; sample sizes are n(ER)=25, n(PO)=30 and n(EE)=32. Triple asterisk indicates statistical difference at P<0.0001, Student t-test. Average frequencies of ER and PO are not significantly different than each other (P=0.4536, Student t-test).

### 4.2.3. Kinesin3 has role in the motility of EE, PO and ER

#### 4.2.3.1 EE and Kin3

As reported previously, Kin3 is the plus end motor transporting EEs in *Ustilago maydis* (Lenz et al., 2006; Wedlich-Söldner et al., 2002b). In this study, dual imaging was performed to visualize EE and Kin3 simultaneously in yeast-like cells of AB33Kin3GChRab5a strain. Photobleaching was applied to capture a few EE movements to do better alignment by reducing background. Kymographs show that Kin3 and EE are moving together (Figure 4.9). In addition, quantitative analysis confirmed that the frequency of EE motility was significantly reduced in the null mutant of *Kin3* when compared with control cells ($P<0.0001$, Student t-test, Figure 4.9).

#### 4.2.3.2 ER and Kin3

To find out Kin3 contribution to the ER tubule motility, AB33Kin3GChHDEL cells were examined. It is observed that ER tubule was pulled by Kin3, moved together and finally connected to another branch of the ER network (Figure 4.10). 100% co-movement was observed between Kin3 and motile ER tubules (n=29 events). Besides, there was significant reduction in the frequency of ER motility in the absence of Kin3 ($P<0.0001$, Student t-test, Figure 4.10).

#### 4.2.3.3 PO and Kin3

Contribution of Kin3 to PO motility was shown in the previous chapter (See Chapter3). In this section, AB33Kin3GChSKL was used to investigate association between Kin3 and PO. Dual imaging revealed that POs are

transported by Kin3 (Figure 4.11). Kin3 accompanied POs in 63 long-range motility events out of 67 (94±1.4% co-localization).

Altogether, these data verifies that Kin3 is involved in transport of EE, ER and PO in *Ustilago maydis.*

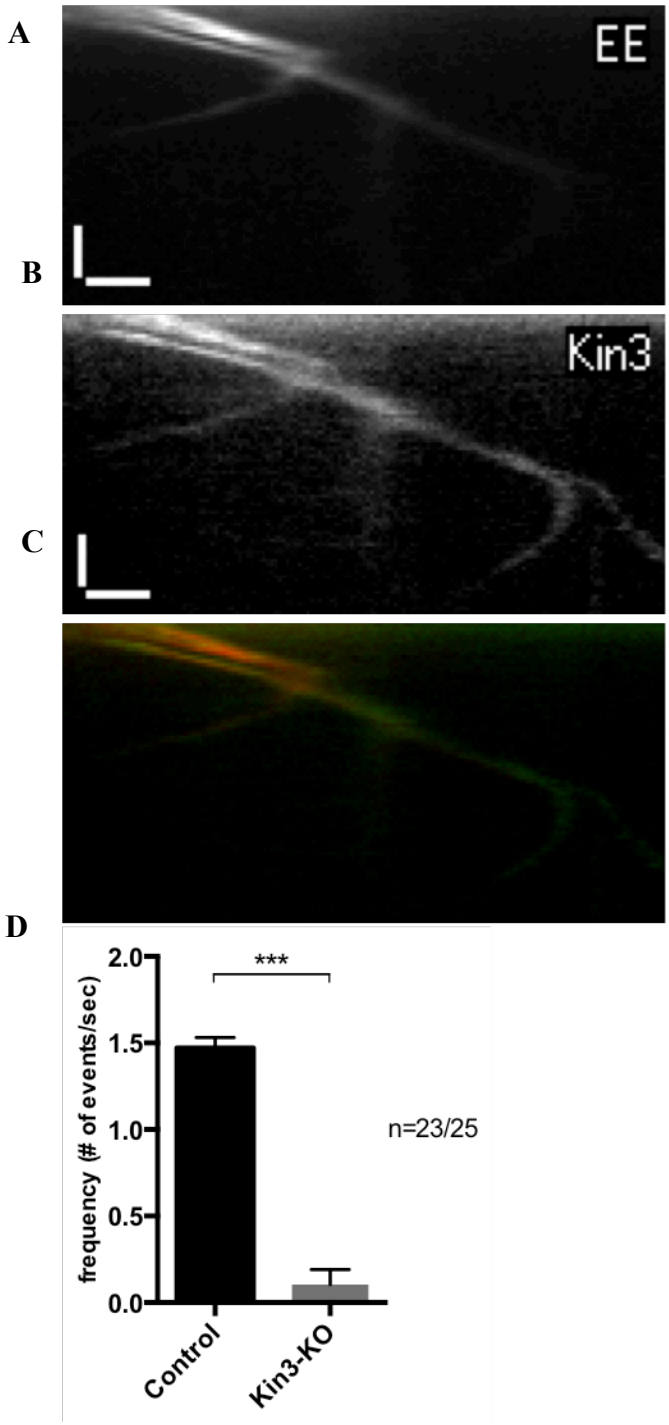


**Figure 4.9 Kin3 transports EEs**

AB33Kin3GmChRab5a strain was examined to observe Kin3 and EE movements simultaneously(C). Kymographs showing EE and Kin3 movement tracks (A and B, respectively). Scale bars= 1µm/2s. Bar chart(D) showing the frequency of EE motility in control and Δ*Kin3* cells. Mean values ± standard error of the mean is given; sample size "n" is indicated. Triple asterisk indicates statistical difference at P<0.0001, Student t-test.

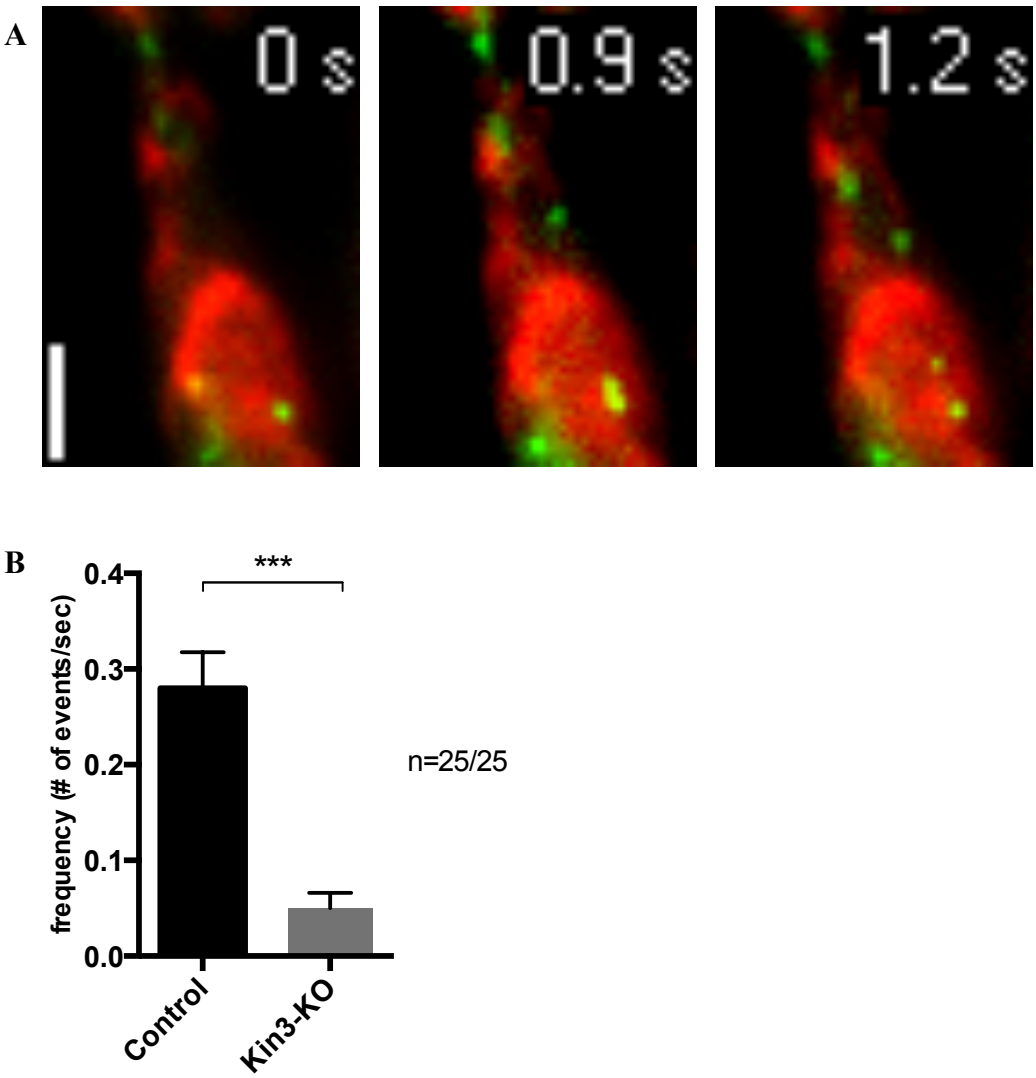


**Figure 4.10 Kin3 transports ER tubules.**
AB33Kin3GChHDEL cell showing Kin3 and ER movements simultaneously. Three image panels of an image stream showing co-movement of Kin3 (green) and ER (red) as the ER tubule extends(A). Time references are given on each image. Scale bar=1 µm. Bar chart(B) showing frequency of ER motility in control and *ΔKin3* cells. Mean values ± standard error of the mean is given; sample size "n" is indicated. Triple asterisk indicates statistical difference at P<0.0001, Student t-test.

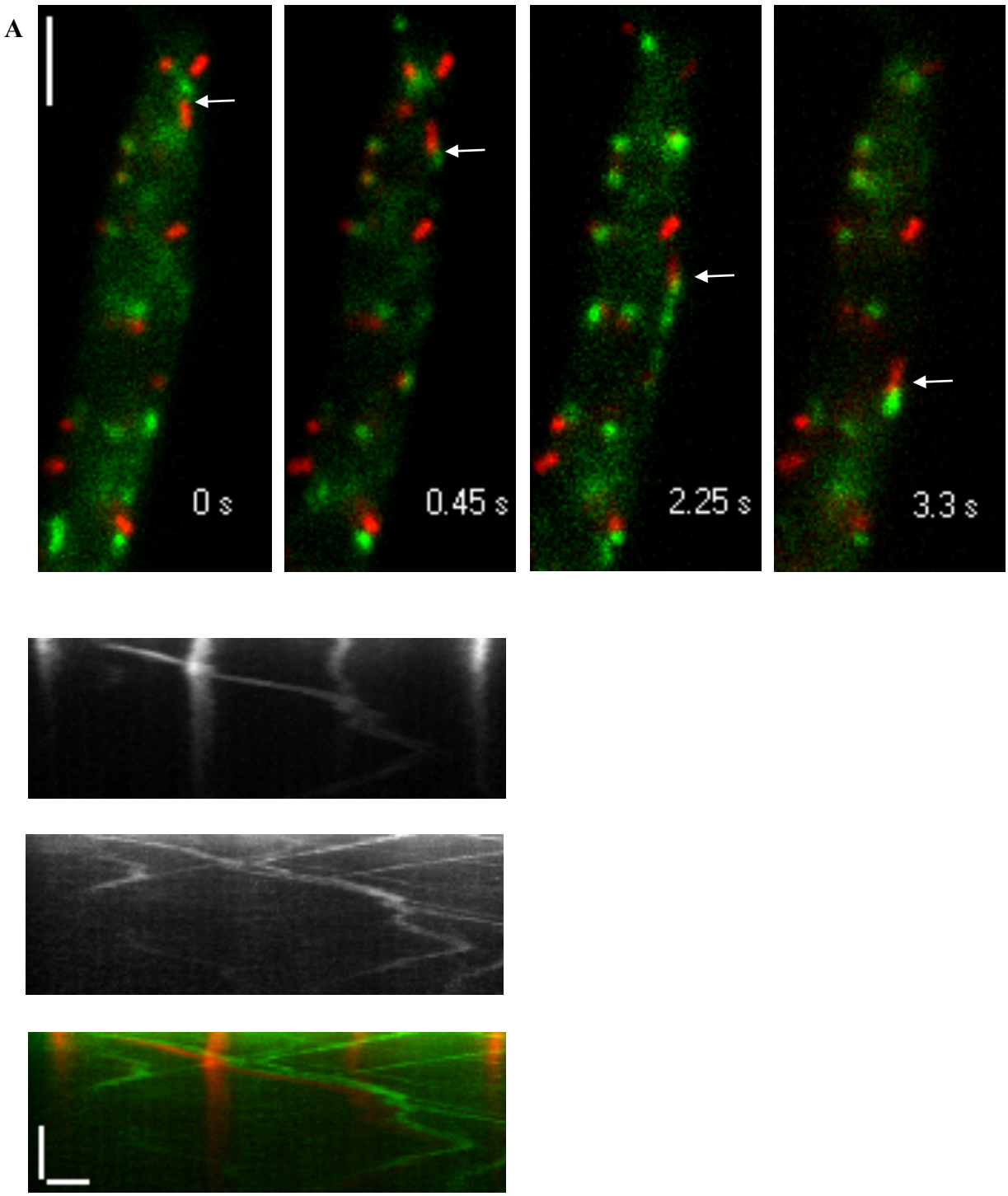


**Figure 4.11 Kin3 mediates PO transport.**
AB33Kin3GChSKL strain showing Kin3 and PO movement simultaneously. Image panels showing co-movement of PO (red) and Kin3(green) (A, white arrows). Note that Kin3 is behind of PO that stands still at t=0 s, Kin3 moves in front and pulls PO at t=0.45 s and both keeps moving together (t=2.25 and t=3.3 s). Scale bar=2µm. Kymograph showing PO and Kin3 co-movement(B1-B3, respectively). Scale bars =1µm/3s.

### 4.2.4 Involvement of EEs in the motility of POs and ER tubules

#### 4.2.4.1 Co-trafficking of EEs with POs and ER tubules

It was previously reported that Kin3 motors co-localizing to EEs at high rates (Schuster et al., 2011b; Wedlich-Söldner et al., 2002b). For that reason, it was tempting to check potential presence of EE during POs and ER tubules transport. To begin with, co-localization studies between EEs and POs and ER tubules were done.

Co-aligned images show that EEs and POs move together in AB33GSKLChRab5a cells (Figure 4.12 and Figure 4.13). Quantitative analysis also showed that among 54 PO motility events, 51 events (94±1.2%) were accompanied with EEs.

Dual imaging in AB33Eca1GChrab5 strain revealed that motile ER tubules are associated with moving EEs (Figure 4.14). ER tubules are travelling with EEs in 53 events out of 56 events (95±1.1%).

These data suggest that EEs are involved in the transport of POs and ER tubules.

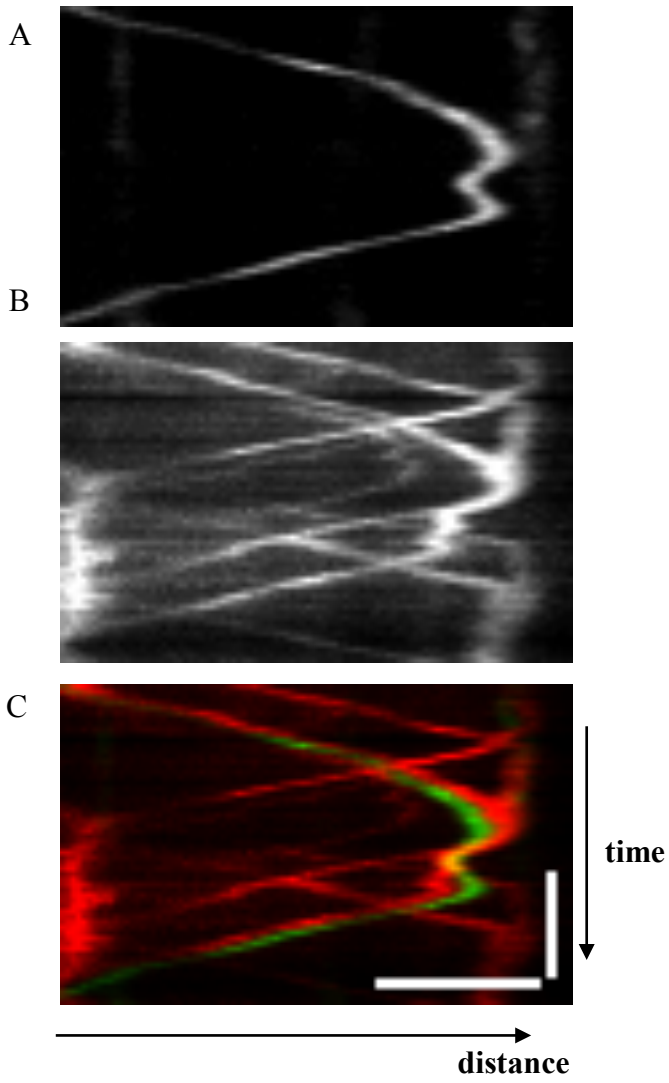


**Figure 4.12 Co-movement of EE and PO**

AB33ChRab5aGSKL cell to indicate movement of PO and EE simultaneously. Kymograph showing co-movement of PO (green, A) and EE (red, B). Merged kymograph(C) showed that EE track is in front of PO track during movement and when the direction changes EE keeps its position in the front (white arrows). Scale bars= 2μm/ 3s.

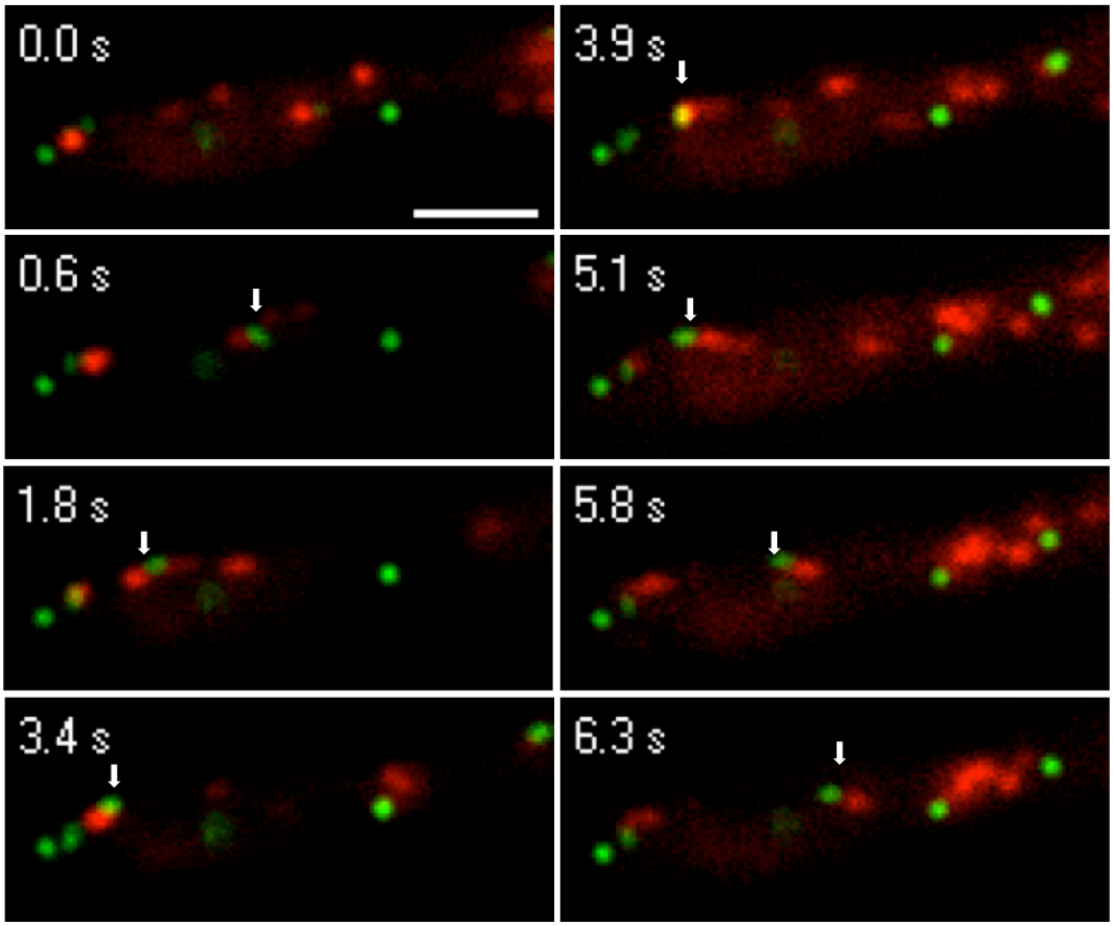


**Figure 4.13 Co-movement of EE and PO**
AB33ChRab5aGSKL strain showing movements of PO and EE simultaneously. Image sections indicate co-movement of PO and EE. Note that EE (red) is in front of PO (green) during transport and keeps the position when the direction of the movement changed after 3.9 seconds (white arrows). Time references are given on each image. Scale bar= 2µm.

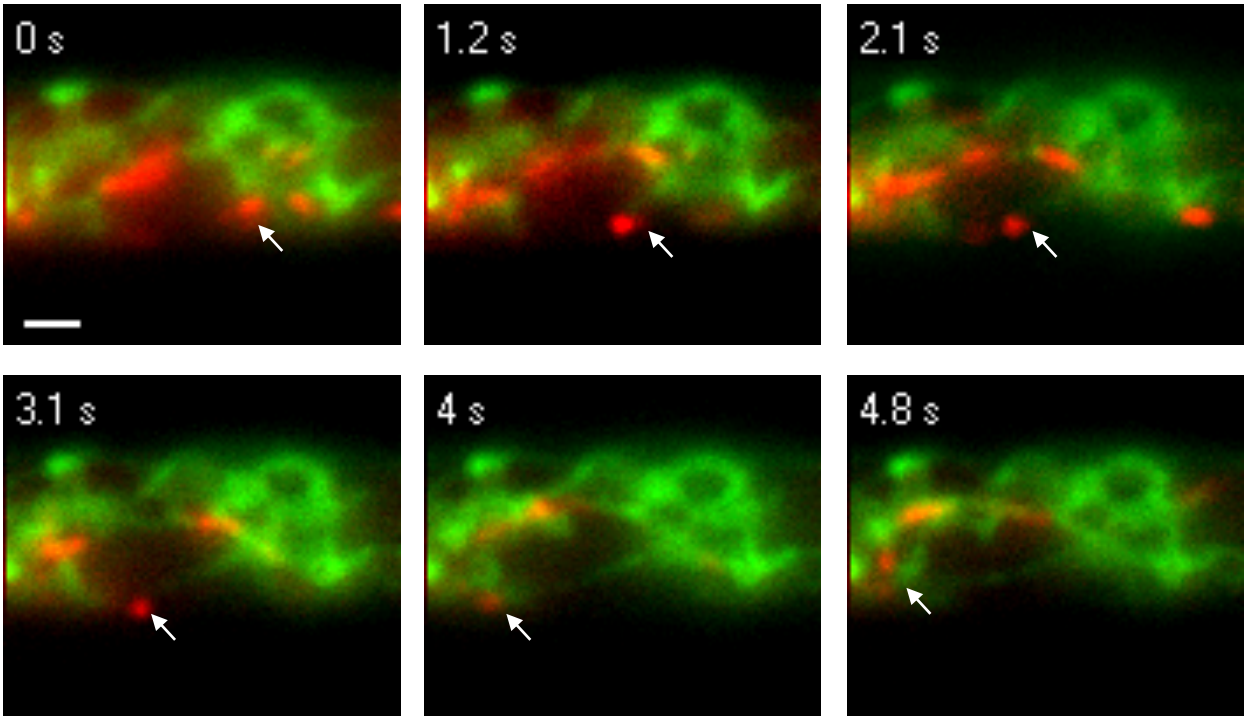


**Figure 4.14 Co-movement of EE and ER tubule.**
AB33Eca1GChRab5a cell to visualize EE and ER tubule motilities simultaneously. Image panels showing co-movement of ER tubule (green) and EE (red). Note that EE got position in front while ER tubule extends out and reconnects to another part of ER network (white arrows). Time references are given. Scale bar= 1µm.

#### 4.2.4.2 Genetic evidence for the role of EE in PO and ER tubule motility

Following co-localization studies, a series of experiments were designed to gain genetic support of EE involvement in PO and ER tubule movement.

##### 4.2.4.2.1 *Yup1ts* mutation and EEs

Yup1 is a putative t-SNARE protein, which mediates the fusion of transport vesicles with EEs (Wedlich-Söldner et al., 2000). When the fusion process is disrupted at restrictive temperature (32 °C) in *Yup1ts* background, the morphology of *Ustilago maydis* cells were altered with larger neck and cell diameter, division by septation, and disruption of polar growth. Besides cell morphology, EE morphology and motility were altered at 32 °C in *Yup1ts* background as well: small dots with no motility dispersed throughout cytoplasm were observed instead of mature EEs with ordinary back and forward long distance motility (Figure 4.15). Kin3 protein was still stably expressed in yup1ts condition (Figure4.16). For these reasons, the *yup1* conditional mutant has been used to provide genetic evidence in establishing the relationship between EE and two organelles by means of motility.

##### 4.3.4.2.2 PO and ER tubule motility in *Yup1ts* at restrictive conditions

To investigate PO motility in *Yup1ts* mutant, mCherry SKL was introduced into FB2*Yup1ts* strain. Cells were incubated at 22 °C and 32 °C for 9 hours to see optimum effect of *Yup1ts* followed by quantitative live cell imaging. The frequency of PO motility was significantly reduced at restrictive temperature compared with the control condition ($P<0.0001$, Student t-test, Figure 4.17).

With the same growth conditions, GFP-HDEL expressing *Yup1ts* cells were cultured and analysed by epifluorescence microscopy. The frequency of ER

motility was significantly reduced at 32 °C compared to 22 °C ($P<0.0001$, Student t-test, Figure 4.18).

These data supports the idea that EEs are involved in the transport of PO and ER.

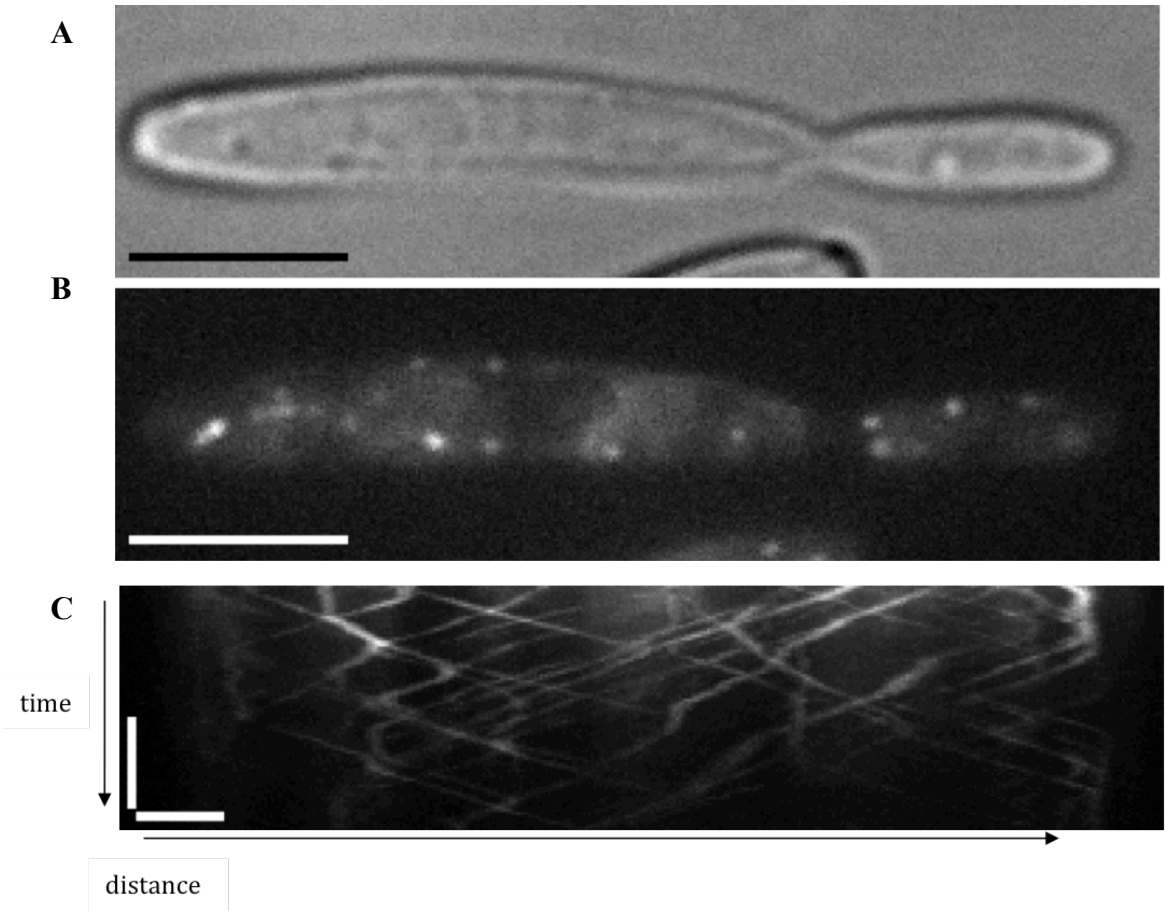


**Figure 4.15 EE morphology in *Yupts* cells at permissive temperature**
AB33*Yup1ts*Grab5 cells at 22 °C is shown as a control where cell phenotype, EE organization and movement are normal(C). Scale bars for DIC(A) and GFP (B) images =5 µm. Scale bars for kymograph= 2 µm/3s.

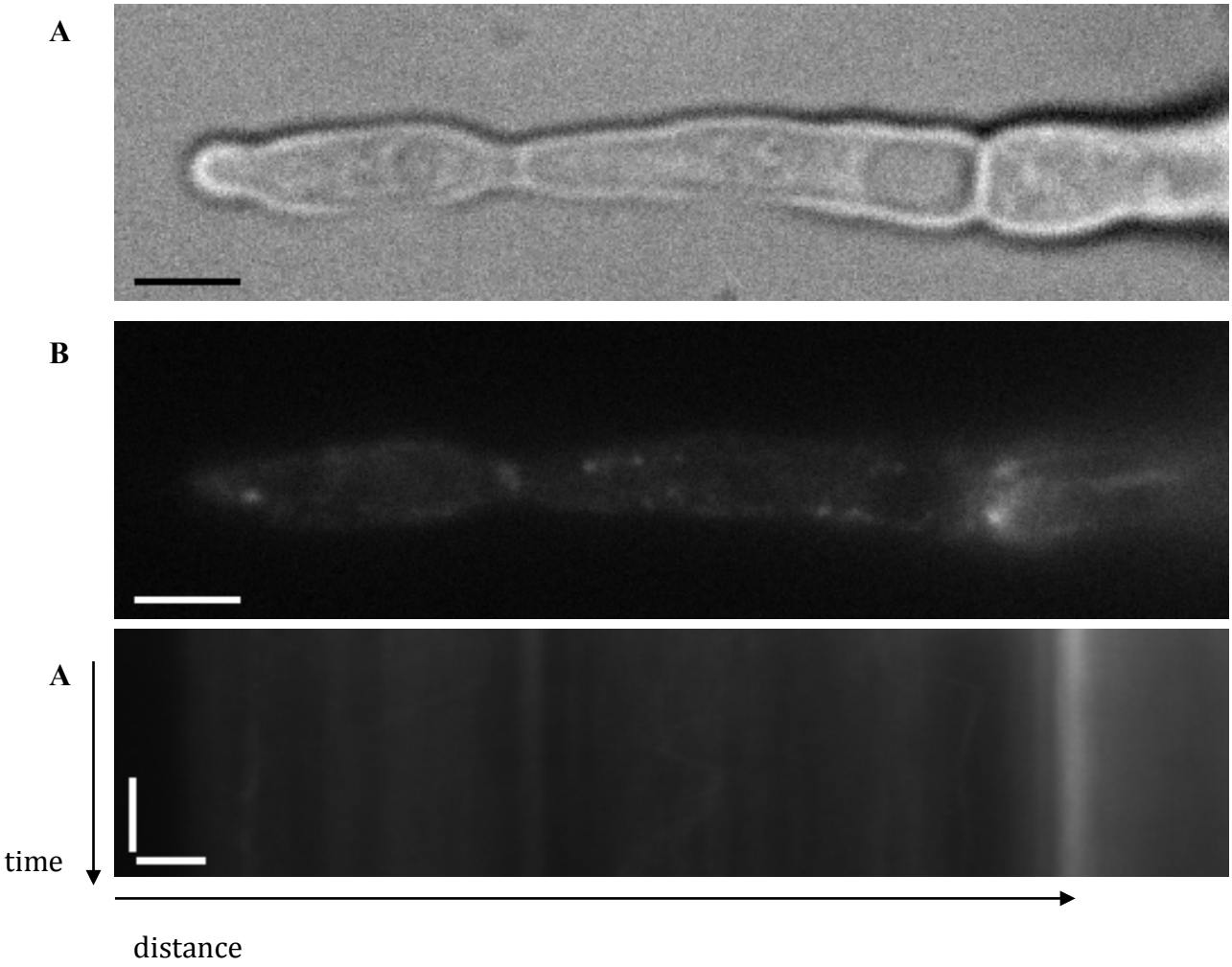


**Figure 4.15 EE morphology and motility are affected in *Yup1ts* .**
(A) AB33*yup1ts*_Grab5a cells at 32°C indicate that cell size and phenotype of yeast like cells change, EEs are smaller and ordinary EE movement is abolished(A,B and C, respectively). Scale bar for DIC and GFP images=5 μm. Scale bars= 2μm/3s

.

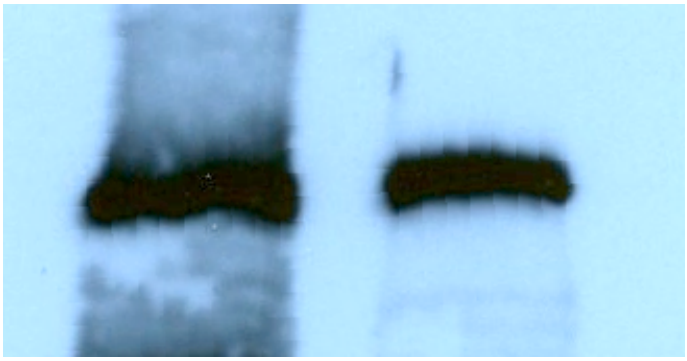


**Figure 4.16 Kin3 expression in *Yup1ts* cells.**
Western blot analysis was done by using FB2 *Yup1ts*Kin3GFP cells grown at permissive (22 °C) and restrictive temperatures (32 °C). Blot result showing that Kin3 is stable at both permissive (lane1) and restrictive temperatures (lane2).

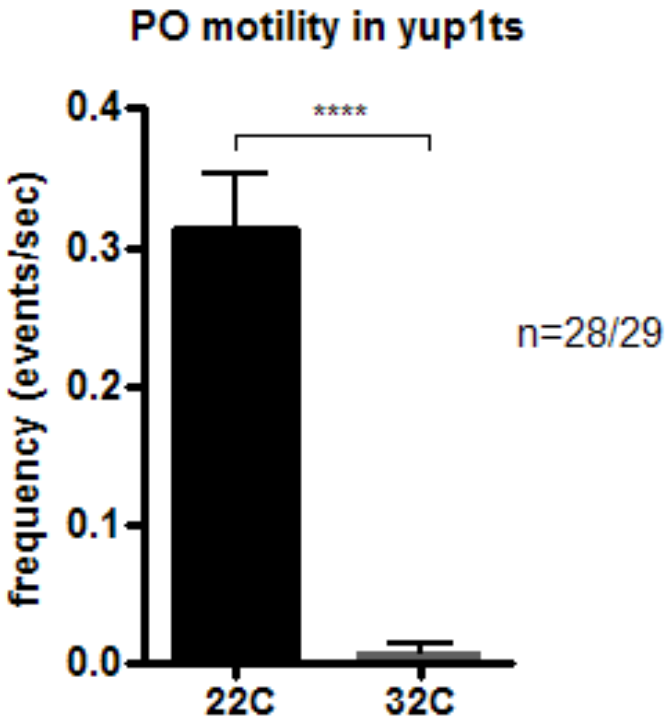


**Figure 4.17 PO motility is affected in Yup1 temperature-sensitive mutants.**
FB2*Yup1ts*GSKL cells were incubated at 22 °C and 32 °C. Bar chart showing frequency of PO motility at restrictive and permissive temperatures. Mean values ± standard error of the mean is given; sample size "n" is indicated. Quadruple asterisk indicates statistical difference at $P<0.0001$, Student t-test.

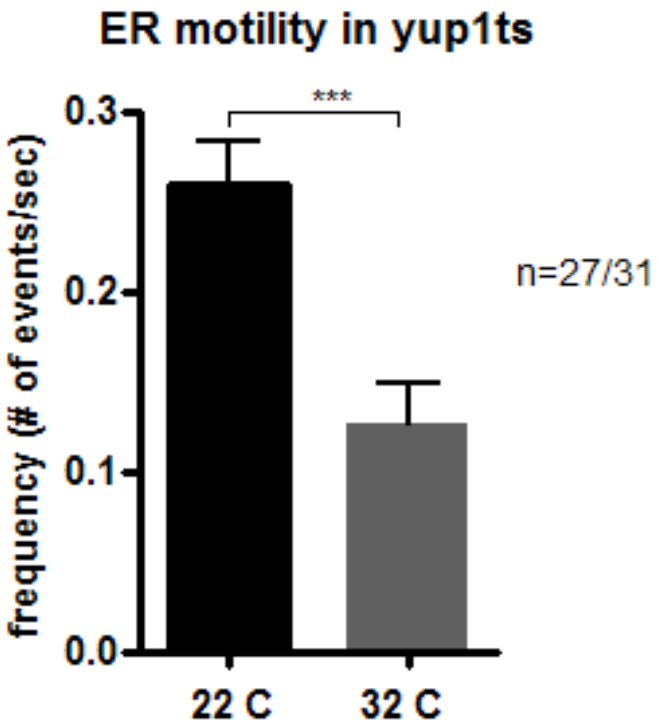


**Figure 4.18 ER motility in *Yup1ts* cells**

FB2*Yup1ts*GFPHDEL cells were incubated at 22 °C and 32 °C. Bar chart showing frequency of ER tubule motility at restrictive and permissive temperatures in *yup1ts* cells. Mean values ± standard error of the mean is given; sample size "n" is indicated. Triple asterisk indicates statistical difference at P<0.0001, Student t-test.

#### 4.2.4.2.2 PO motility in *Δrab5a* cells

Rab5, used as an EE marker in *Ustilago maydis*, is reported to have function in membrane fusion into EEs (Bucci et al., 1992; Stenmark et al., 1994). In addition to membrane fusion, it has a role in association of EE to microtubules and regulation of EE motility (Nielsen et al., 1999). For that reason, EE and PO motilities were investigated in the absence of Rab5a.

Firstly, EE morphology and motility was analysed in *Δrab5a* background by using Yup1GFP fusion protein as EE marker (Wedlich-Söldner et al., 2000). Microscope analysis showed that number of EEs is reduced (Figure 4.19) compared with the control conditions (see Figure4.1) and also EE motility is distorted (Figure 4.19) in the absence of rab5. This result confirmed that rab5 has a role in the regulation of EE transport.

PO motility was analysed in *Δrab5a* background. Microscopic analysis of AB33Δ*rab5a*GSKL strain showed that POs tend to cluster and PO motility is abolished (Figure 4.20).

This data supports previous findings on EE-dependency of PO transport.

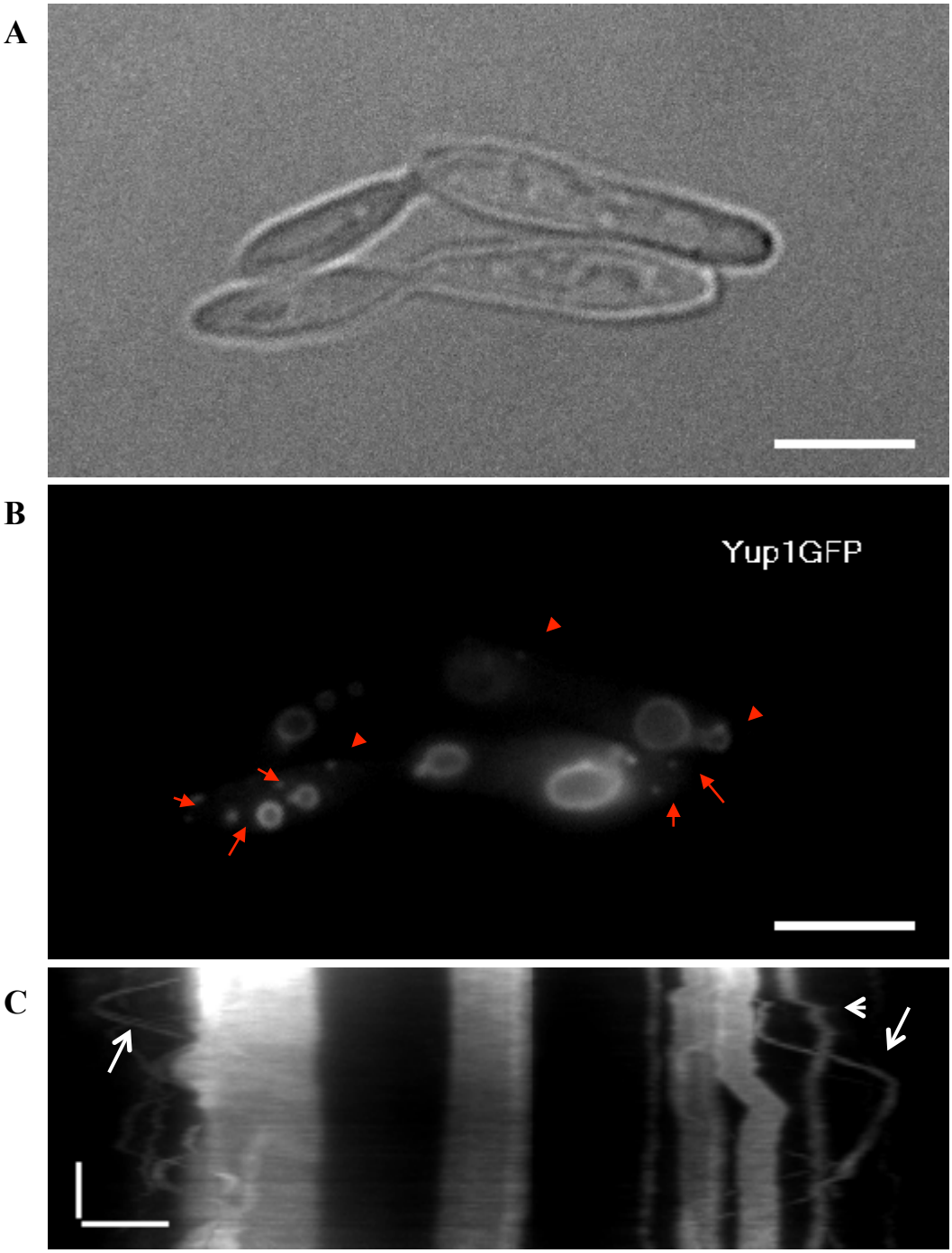


**Figure 4.19 EE morphology and movement is affected in *Δrab5a* cells**
(A)AB33*Δrab*5ayup1GFP strain was analysed for EE motility. DIC image of the Δrab5a cells. Scale bar= 5μm. (B) Yup1GFP signal localizes on EE (red arrows) and vacuoles. Note that number of EEs is reduced in Δrab5a cells. Scale bar= 5μm. (C) Kymograph showing EE movement in the absence of rab5 (white arrows). Scale bar= 2μm/2s .

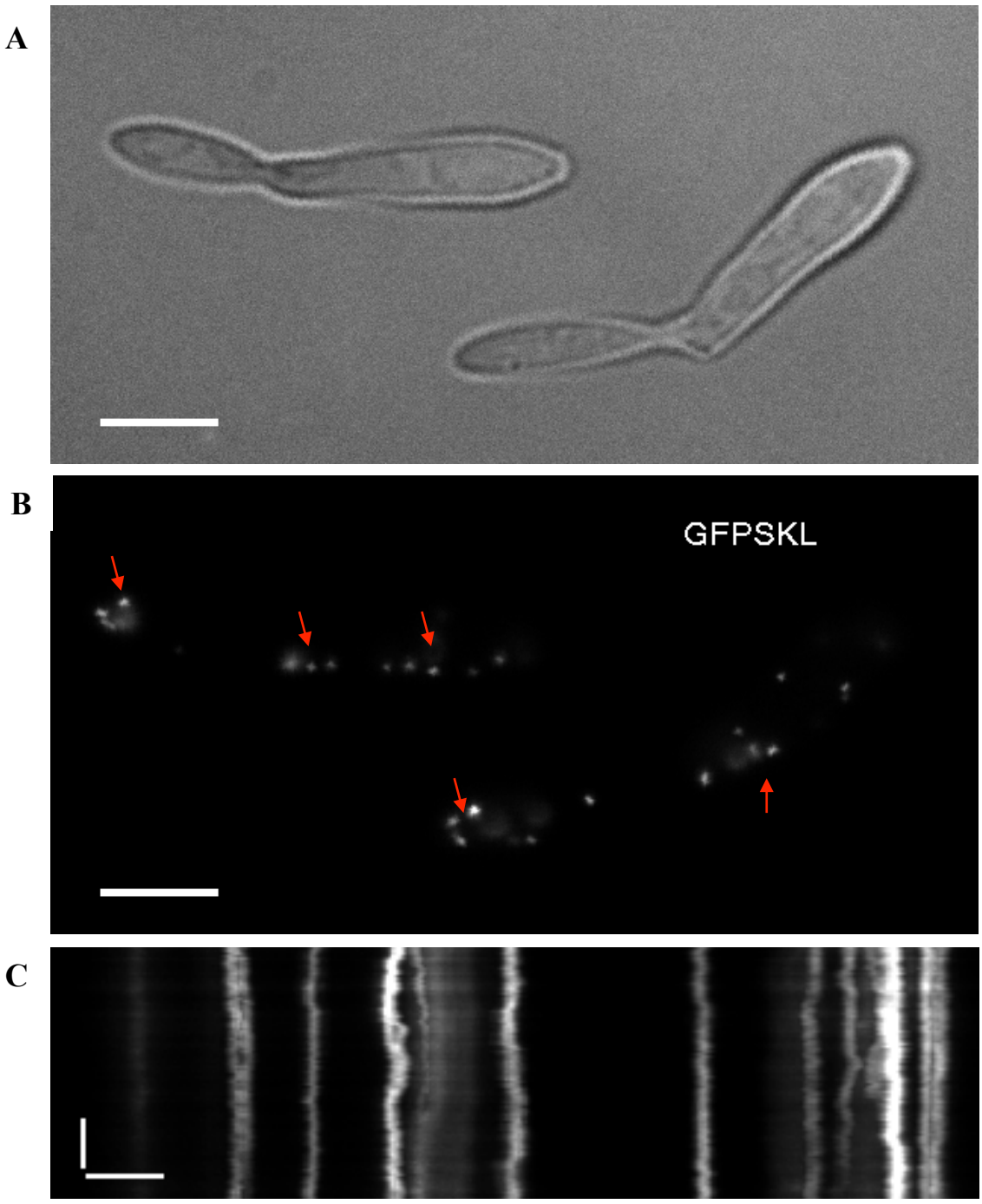


**Figure 4.20 PO organization and movement are affected in Δrab5 cells.**
(A) AB33*Δrab5a*GSKL strain was analysed for PO motility. DIC image of the cells. Scale bar=5μm. (B) GFP image showing that POs cluster (red arrows) in *Δrab5a* cells. Scale bar=5μm. (C) Kymograph showing PO movement in the absence of *rab5a*. Scale bar=2μm/2s.

## 4.3 Discussion

Long-range motility of EEs and ER tubules are reported as MT-dependent in *Ustilago maydis* (Lenz et al., 2006; Wedlich-Söldner et al., 2002a; Wedlich-Söldner et al., 2002b). PO motility is also MT dependent as shown in the previous chapter (see chapter 3). Microscopic analysis showed that EEs are moving in forward and reverse directions rapidly at high frequency rates, whereas only a small portion of POs and ER tubules are moving in a long-range fashion. Both the frequency and average run length of EE motility is found to be significantly different than the frequencies and run lengths of PO and ER tubule motilities. These organelles show different motility behaviours except their average velocities. Different motility behaviours can be the result of different functions and morphology of the organelles within the cell (Egan et al., 2012b).

Previous studies showed that Dynein is the minus end motor for EEs and ER tubules' traffic ((Wedlich-Söldner et al., 2002a; Wedlich-Söldner et al., 2002b). PO motility also depends on dynein motor, which was discussed in the previous chapter (see chapter 3). As Kin3 is known as plus end motor for EEs (Schuster et al., 2011b; Wedlich-Söldner et al., 2002b), the contribution of Kin3 in the motility of three organelles was investigated. Kin3 knockout strains transformed with fluorescence organelle markers were analysed and revealed that motility of all three organelles ceased. For further investigation, fluorescent labelled Kin3 and each organelle marker were visualized simultaneously. Co-localization studies showed that Kinesin3 is moving with EE, ER and PO during their transports. There was an interesting observation regarding to Kin3 position in the co-alignment that Kinesin3 is not fully co-

aligned with POs instead it appears like Kin3 is pulling POs during motility. For that reason, it might be more convenient to call this movement as co-movement.

As previously reported Kin3 is the responsible molecular motor for the EE transport with high co-localization rate (Wedlich-Söldner et al., 2002b). For that reason, a potential EE dependency of PO and ER tubule motility was investigated. Co-localization studies revealed that PO and ER tubule motilities are not independent from EEs. Dual images showed that EEs are pulling POs and ER tubules and changing their positions in the cell. This result suggests that PO and ER tubules are hitchhiking on EEs.

Since EEs are moving with high frequencies along microtubules, there is a possibility that these interactions are incidental and misleading. To eliminate these concerns, in addition to co-trafficking data, genetic data by using conditions where EE motility was abolished was also provided. These conditions are Yup1 temperature-sensitive and Rab5a knockout mutants as they were previously reported to regulate early endosome dynamics. In *Yup1ts* cells, EEs did not form properly and small vesicles were observed. In addition to the aberrant cell morphology, motility of these small vesicles is abolished in *Yup1ts* cells at restrictive temperatures. Quantitative analysis showed that PO and ER tubule motilities are significantly reduced in yup1ts cells. In *Δrab5* cells, number of EEs is reduced in the cell and motility of EEs is disturbed. In this study, we only analysed PO transport in *Δrab5a* cells, which showed that long range PO motility is stopped when EE transport is distorted. *Δrab5* study needs further analysis to quantify effect of rab5 on PO transport. Analysis of the ER tubule movement in *Δrab5a* cells is needed to

further support EE contribution in transport. Although, I observed drastic effect of *Yup1ts* and *Δrab5a* on peroxisome motility, these results might be misleading. Early endosomes are important elements of endocytic pathways, which is linked to various processes such as intracellular communication and cellular morphogenesis (Higuchi et al., 2014; Mateus et al., 2011). It should be noted that in these mutants abolishing early endosome formation and function might exert pleitrophic effect in the cell. So, the results should be interpreted with caution and further experiments should be done to support these results. In a recent study, it was shown that an adaptor protein, hok1, is coordinating binding of EEs to Kin3 and dynein (Bielska et al., 2014). So, analysing PO motility in hok1 mutants would provide further insights.

To sum up, these data suggests that EEs may serve as a platform for transport of PO and ER tubules as well as polysomes and mRNPs by Kin3 (Baumann et al., 2012; Higuchi et al., 2014). In *N. crassa*, Kin3 transports mitochondria and early endosome. It has been proposed that mitochondria movement is mediated by early endosomes (Fuchs and Westermann, 2005; Seidel et al., 2013).

## 5. Peroxisome motility and Function

### 5.1 Introduction

Peroxisome association with the cytoskeleton mediates spatio-temporal organization of peroxisomes. Inhibition of microtubule polymerization resulted in formation of peroxisome clusters in the cell (Wiemer et al., 1997). Mutations in peroxisome transporting motors resulted in polar distribution of peroxisomes (Egan et al., 2012b). A mutation in peroxisome recognition site of Myo2p of yeast reduced inheritance of peroxisomes to the bud cells (Fagarasanu et al., 2009). Microtubules have role in biogenesis including proliferation and division. In fibroblast cells of patients suffering from Zellweger syndrome, a peroxisome biogenesis disorder, microtubule-based peroxisome motility was disturbed. This led to alterations in peroxisome abundance and morphology (Nguyen et al., 2005). Thus, peroxisomal dynamics might be linked to peroxisomal movements.

Peroxisome studies in different organisms suggested various roles to peroxisome motility. In plants, peroxisomes move and contact transiently with each other. Sometimes fusion or division events are observed (Mathur et al., 2002). Another proposed function in plants is linking peroxisome motility to provide close proximity to peroxisomal proteins, which needs to be imported into peroxisome matrix (Muench and Mullen, 2003). In fission yeast, peroxisomes are found to be associated to mitochondria and peroxisome motility is an indirect effect of mitochondrial dynamics (Jourdain et al., 2008). In yeast, peroxisome motility is important for inheritance of peroxisomes from mother to bud during cell division (Fagarasanu et al., 2005b; Hoepfner et al., 2001). In mammalian cells, peroxisome-peroxisome interactions and

maintaining of peroxisome distribution are linked to peroxisome motility (Bonekamp and Schrader, 2012). To sum up, peroxisome motility may relate to four processes of peroxisome life cycle including i) peroxisome distribution, ii) peroxisome inheritance, iii) peroxisome-peroxisome interaction and iv) division of peroxisomes. In the first part of this chapter, I address potential functions of peroxisomal motility in *U. maydis*. To this end, Kin3 knockout and benomyl-treated cells where peroxisome motility was abolished (See Chapter3) were analysed. In addition, peroxisomal interactions between each other were investigated in GFPSKL expressing cells.

In the second part of this chapter, a hypothetical protein of *Ustilago maydis* is characterized. This study was performed as an wet-lab experimental step of the bioinformatics research revealing homolog proteins in *U. maydis* and *H. sapiens* genomes which are not present in *S. cerevisae* genome (Münsterkötter and Steinberg, 2007). In this report, proteome information of *Ustilago* , yeast and human were compared and found that *Ustilago maydis* is closer to human than yeast. There are a number of common proteins shared by *Ustilago* and human which are not present in the yeast. As a result of FunCat database search, these proteins have potential roles in certain cellular activities. Most of these proteins are unidentified which makes *U. maydis* a potential model organism to study functions of these common proteins. One of these proteins, um05592 a hypothetical protein with high homology to a human protein with unknown function, was chosen in this study. Project was suspended after a series of experiments (J. Klarig unpublished). I continued the project and reported functional characterization of um05592. Firstly, corresponding human homolog to um05592 was found by NCBI/BLAST

(http://blast.ncbi.nlm.nih.gov/Blast.cgi). Conserved domains of um05592 were found by online protein domain resource SMART (http://smart.embl.de/). Then, subcellular localization of um05592 was visualized in *Ustilago maydis* cells. Once the gene was knocked out, various growth tests were applied with control and mutant cells. Finally, pathogenicity in um05592 background was assayed.

## 5.2 Results

### 5.2.1 Peroxisome motility and related functions

#### 5.2.1.1 Peroxisome organization does not exclusively depend on long-range motility

Intracellular organelle traffic has been important to maintain proper organelle distribution within the cell (Burkhardt et al., 1997; Higuchi et al., 2014; Requena et al., 2001). To investigate the influence of peroxisome transport on peroxisome organization in Ustilago cells, I analysed peroxisome distribution in AB33GSKL (Control) and AB33*ΔKin3*_GSKL cells where long-range peroxisome motility is widely diminished (See Chapter3). When the two strains were compared by live cell fluorescence imaging, I observed peroxisome clusters (Figure5.1).

To see the effect of failure of long-range movement, I analysed peroxisome distribution during longer (than the elapsed time of video sequences for motility measurements) periods. After observing over 20 minutes, I found that peroxisomes could still relocate in both conditions (Figure 5.2). This result shows that, in the absence of long-range transport, peroxisomes can still change location in the cell but the process seems to be slower resulting in clustering phenotype.

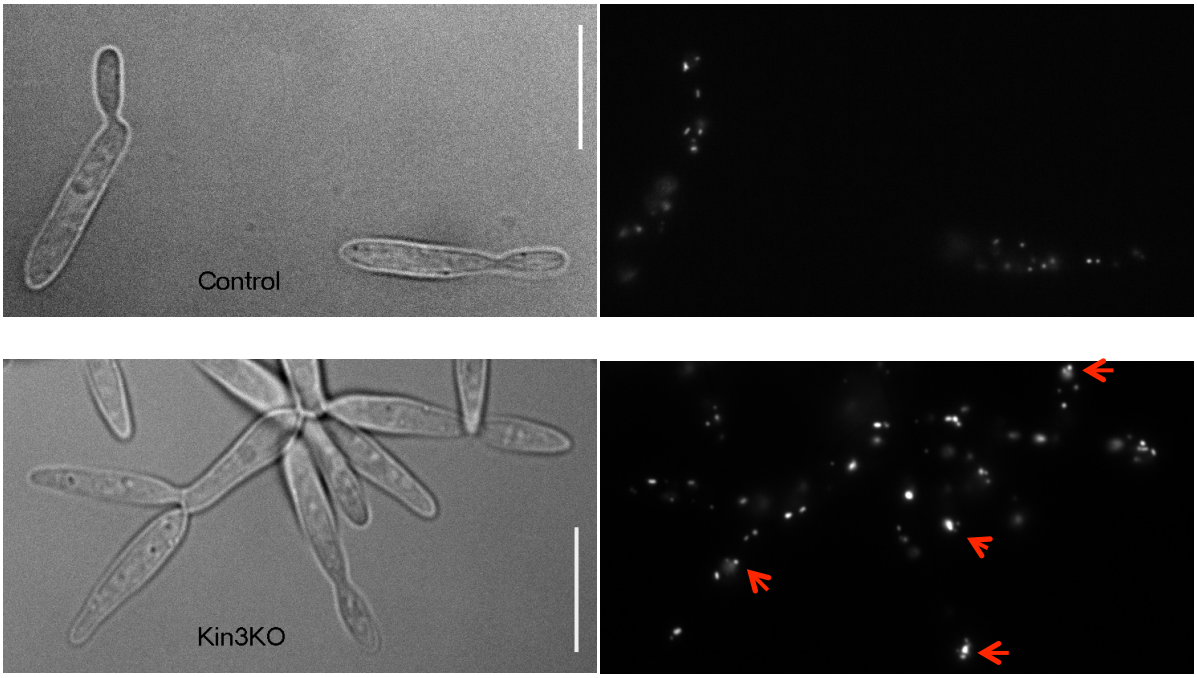


**Figure 5.1 Peroxisome distribution in Control and *ΔKin3* cells.**

AB33GSKL and AB33*ΔKin3*GSKL strains were cultured in liquid CM-glucose medium overnight and examined by epifluorescence microscopy. DIC images showing phenotypes of control and *ΔKin3* cells. GFP expressing cells showing peroxisome distribution, Red arrows indicating peroxisome clusters *ΔKin3* cells. Scale bars= 10 μm.

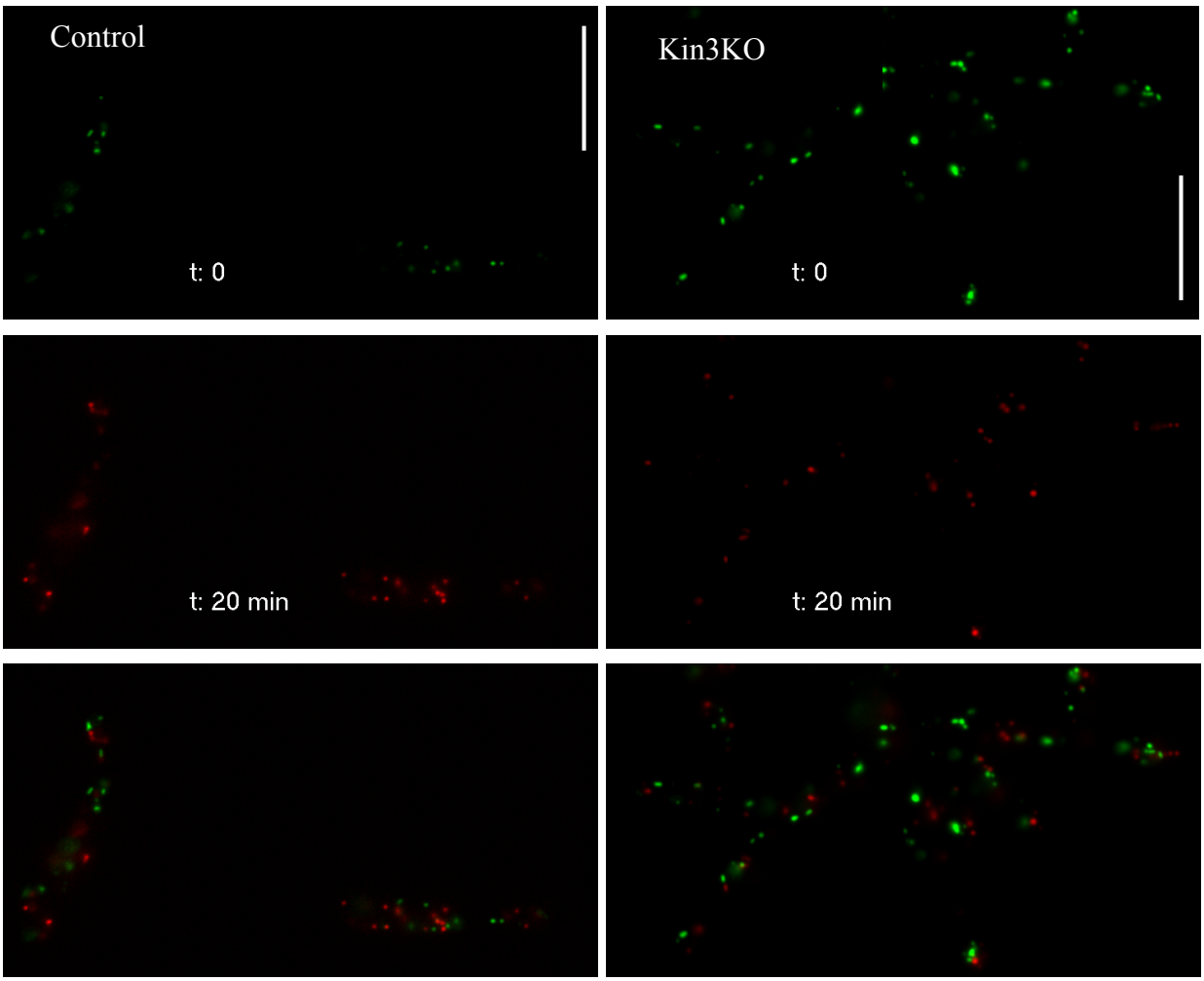


**Figure 5.2 Peroxisome redistribution in *ΔKin3* cells**

AB33GSKL and AB33*ΔKin3*_GSKL strains were examined to analyse peroxisome organization. Distribution of peroxisomes is shown with image planes at t:0 (green) and t=20 min (red). Note that peroxisomes change their positions in both Control and *ΔKin3* cells after 20 min. Scale bars=10 µm.

#### 5.2.1.2 Peroxisome inheritance does not depend on long-range motility of peroxisomes

To address whether peroxisome movements occur randomly anywhere or at particular regions in the cell, peroxisome motility movies in medium-budded cells were analysed and motility events were grouped according to specific regions: mother side, nucleus region, neck region and bud side (Figure 5.3A). By using kymographs, each motility event was quantified and motility region was addressed. The results showed that 18.70% of the events take place around mother cell end, 21.60% of the events occurs around bud cell and the rest of the motility events, approximately 60% of the peroxisome transport, takes place around neck and nucleus regions. This result suggests that peroxisome traffic mostly occurs in the region between bud and mother cells. Figure 5.3B represents an example from a stack that is analysed for motility regions showing peroxisome traffic between mother and bud cells.

Organelle movement is an essential step for equal segregation of organelles between the cells (Fagarasanu et al., 2007). Mother-bud communication could be important for peroxisome inheritance between mother and bud cells. To ascertain connection between peroxisome inheritance and peroxisome motility, FB2GFPSKL strain was treated with benomyl to abolish peroxisome transport (see Chapter3) and investigate the presence of peroxisomes in the bud cells. Benomyl was applied for short (30 min) and long (2 h) periods: (i) to observe and compare the effect at two different time points and (ii) to allow enough time for cell doubling to see peroxisome inheritance into the bud. Doubling time for wild type cells (FB2) was reported as 2.0 h previously (Weber et al., 2003). Peroxisomes were detected in the bud cells after 2 hours

benomyl treatment (Figure 5.4). There was no bud without peroxisomal signals. Peroxisome organization shows differences in control and benomyl-treated cells (Figure 5.4). Peroxisome clusters were detected and the number of peroxisomes in the bud increased, mostly clustered at bud tip, in benomyl-treated cells.

Yet, this result suggests that long-range peroxisome motility is not essential for peroxisome inheritance.

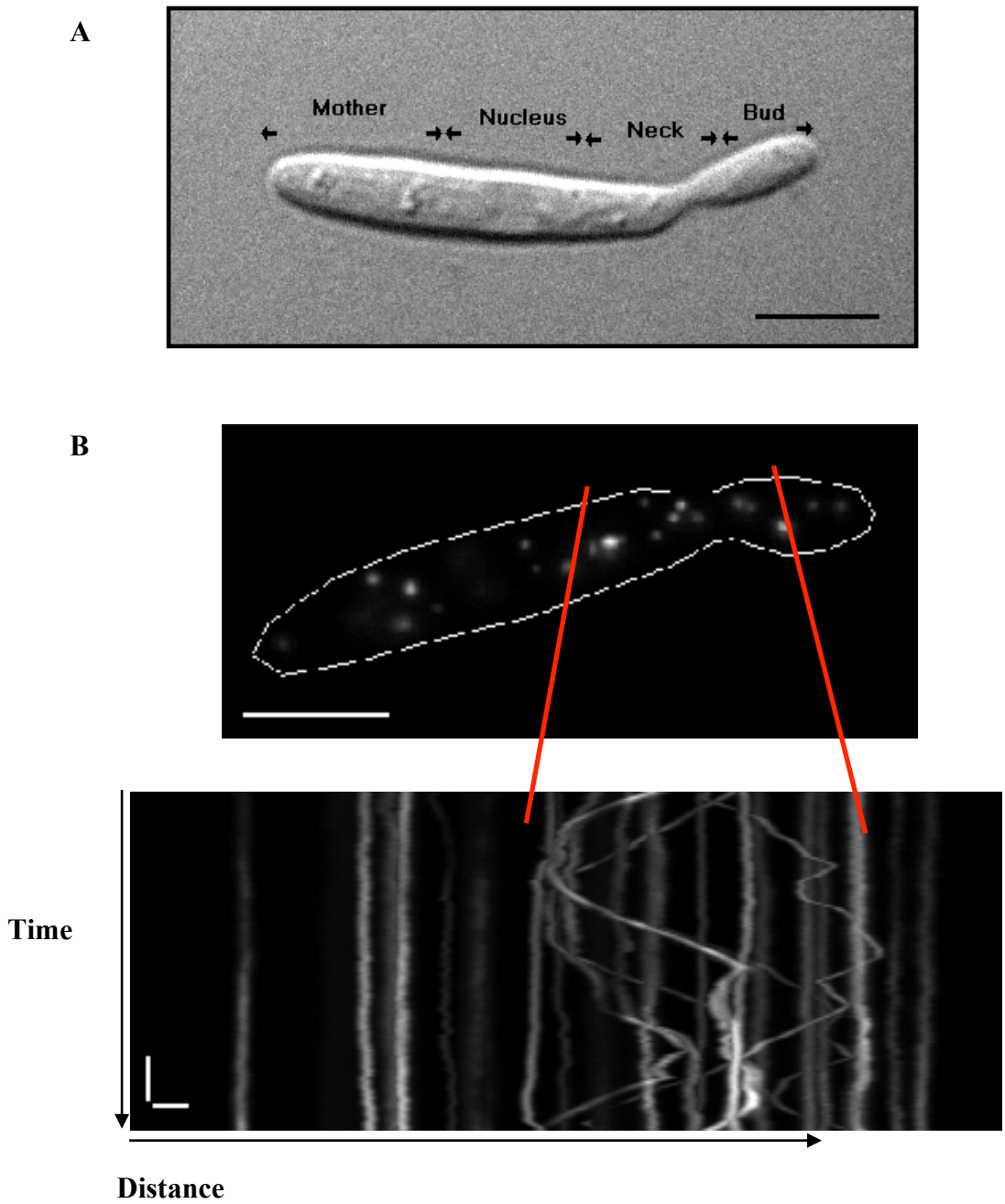


**Figure 5.3 Peroxisome traffic between mother and bud cells**
**(A**) FB2GSKL cells were examined to elucidate the link between cellular regions and peroxisome motility. Regional division in medium budded *U. maydis* yeast-like cell is shown with arrow borders and region names. Scale bar=5μm. (**B)** GFP image from FB2-GFPSKL cell and kymograph showing busy peroxisome traffic between mother and bud cells. Scale bar for still image= 5μm. Scale bars for kymograph= 2μm/2s.

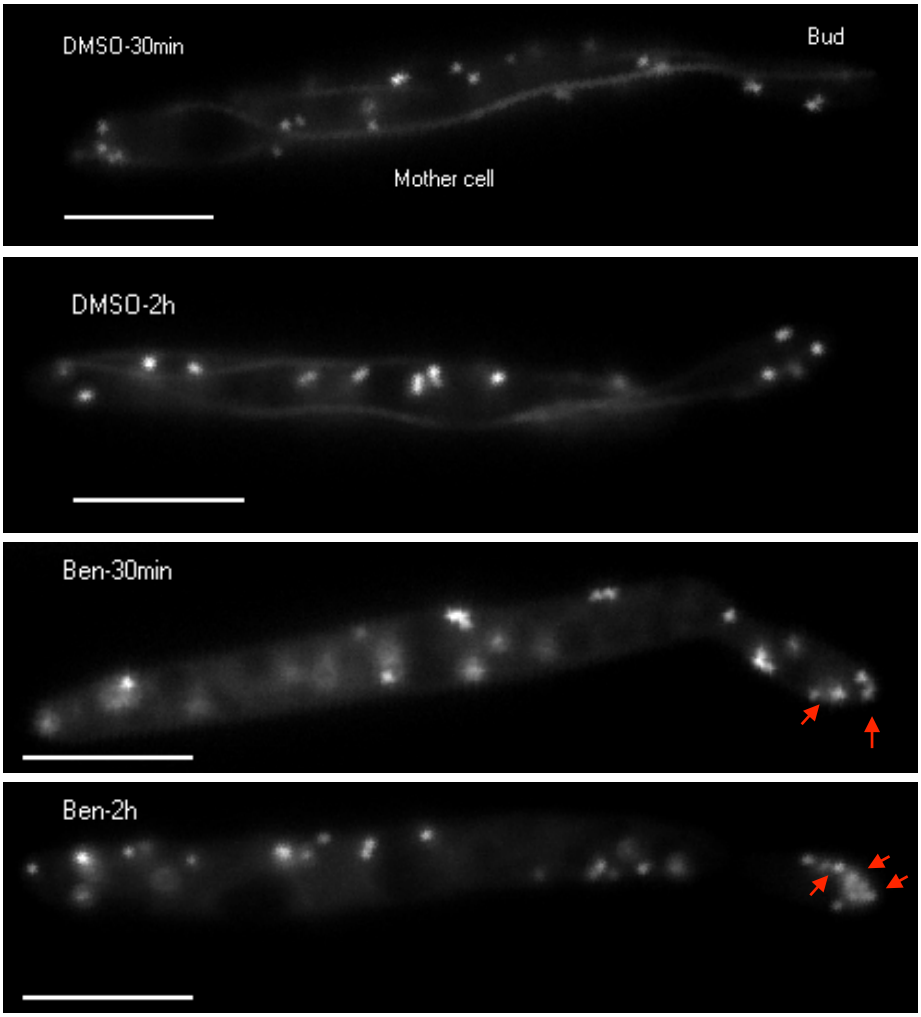


**Figure 5.4 Peroxisome inheritance in DMSO and benomyl-treated cells**

FB2GSKLGT strain was treated with benomyl and DMSO(Control) followed by microscopic analysis. Short and long-time drug treatments revealed that peroxisomes are inherited to bud cells even though peroxisome movement is disrupted. Note that there are more peroxisomes in bud cells and also peroxisome accumulation is observed at the bud tip (red arrows) in benomyl-treated condition. Scale bars= 5μm.

### 5.2.1.3 Transient interactions between moving peroxisomes

Peroxisomes in *Ustilago maydis* cells can be regarded as morphologically heterogeneous, i.e they are present in various forms such as round, elongated, duplets or multiplets. Different forms of peroxisomes were also reported in the plant and mammalian cells (Muench and Mullen, 2003; Schrader et al., 2000).

In order to visualize peroxisomes, FB2GFPSKL cells were analysed by epifluorescence microscopy. Figure 5.5 represent examples for different peroxisome morphologies observed in *Ustilago maydis* cells. Peroxisomes can be observed in round shape or having small tails (Figure 5.5a). They could be observed in duplets and just ready for fission (Figure 5.5b). Also some peroxisomes are in elongated or long-tailed forms (Figure 5.5c). Finally, peroxisomes are sometimes in multiplets like a long chain with small beads on it (Figure5.5d).

In some motility events, it is observed that elongated peroxisomes move and after a while " off-loading" of a peroxisome occurs. In other words, peroxisome division seems to happen while they are moving. Figure 5.6 shows that an elongated peroxisome is moving and after 3.3 seconds one peroxisome is separated from the elongated peroxisome. Although signal quality is poor at later time points, division can be seen well with the kymograph (Figure5.6C). Similar events in which peroxisomes are observed as dividing were reported in plant and mammalian studies (Mano et al., 2002; Mathur et al., 2002). Occasionally an elongated peroxisome is pulled to opposite sites during movement implying that movement back and forth helps for division (not shown).

In addition to division, peroxisomes are observed to interact with each other during peroxisome transport. Peroxisome-peroxisome interactions are quite common in motility events. These interactions are observed in various modes. In some occasions, one interacting partner is mobile and the other one is stationary. The mobile one picks up the other one and they interact followed by continuing to move with long-range movement or oscillate together at the meeting spot. In other occasions, both interacting organelles are moving in different parts of the cell and come together followed by moving or just oscillating together. Occasionally, it was observed that two or more peroxisomes could interact with each other in some motility events.

In the Figure 5.7, an example for the interaction of three peroxisomes is given with a still image of the cell and sections from stacks of peroxisome movements. At first, two peroxisomes from opposite site (#1&#2) move to each other, unite and continue their movements together. Later, another peroxisome (#3) comes towards and joins to moving peroxisomes. These interactions are also shown by kymograph of the same movie with time and distance references (Figure 5.8).

In another example given in the Figure 5.9, one peroxisome (#1) moves, joins to another peroxisome (#2) and they move together shortly followed by separation. Then, first peroxisome (#1) continues to move by itself, joins to another peroxisome (#3) which is a duplet and they start to oscillate together by short range movement after the interaction.

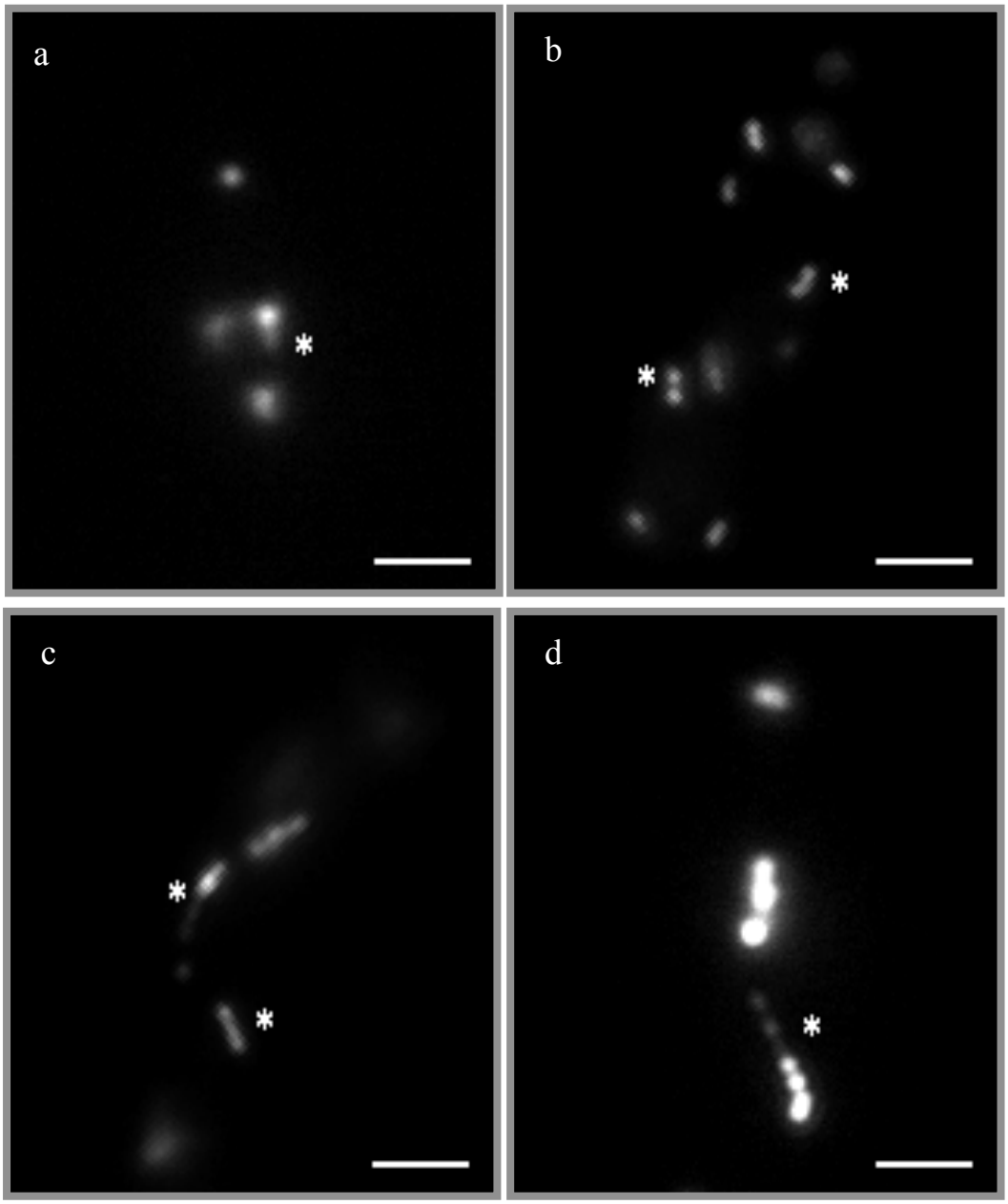


**Figure 5.5 Peroxisome morphology in *U. maydis* cells**

FB2GSKL cells were examined by fluorescence microscopy to visualize peroxisome morphology. Image panels showing examples of peroxisomes in single, duplet, tailed and multiplets (a-d, respectively). Asterisk indicates different forms of peroxisomes

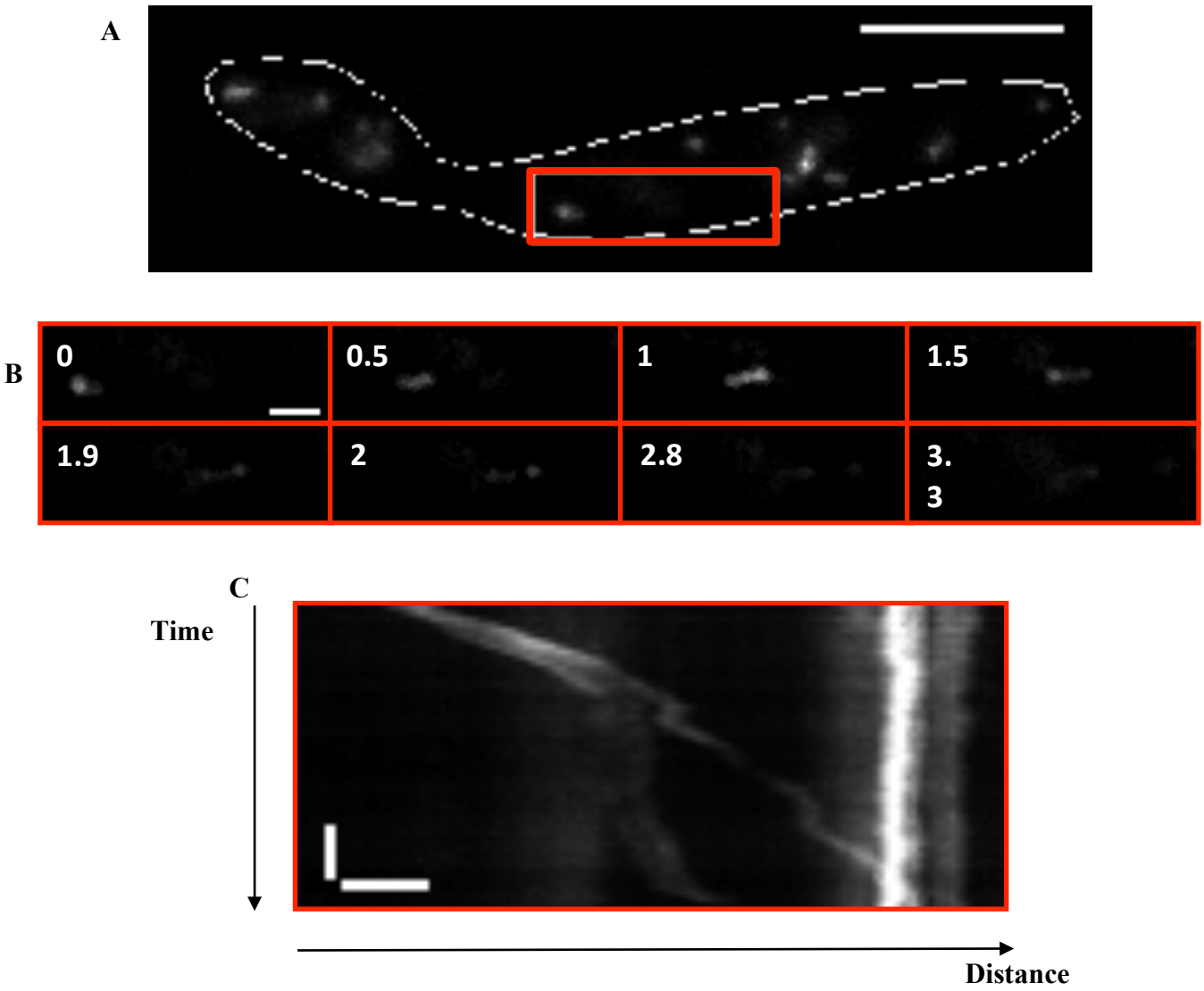


**Figure 5.6 Peroxisome division during peroxisome movement**

FB2GSKL strain was examined to analyze peroxisome motility(A). Eight image panels summarize a 3.3s motility event (red insets,B). Note that an elongated peroxisome with constrictions(t=1s) is moving and one peroxisome is pinched off after 1.9s. Respective kymograph(C) demonstrating movement and division of peroxisomes within 3.3s. Scale bars= 5µm, 1µm, 1µm/1s respectively.

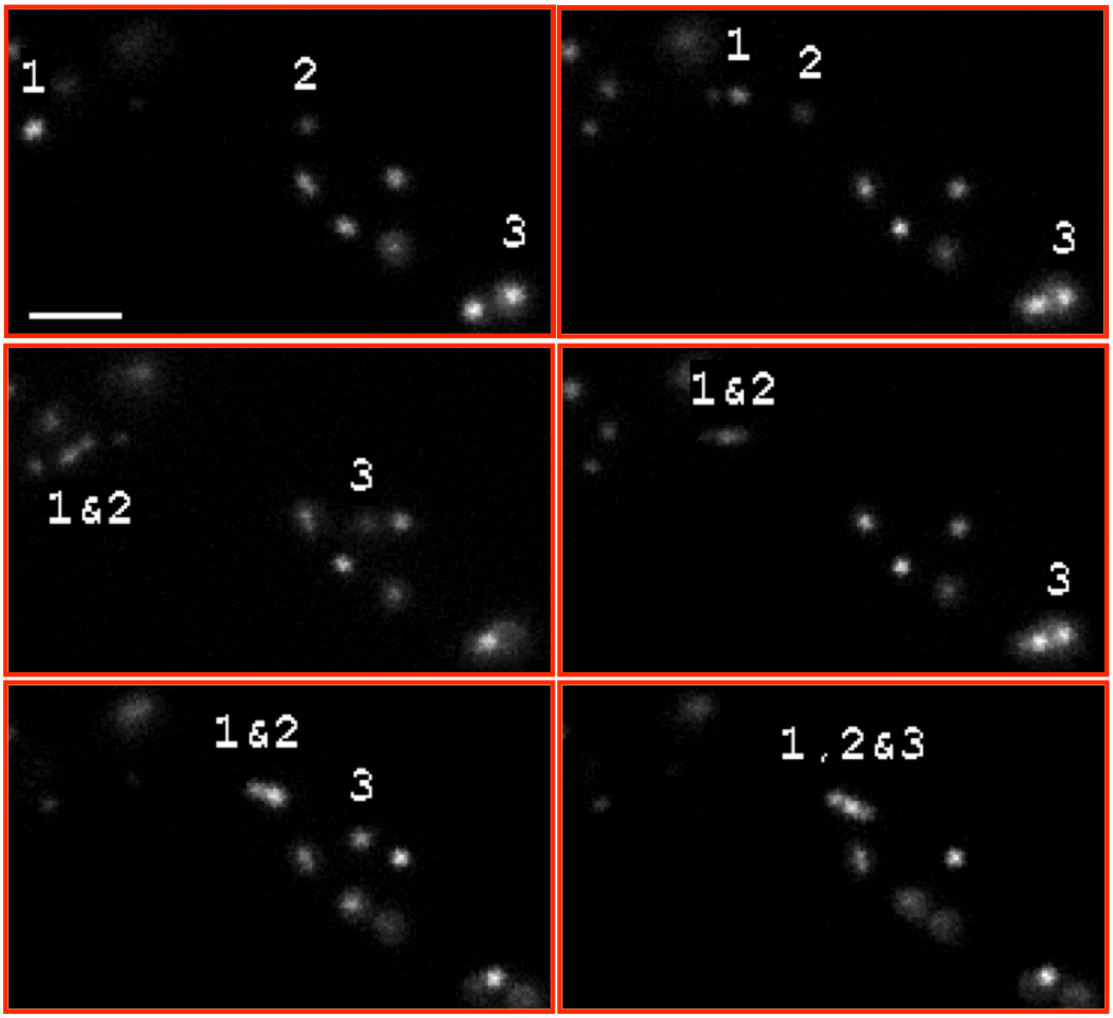


**Figure 5.7 Peroxisome-peroxisome interactions during peroxisome transport**

FB2GFP SKL cells were examined by microscopy and stacks were acquired to analyze peroxisome movements. Six panels (a-f) in red rectangular boxes showing movements and interactions of three peroxisomes while moving. In panels a and b, peroxisomes #1 and #2 run towards each other, make a "couple" (c) and move together (d). In the panel e, the "couple" and peroxisome #3 move towards each other and join together (f).Scale bar=2μm.

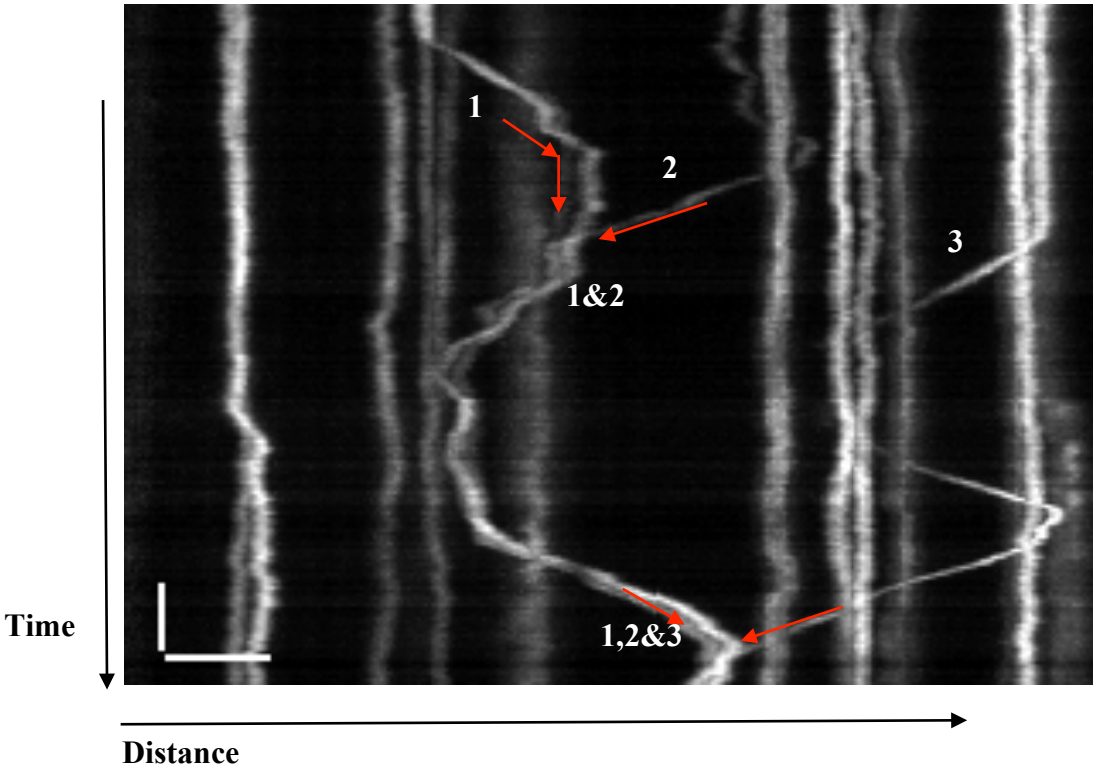


**Figure 5.8 Peroxisome-peroxisome interactions by kymograph**
Stack movie of the previous image (see Figure 5.7) was processed into kymograph to show tracks of three interacting peroxisomes. Movements and interactions of three peroxisomes are given by kymograph. Moving peroxisomes are numbered respectively. Red arrows to highlight movements of peroxisomes towards each other and the moment they interact. Scale bars=2μm/2s

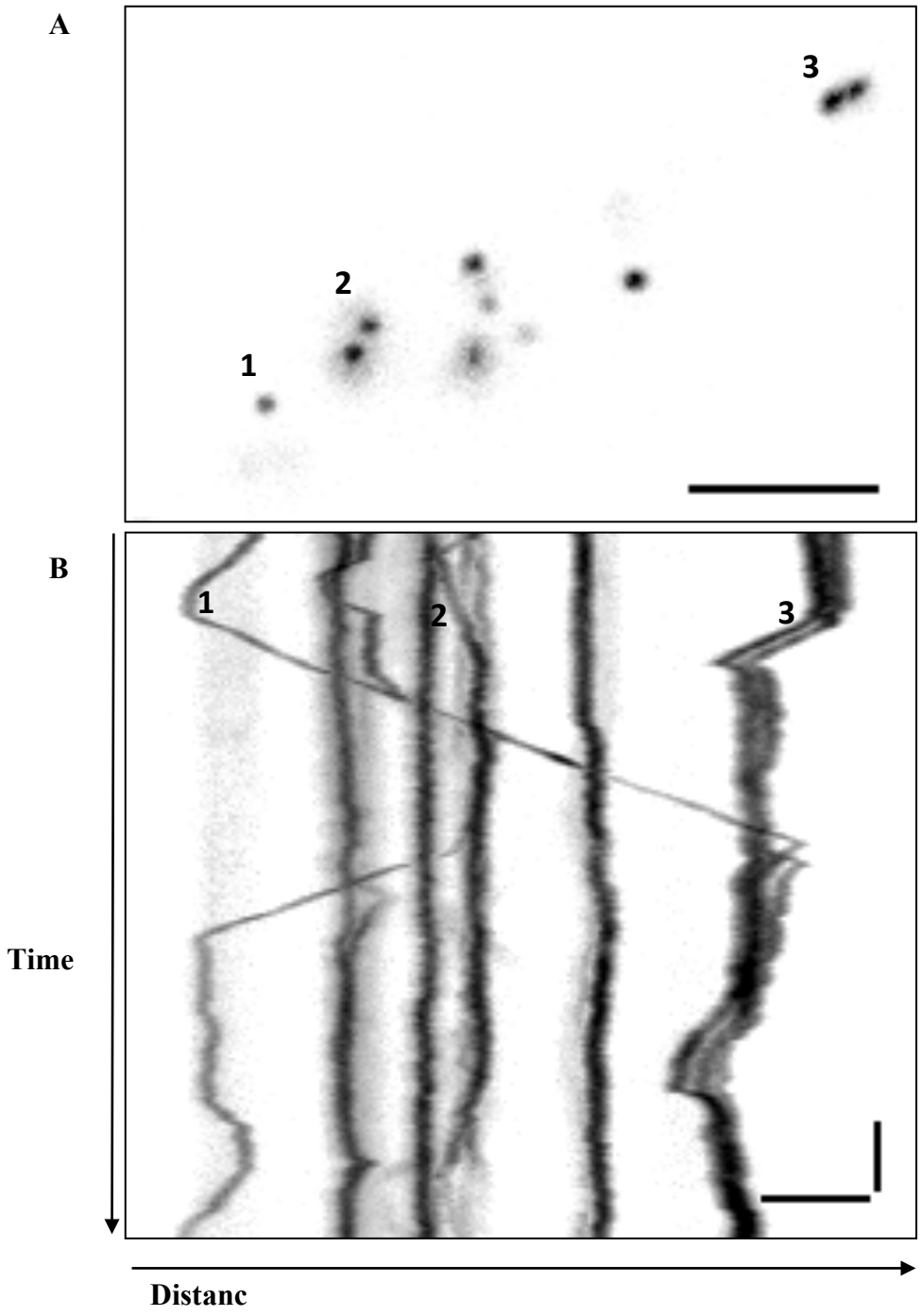


**Figure 5.9 Peroxisome-peroxisome interactions during peroxisome movement**
FB2GFP SKL cells were examined by microscopy and stacks were acquired to analyze peroxisome movements. A still image(A) and respective kymograph(B) of GFP expressing cell is given. Interacting peroxisomes are given in numbers. Kymograph shows that peroxisome #1 and peroxisome #2 join together followed by separation. Then, peroxisome #1 unites with oscillating peroxisome #3 and they oscillate together. Scale bars=3 μm, 2 μm/2s respectively.

### 5.2.2 Functional characterization of um05592- a hypothetical protein of *U.maydis*

#### 5.2.2.1 Homology between *Ustilago maydis* and human proteins

Bioinformatics study showed that *Ustilago maydis* and human proteome contain common proteins, which are important in cellular processes and not present in the yeast proteome (Münsterkötter and Steinberg, 2007). Among these, there are 222 common proteins with unknown function. Human homologs of 42 *Ustilago maydis* proteins are implicated to have potential role in human diseases (Münsterkötter and Steinberg, 2007).

Previous studies did show that Um05592 is a putative AAA ATPase that localizes in peroxisomes (J. Klaerig and G. Steinberg, unpublished). Here, I repeat these initial experiments and confirm those findings. I extend these studies by adding pathogenicity assays and functional studies. Amino acid sequence of um00592 was obtained from MIPS Ustilago maydis database MUMDB (http://mips.helmholtz-muenchen.de/genre/proj/ustilago/) and human homolog was identified as NP_055873 by blasting the sequence in NCBI/BLASTP. Next, sequence similarity (Figure 5.10) and conserved domains (Figure 5.11) of the protein homologs were established by using ClustalW and Smart-PFAM software resources (Larkin et al., 2007; Letunic et al., 2012; Schultz et al., 1998). Conserved domain search revealed that both proteins have 2 AAA_5 ATPase domains (pfam07728) and one WA domain (cd01455). AAA is abbreviation for ATPases Associated with diverse cellular activities and as the name suggests that the members of the superfamily have various functions in the cell such as actin and microtubule based transport, membrane modification, proteolysis (Babst et al., 1998; Esaki and Ogura, 2010; Kress et al., 2009; Wang et al., 2001; Wendler et al., 2012). Von

Willebrand factor type A domain is also found in many proteins having various functions mostly in the cell surface such as membrane formation, cell adhesion, migration, signalling (De Luca et al., 2000; Lyons et al., 1992; Springer, 2006)

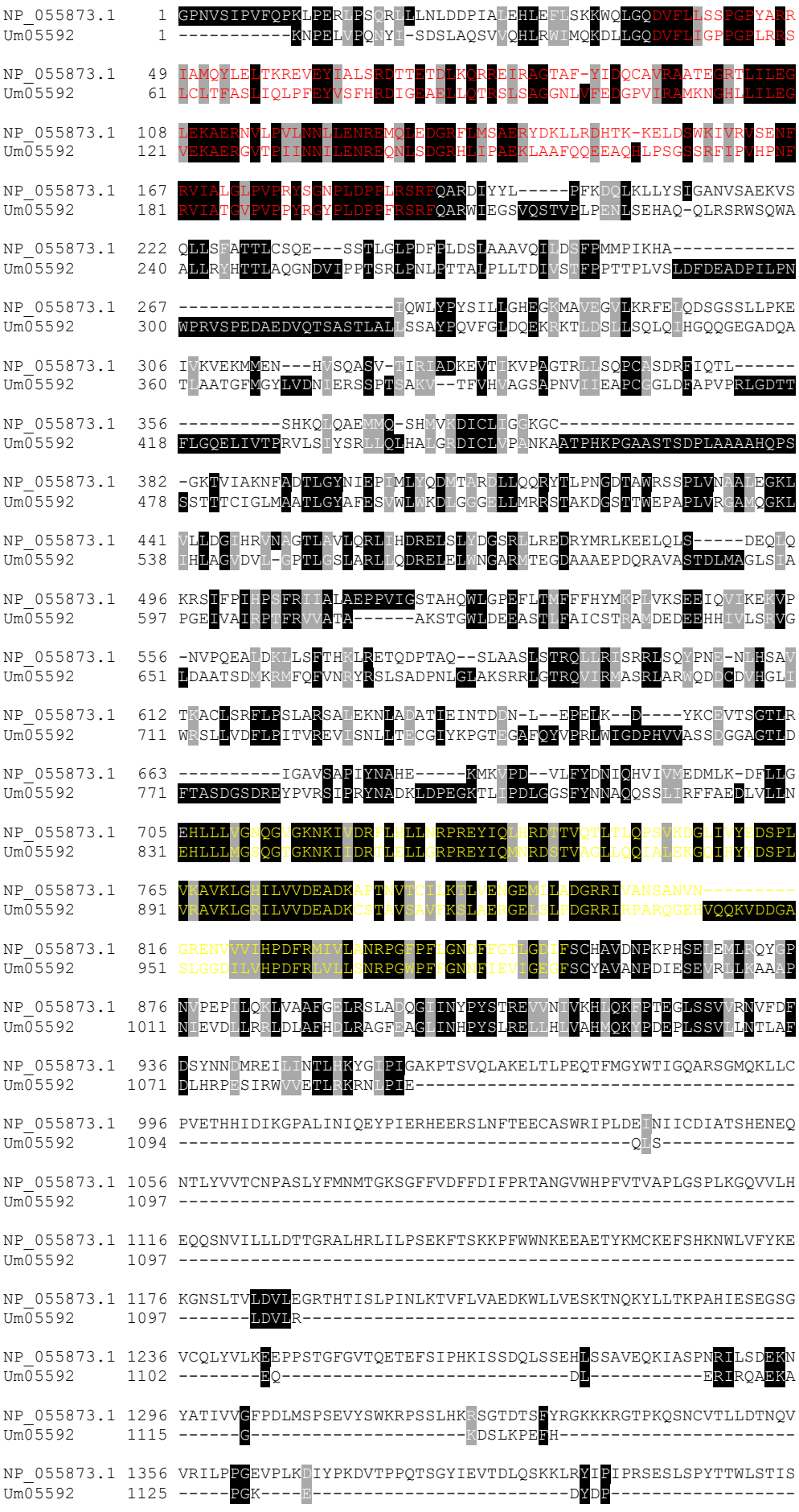

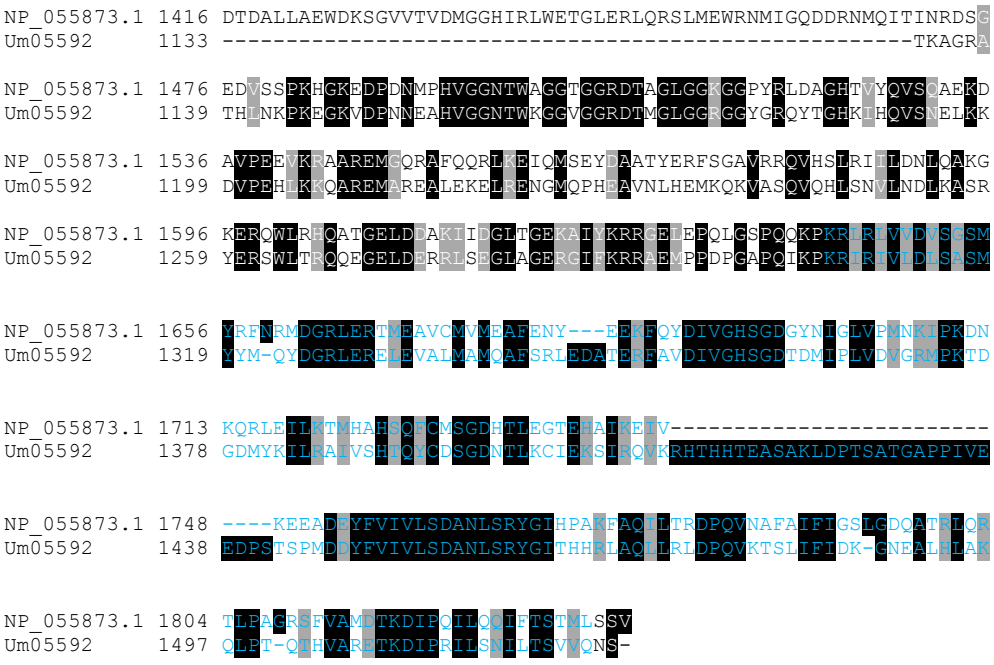


**Figure 5.10 Comparison of amino acid sequences of um05592 and NP_055873.1**

Amino acid sequences were aligned by using ClustalW (Thompson et al., 1994). Identical amino acids are marked by black boxes and similar amino acids are marked with grey boxes. Dashes indicate the gaps in the alignment. Red colored sequence showing first AAA_5 domain and yellow colored sequence showing second AAA_5 domain. Blue colored part highlighting vWA domain in both proteins.

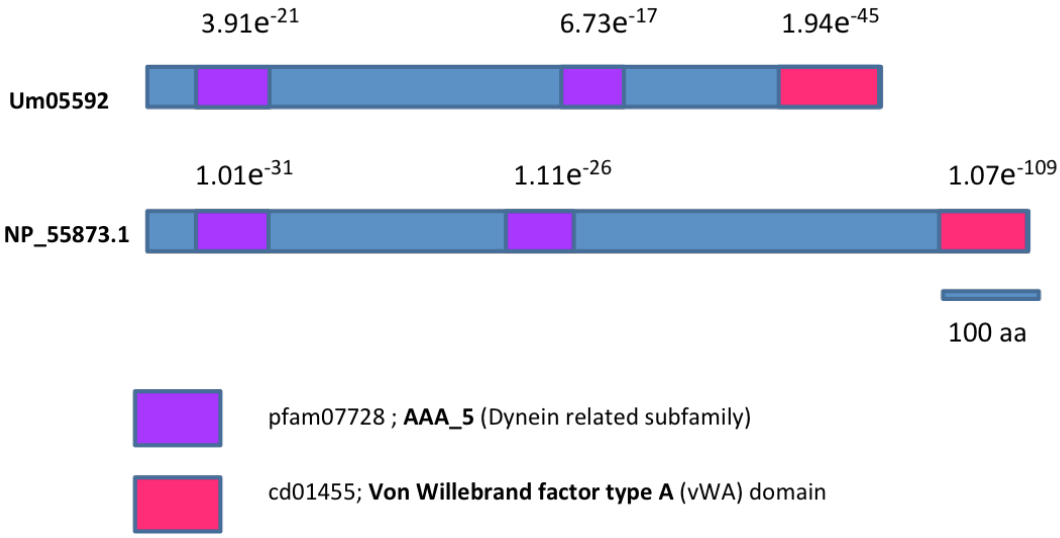


**Figure 5.11 Schematic representation of conserved domains in um05592 and NP_055873.1**

The putative gene product of um05592 to show relative positions of AAA_5 (purple) and vWA (pink) domains (**A**). The putative gene product of NP_055873.1 to show relative positions of conserved domains (**B**).

### 5.2.2.2 Subcellular localization of um05592

Prior to functional analysis of um05592, I set out to investigate subcellular localization of um05592. To this end, the ORF of the hypothetical protein was fused with GFP at C terminus under control of otef promoter. Um05592-GFP was found to localize to spherical structures. Co-expression with mCherry SKL proved that um05592 GFP signals are peroxisomal (Figure 5.12). Protein was also tagged with GFP from N-terminus and showed same subcellular localization (J. Klarig unpublished).

### 5.2.2.3 Targeted gene deletion of um05592

In order to analyse function of um05592, the ORF of the hypothetical protein was replaced with the Nat resistance gene cassette and um05592 knockout strain was obtained. Genomic DNA of the putative transformants was extracted and digested overnight with the *HindIII* enzyme. 1kb downstream sequence of um05592 was amplified with fluorescent-labelled nucleotides and used as a probe for southern blot. Replacement of gene with the resistance gene created size difference between wild type and mutant loci. Figure 5.13 shows relative band sizes for control (FB2 and SG200; 1 and 1.6kb) and Δum05592 transformants (1.6 and 3.9kb). The presence of 3.9kb band in transformants 3,4,5 and 6 confirmed the deletion of the um05592 gene.

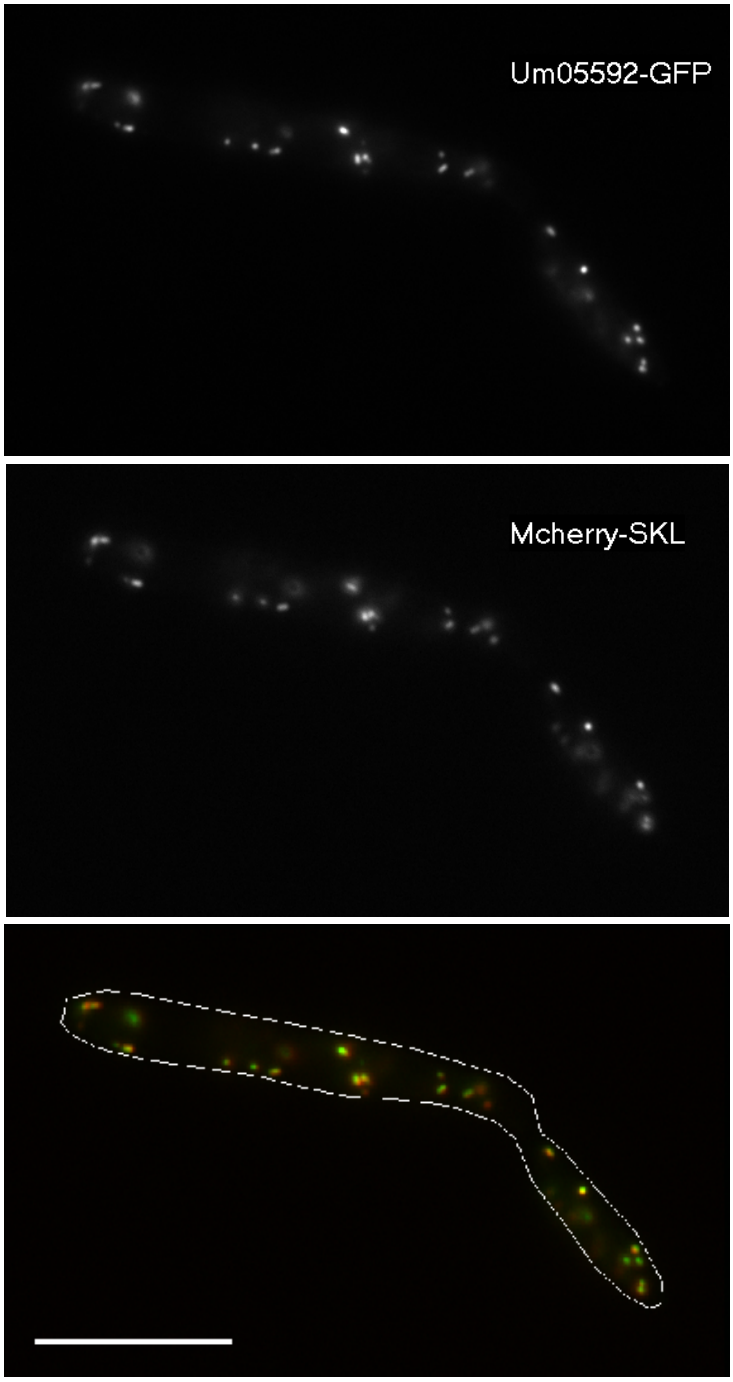


**Figure 5.12 Subcellular localization of um05592 in *U. maydis* cells.**
AB33*um*05592GChSKL strain was visualized to investigate subcellular localization of um05592. Yellow spots in merged image shows that um05592GFP localizes to peroxisomes. Scale bar= 10 µm.

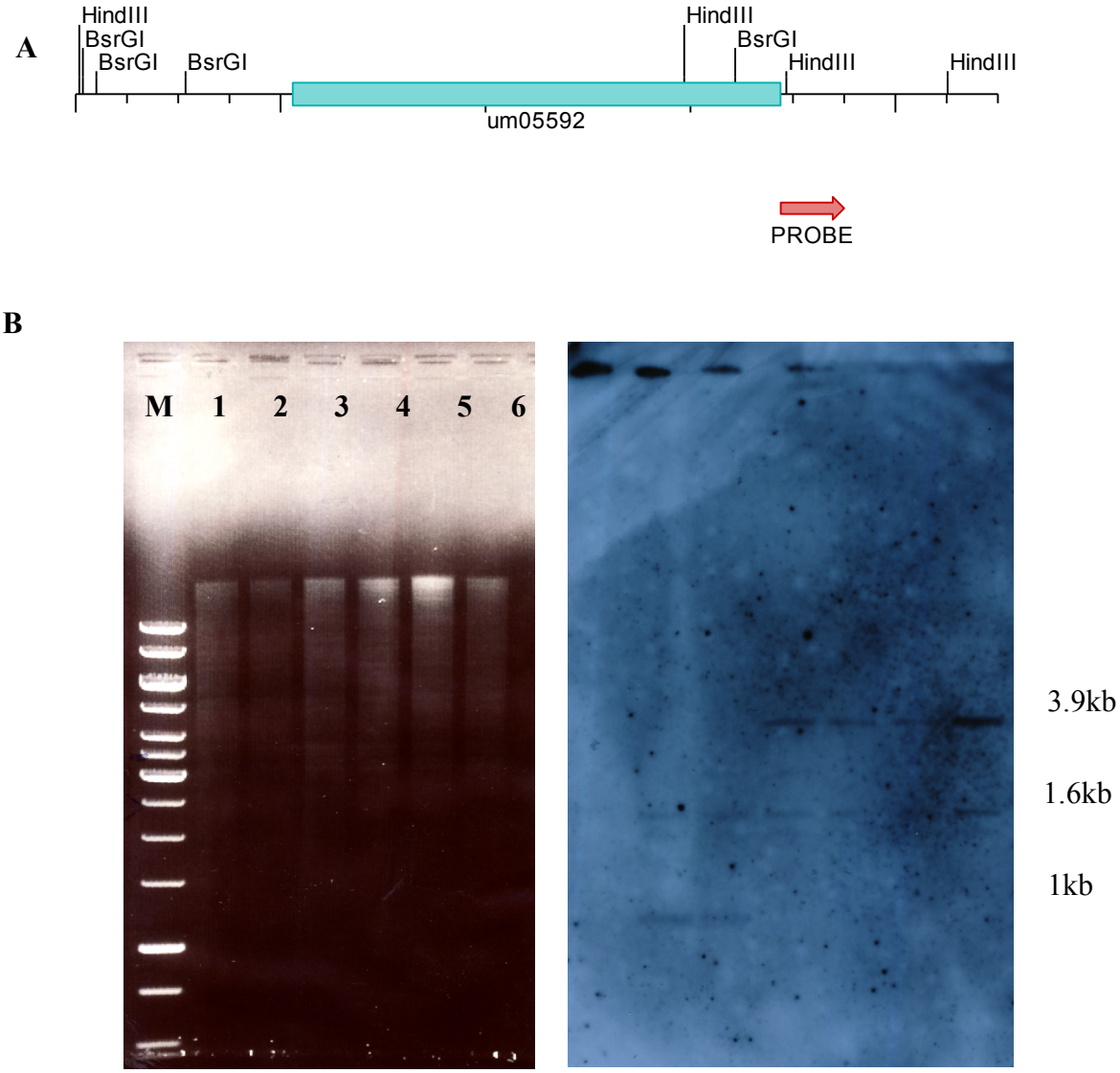


**Figure 5.13 Targeted gene deletion of um05592 in *U.maydis* FB2 and SG200 backgrounds**

(A) Targeted locus of um05592 which is replaced by resistance cassette and probe region to detect positive transformants are presented schematically. (B) Agarose gel showing fractionation of genomic DNAs digested with *Hind*III and corresponding southern blot probed with downstream 1 kb region of um05592 locus. Lanes 1 and 2 are control strains: FB2 and SG200 respectively. Lanes 3,4,5 and 6 are transformants confirmed as positive due to correct size difference after replacement of um05592 with resistance cassette.

#### 5.2.2.4 Lipid metabolism in Δ*um05592* cells

After finding out um05592 localization to peroxisomes, I checked potential role of um05592. There is no growth defect or obvious phenotype observed in yeast-like cells (J. Klarig, unpublished). Δ*um05592* cells were grown in rich media then inoculated serially onto minimal media plates supplemented with long (oleic acid-C18) and short chain (butyric acid-C4) fatty acids as sole carbon sources (Hynes et al., 2008). The results showed that absence of um05592 did not show colony phenotype or detectable growth defect on either butyric acid or oleic acid plates when compared with control plates (glucose) as presented in the Figure 5.14.

#### 5.2.2.5 Plant pathogenicity assay with Δ*um05592* cells

Although um05592 was found to be not essential for *Ustilago maydis* yeast cells to survive on fatty acid media, it might be important in lipid metabolism during hyphal growth which, in turn, may affect pathogenicity of the fungus. To test this, um05592 was deleted in solo pathogenic *U. maydis* strain (SG200) and plant infection was done accordingly. The results showed that, SG200*Δum05592* cells were able to infect plants and form tumours (Figure 5.15) as well as control cells (SG200). Quantitative analysis for tumour formation was done by counting maize leaves with tumours (Fuchs et al., 2005). When the results were compared between wild type and mutant cells statistically, it was found that there is no significant difference in tumour formation ratio between SG200 and SG200*Δum05592* infected plants (P=0.5994, Student t-test, Figure5.15).

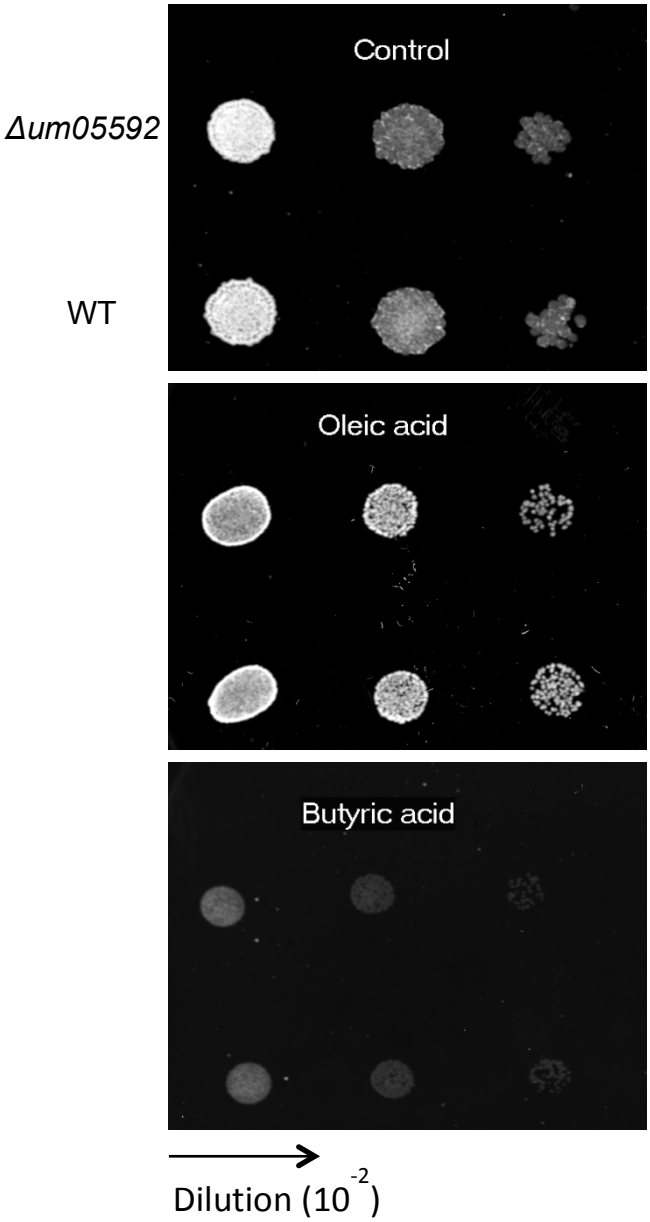


**Figure 5.14 Growth of Δ*um05592* cells on fatty acid containing media**

WT (FB2) and FB2Δ*um05592* strains were grown in CM-glucose liquid media overnight and applied by serial dilutions onto growth plates supplemented with minimal media containing glucose (1% w/v, control), oleic acid (1% v/v) and butyric acid (0,1% v/v) as carbon sources. Followed by three days incubation, *U. maydis* colonies showed that um05592 null mutant cells were able to grow on fatty acid containing media.


**Figure 5.15 Pathogenicity of SG200Δ*um05592* cells**

**(A)** Symptoms on maize leaves infected with progenitor strain (SG200) and um05592 deleted strain (SG200Δ*um05592*) are shown. Both strains are able to induce tumours. (**B**) Quantitative analysis of disease development after 12d infection with SG200 and SG200*Δum05592*. Bar chart showing no significant difference in tumor formation ratio (P=0.5994, Student t-test). Mean values ± standard error of the mean is given; P is indicated. n=53/46

## 5.3 Discussion

In the absence of long-range motility of peroxisomes, in Δ*Kin3* background, the cell shows a phenotype compared to control cells. In this phenotype, peroxisomes seem to localize as clusters rather than equal distribution all over the cell. Clustering might be a serious problem for the cell during cell division as reported in chloroplast clustering mutant in plants (Yang et al., 2011). When the peroxisome motility was analysed for 20 minutes, peroxisomes seemed to be able to redistribute but still present in clusters. So, long-range motility is not necessarily needed for peroxisome to change its position, i.e. re-distribute, within the cell. Redistribution of peroxisomes might be an indirect effect of other motility events in the cell such as cytoplasmic streaming, microtubule movements, and endoplasmic reticulum movements on peroxisome distribution (Barton et al., 2013; Kulic et al., 2008). This result suggests that long-range motility is important for even distribution of individual peroxisomes in the cell.

Organelle inheritance is important for the cells to maintain healthy cell function in the newly formed bud cells (Fagarasanu et al., 2005b). In the movies that were analysed, there is peroxisome traffic between mother and bud in both directions. Some long-range organelle motility events take place between mother and bud cells, which suggests that peroxisome transport may serve mother-bud communication and organelle inheritance. In 2h benomyl-treated cells, there were more peroxisomes in the bud cells with clustering phenotype at tip in the absence of peroxisome motility compared with control (DMSO-treated cells). This result implies that that long-range motility is not needed for peroxisome inheritance.

Video sequences of GFPSKL signals suggested that long-range motility is linked to peroxisome-peroxisome communications and division (budding) of peroxisomal vesicles in the cell. As reported for other organelles (e.g. mitochondria) and also for peroxisome in plant and mammalian cells, interaction between same kind of organelles is a common phenomenon which might be providing material transfer between organelles (Bonekamp et al., 2012; Jedd and Chua, 2002; Liu et al., 2009). In the video sequences analysed, it is a very common event that a moving peroxisome to engage with another peroxisome. These interactions may last long time with moving together or short time followed by a separation. In some cases it is observed that peroxisomal bodies are pinched off the peroxisomes during motility. Similar interactions were observed in mitochondria and called as transient fusions where organelles exchange proteins. Transient fusions are supported by motility and important for sufficient mitochondria function (Liu et al., 2009). Same phenomenon was investigated in mammalian peroxisomes but material exchange was not detected (Bonekamp et al., 2012). Further investigation is needed by using combination of peroxisome targeted different photoactivable fluorescent proteins to clarify role of peroxisome motility on transient interactions and peroxisomal buddings in *Ustilago maydis*.

In the second part of the chapter, function of a hypothetical protein of *Ustilago maydis*, um05592, was investigated. This protein is chosen because: i) it shows high identity to a homolog protein in human genome and ii) it has no corresponding homolog protein in the yeast genome. Besides, human homolog might have a potential role in disease related processes. Therefore, *Ustilago* cell system was used as a model to find out function of this protein.

Conserved domain search identified 2 functional domains: AAA_5(ATPases Associated with diverse cellular Activities) and vWA (von Willabrand factor type A) in both homolog proteins. Unfortunately, domain search did not provide selective information since both domains happen to be very general domains that have function in various different cellular events. When I checked the localization of um00592 protein we found that it is a peroxisomal protein. Localization was confirmed by mcherry SKL protein that is a widely used peroxisomal marker (see Chapter3). Once the localization was established I checked whether the protein has a role in fatty acid metabolism due to localization to POs and having ATPase domain. However, I could not observe any growth defect as um05592 deficient cells were still able to grow on long and short chain fatty acid media. A wide range of fatty acids has also been tested and the mutant did not give any growth phenotype that is different than wild type (S. Guimareas unpublished). This result suggests that um00592 is not essential for fatty acid metabolism. Finally, pathogenicty test was performed with Δ*um05592* cells in order to see if the protein has any role in hyphal growth and disease development. Plant pathogenicity assays showed that Δ*um05592* cells were able to develop corn smut disease as successfully as control cells. Therefore, um05592 was not essential for the cells to infect the maize plants.

## 6. General Conclusion

In this study, I report results that have provided fundamental information on peroxisome motility in filamentous fungi *Ustilago maydis*. The objectives were to analyse peroxisome motility along with underlying transport machinery, address motor-cargo interaction in peroxisome transport and determine the importance of peroxisome motility.

### 6.1 Peroxisomes switch between motility states: from static to fast moving

Microscopic analysis showed that peroxisomes are mobile organelles changing positions in the cell within a few seconds. Peroxisomes are sometimes static, sometimes oscillating and sometimes moving in long bidirectional manner. Quantitative analysis of motility in yeast-like and hyphal cells showed that run-length and frequency change according to cell types. Inhibitor studies indicated that long-range peroxisome motility is an energy-driven process. Both inhibitor and co-localization studies revealed that peroxisomes move along microtubules not actin filaments. Co-localization studies also revealed that only half of the peroxisomes were located on microtubules. Among these, half of the peroxisomes (25% of the total peroxisomes) moved in long-distance manner. A group of peroxisomes that seem independent from microtubules were only oscillating in short-range with a undirectional manner. This suggested that there are different peroxisome subpopulations in the cell; two groups are located on microtubules (see 6.3 for further discussion).

This work reports that Dynein and Kin3 are the molecular motors mediating peroxisome transport. Kin1 might have an indirect role in peroxisome movement by transporting dynein to plus ends of microtubules. Dynein and Kin3 transport early endosomes, secretory vesicles, polysomes and mRNPs in *Ustilago maydis* (Baumann et al., 2012; Higuchi et al., 2014; Schuster et al., 2011b; Wedlich-Söldner et al., 2002b).

### 6.2 Peroxisomes 'hitch a ride' on early endosomes

Kin3 is the predominating plus end motor in *Ustilago maydis*. It has role in the transport of early endosomes, secretory vesicles, polysomes, mRNPs and peroxisomes (Baumann et al., 2012; Higuchi et al., 2014; Schuster et al., 2011b; Wedlich-Söldner et al., 2002b)(see Chapter 3). Kin3 interacts with early endosomes via hok1 adaptor complex in *U. maydis* (Bielska et al., 2014). Recent reports showed that mRNPs and polysomes hitchhike on moving early endosomes (Baumann et al., 2012; Higuchi et al., 2014). This study validates that endoplasmic reticulum is another cargo of Kin3. It also presents evidence for that Kin3 transports peroxisomes and endoplasmic reticulum on early endosomes. Rrm4 serves as an adapter protein for early endosome interacting to mRNPs and polysomes (Baumann et al., 2012; Higuchi et al., 2014). Any accessory protein involved in early endosome interaction with peroxisome and/or endoplasmic reticulum remains to be shown.

### 6.3 Peroxisome dynamics is closely linked to peroxisome movements

When peroxisome motility is disturbed, in Δ*Kin3* and benomyl-treated cells, peroxisomes cluster particularly at the bud tip in yeast-like cells and hyphal tip in hyphae. This concludes that peroxisome motility might be important for even distribution of peroxisomes.

On many occasions, long-range peroxisome traffic was observed between mother and bud cells. In *S. cerevisae*, peroxisomes are inherited into bud cell via myosin-dependent transport from mother to bud cells (Fagarasanu et al., 2006; Fagarasanu et al., 2005a; Hoepfner et al., 2001). *In Ustilago maydis*, experimental line and direct observations verified that peroxisome traffic between mother and bud cell is not critical for peroxisome inheritance. Firstly, in Δ*Kin3* cells peroxisomes are accumulated in bud tips. There was no bud cell lacking peroxisome. Secondly, when benomyl was applied to stop peroxisome transport, many peroxisomes were observed at bud cells even after 2h treatment. These results indicate that long-range peroxisome motility does not mediate peroxisome inheritance.

Peroxisomes interact with other peroxisomes while moving. This study presents data showing that peroxisome motility couples with peroxisome fusion or fission. In some cases, peroxisomes that are moving opposite directions interact and move one direction together followed by separation. In mammalian cells, mitochondrial movements involve transient fusion events where mitochondria interact and exchange material while moving (Liu et al., 2009). Peroxisomes also interact on many occasions but no protein exchange was detected (Bonekamp et al., 2012). Besides transient fusion events, peroxisome division was also observed. It is likely that microtubules exert

forces for peroxisomes to divide while peroxisomes are moving. However, peroxisome fusion and fission events must be supported with more experiments.

In the last part of this study, I report findings on functional characterization of hypothetical protein um05592. Although it locates to peroxisomes, absence of this protein did not produce any defect in the growth of *Ustilago maydis*, which was tested in different conditions. This concludes that um05592 is a nonessential protein.

To sum up, major findings of this study are that (1) A group of peroxisomes are moving in long distances and directionally on microtubules, (2) Kin3 and dynein mediate peroxisome transport, (3) Early endosomes have role in peroxisome transport as well as endoplasmic reticulum and polysome transports, (4) Peroxisomes are interacting with each other while moving in *U. maydis.*

Along with these outcomes, this study raised many questions regarding to peroxisome motility and dynamics: if almost half of peroxisomes are present on microtubules, where are the other peroxisomes located, cytoplasm or anchored to somewhere in the cell? Is there any material transfer between peroxisomes and early endosomes? Are peroxisomes passive cargos of early endosome traffic?

This work attempts to present a comprehensive analysis on peroxisome transport and implications in peroxisomal dynamics. Although objectives of the study were achieved, still experimental set up and analysis was restricted by technical and time-related factors for in detail investigation. For example peroxisomes should be examined longer under microscope to observe

division and fusion events. However, gradual decrease and finally fading off of the fluorescence intensity prevents to assaying division and fission incidents. Findings of this study need to be supported especially by biochemical methods to unravel accessory proteins that mediate peroxisome interaction with other peroxisomes, early endosomes and other subcellular structures.

This study contributed to fundamental information in membrane traffic of *Ustilago maydis*. *Ustilago maydis* became an important tool to observe hitchhiking of organelles. Outcome of peroxisome motility indicated that intracellular traffic composition is closer to that of animal cells rather than yeast and plant cells.

## Bibliography


Adamikova, L., A. Straube, I. Schulz, and G. Steinberg. 2004. Calcium signaling is involved in dynein-dependent microtubule organization. *Mol Biol Cell*. 15:1969-1980.

Akhmanova, A., and J.A. Hammer, 3rd. 2010. Linking molecular motors to membrane cargo. *Curr Opin Cell Biol*. 22:479-487.

Alberti-Segui, C., F. Dietrich, R. Altmann-Johl, D. Hoepfner, and P. Philippsen. 2001. Cytoplasmic dynein is required to oppose the force that moves nuclei towards the hyphal tip in the filamentous ascomycete Ashbya gossypii. *Journal of cell science*. 114:975-986.

Ali, M.Y., S. Uemura, K. Adachi, H. Itoh, K. Kinosita, Jr., and S. Ishiwata. 2002. Myosin V is a left-handed spiral motor on the right-handed actin helix. *Nature structural biology*. 9:464-467.

Amos, L.A., and D. Schlieper. 2005. Microtubules and maps. *Advances in protein chemistry*. 71:257-298.

Araki, K., T. Horikawa, A.K. Chakraborty, K. Nakagawa, H. Itoh, M. Oka, Y. Funasaka, J. Pawelek, and M. Ichihashi. 2000. Small Gtpase rab3A is associated with melanosomes in melanoma cells. *Pigment cell research / sponsored by the European Society for Pigment Cell Research and the International Pigment Cell Society*. 13:332-336.

Aronov, S., R. Gelin-Licht, G. Zipor, L. Haim, E. Safran, and J.E. Gerst. 2007. mRNAs encoding polarity and exocytosis factors are cotransported with the cortical endoplasmic reticulum to the incipient bud in Saccharomyces cerevisiae. *Mol Cell Biol*. 27:3441-3455.

Babst, M., B. Wendland, E.J. Estepa, and S.D. Emr. 1998. The Vps4p AAA ATPase regulates membrane association of a Vps protein complex required for normal endosome function. *Embo J*. 17:2982-2993.

Bahadoran, P., E. Aberdam, F. Mantoux, R. Busca, K. Bille, N. Yalman, G. de Saint-Basile, R. Casaroli-Marano, J.P. Ortonne, and R. Ballotti. 2001. Rab27a: A key to melanosome transport in human melanocytes. *J Cell Biol*. 152:843-850.

Barton, K., N. Mathur, and J. Mathur. 2013. Simultaneous live-imaging of peroxisomes and the ER in plant cells suggests contiguity but no luminal continuity between the two organelles. *Frontiers in physiology*. 4:196.

Basse, C.W., S. Kolb, and R. Kahmann. 2002. A maize-specifically expressed gene cluster in Ustilago maydis. *Molecular microbiology*. 43:75-93.

Baumann, S., T. Pohlmann, M. Jungbluth, A. Brachmann, and M. Feldbrugge. 2012. Kinesin-3 and dynein mediate microtubule-dependent co-transport of mRNPs and endosomes. *J Cell Sci*. 125:2740-2752.

Bearer, E.L., J.A. DeGiorgis, R.A. Bodner, A.W. Kao, and T.S. Reese. 1993. Evidence for myosin motors on organelles in squid axoplasm. *Proceedings of the National Academy of Sciences of the United States of America*. 90:11252-11256.

Becht, P., J. Konig, and M. Feldbrugge. 2006. The RNA-binding protein Rrm4 is essential for polarity in Ustilago maydis and shuttles along microtubules. *J Cell Sci*. 119:4964-4973.

Belgareh, N., G. Rabut, S.W. Bai, M. van Overbeek, J. Beaudouin, N. Daigle, O.V. Zatsepina, F. Pasteau, V. Labas, M. Fromont-Racine, J. Ellenberg, and V. Doye. 2001. An evolutionarily conserved NPC

subcomplex, which redistributes in part to kinetochores in mammalian cells. *The Journal of cell biology*. 154:1147-1160.
Berepiki, A., A. Lichius, J.Y. Shoji, J. Tilsner, and N.D. Read. 2010. F-actin dynamics in Neurospora crassa. *Eukaryot Cell*. 9:547-557.
Beushausen, S., A. Kladakis, and H. Jaffe. 1993. Kinesin light chains: identification and characterization of a family of proteins from the optic lobe of the squid Loligo pealii. *DNA and cell biology*. 12:901-909.
Bharti, P., W. Schliebs, T. Schievelbusch, A. Neuhaus, C. David, K. Kock, C. Herrmann, H.E. Meyer, S. Wiese, B. Warscheid, C. Theiss, and R. Erdmann. 2011. PEX14 is required for microtubule-based peroxisome motility in human cells. *J Cell Sci*. 124:1759-1768.
Bielska, E., M. Schuster, Y. Roger, A. Berepiki, D.M. Soanes, N.J. Talbot, and G. Steinberg. 2014. Hook is an adapter that coordinates kinesin-3 and dynein cargo attachment on early endosomes. *J Cell Biol*. 204:989-1007.
Binns, D., T. Januszewski, Y. Chen, J. Hill, V.S. Markin, Y. Zhao, C. Gilpin, K.D. Chapman, R.G. Anderson, and J.M. Goodman. 2006. An intimate collaboration between peroxisomes and lipid bodies. *J Cell Biol*. 173:719-731.
Birnboim, H.C. 1983. A rapid alkaline extraction method for the isolation of plasmid DNA. *Methods in enzymology*. 100:243-255.
Boevink, P., K. Oparka, S. Santa Cruz, B. Martin, A. Betteridge, and C. Hawes. 1998. Stacks on tracks: the plant Golgi apparatus traffics on an actin/ER network. *The Plant journal : for cell and molecular biology*. 15:441-447.
Bonekamp, N.A., P. Sampaio, F.V. de Abreu, G.H. Luers, and M. Schrader. 2012. Transient complex interactions of mammalian peroxisomes without exchange of matrix or membrane marker proteins. *Traffic*. 13:960-978.
Bonekamp, N.A., and M. Schrader. 2012. Transient complex peroxisomal interactions: A new facet of peroxisome dynamics in mammalian cells. *Commun Integr Biol*. 5:534-537.
Bottin, A., J. Kamper, and R. Kahmann. 1996. Isolation of a carbon source-regulated gene from Ustilago maydis. *Molecular & general genetics : MGG*. 253:342-352.
Brachmann, A., G. Weinzierl, J. Kamper, and R. Kahmann. 2001. Identification of genes in the bW/bE regulatory cascade in Ustilago maydis. *Molecular microbiology*. 42:1047-1063.
Brefort, T., G. Doehlemann, A. Mendoza-Mendoza, S. Reissmann, A. Djamei, and R. Kahmann. 2009. Ustilago maydis as a Pathogen. *Annual review of phytopathology*. 47:423-445.
Bridgman, P.C. 2004. Myosin-dependent transport in neurons. *Journal of neurobiology*. 58:164-174.
Brocard, C., and A. Hartig. 2006a. Peroxisome targeting signal 1: is it really a simple tripeptide? *Biochim Biophys Acta*. 1763:1565-1573.
Brocard, C., and A. Hartig. 2006b. Peroxisome targeting signal 1: is it really a simple tripeptide? *Biochim Biophys Acta*. 1763:1565-1573.
Brocard, C.B., K.K. Boucher, C. Jedeszko, P.K. Kim, and P.A. Walton. 2005. Requirement for microtubules and dynein motors in the earliest stages of peroxisome biogenesis. *Traffic*. 6:386-395.

Bucci, C., R.G. Parton, I.H. Mather, H. Stunnenberg, K. Simons, B. Hoflack, and M. Zerial. 1992. The small GTPase rab5 functions as a regulatory factor in the early endocytic pathway. *Cell*. 70:715-728.

Burkhardt, J.K., C.J. Echeverri, T. Nilsson, and R.B. Vallee. 1997. Overexpression of the dynamitin (p50) subunit of the dynactin complex disrupts dynein-dependent maintenance of membrane organelle distribution. *J Cell Biol*. 139:469-484.

Carazo-Salas, R.E., C. Antony, and P. Nurse. 2005. The kinesin Klp2 mediates polarization of interphase microtubules in fission yeast. *Science*. 309:297-300.

Chang, J., A. Fagarasanu, and R.A. Rachubinski. 2007. Peroxisomal peripheral membrane protein Yllnp1p is required for peroxisome inheritance and influences the dimorphic transition in the yeast Yarrowia lipolytica. *Eukaryot Cell*. 6:1528-1537.

Chang, J., F.D. Mast, A. Fagarasanu, D.A. Rachubinski, G.A. Eitzen, J.B. Dacks, and R.A. Rachubinski. 2009. Pex3 peroxisome biogenesis proteins function in peroxisome inheritance as class V myosin receptors. *J Cell Biol*. 187:233-246.

Cho, C., and R.D. Vale. 2012. The mechanism of dynein motility: insight from crystal structures of the motor domain. *Biochimica et biophysica acta*. 1823:182-191.

Clayton, P.T., B.D. Lake, M. Hjelm, J.B. Stephenson, G.T. Besley, R.J. Wanders, A.W. Schram, J.M. Tager, R.B. Schutgens, and A.M. Lawson. 1988. Bile acid analyses in "pseudo-Zellweger" syndrome; clues to the defect in peroxisomal beta-oxidation. *J Inherit Metab Dis*. 11 Suppl 2:165-168.

D'Angelo, M.A., D.J. Anderson, E. Richard, and M.W. Hetzer. 2006. Nuclear pores form de novo from both sides of the nuclear envelope. *Science*. 312:440-443.

De Luca, M., D.A. Facey, E.J. Favaloro, M.S. Hertzberg, J.C. Whisstock, T. McNally, R.K. Andrews, and M.C. Berndt. 2000. Structure and function of the von Willebrand factor A1 domain: analysis with monoclonal antibodies reveals distinct binding sites involved in recognition of the platelet membrane glycoprotein Ib-IX-V complex and ristocetin-dependent activation. *Blood*. 95:164-172.

Delille, H.K., B. Agricola, S.C. Guimaraes, H. Borta, G.H. Luers, M. Fransen, and M. Schrader. 2010. Pex11pbeta-mediated growth and division of mammalian peroxisomes follows a maturation pathway. *J Cell Sci*. 123:2750-2762.

Diefenbach, R.J., E. Diefenbach, M.W. Douglas, and A.L. Cunningham. 2002. The heavy chain of conventional kinesin interacts with the SNARE proteins SNAP25 and SNAP23. *Biochemistry*. 41:14906-14915.

Diefenbach, R.J., M. Miranda-Saksena, M.W. Douglas, and A.L. Cunningham. 2008. Transport and egress of herpes simplex virus in neurons. *Reviews in medical virology*. 18:35-51.

Dienstbier, M., F. Boehl, X. Li, and S.L. Bullock. 2009. Egalitarian is a selective RNA-binding protein linking mRNA localization signals to the dynein motor. *Genes Dev*. 23:1546-1558.

Djamei, A., and R. Kahmann. 2012. Ustilago maydis: dissecting the molecular interface between pathogen and plant. *PLoS pathogens*. 8:e1002955.

Doehlemann, G., R. Wahl, M. Vranes, R.P. de Vries, J. Kamper, and R. Kahmann. 2008. Establishment of compatibility in the Ustilago maydis/maize pathosystem. *Journal of plant physiology*. 165:29-40.

Egan, M.J., M.A. McClintock, and S.L. Reck-Peterson. 2012a. Microtubule-based transport in filamentous fungi. *Current opinion in microbiology*. 15:637-645.

Egan, M.J., K. Tan, and S.L. Reck-Peterson. 2012b. Lis1 is an initiation factor for dynein-driven organelle transport. *J Cell Biol*. 197:971-982.

Esaki, M., and T. Ogura. 2010. ATP-bound form of the D1 AAA domain inhibits an essential function of Cdc48p/p97. *Biochemistry and cell biology = Biochimie et biologie cellulaire*. 88:109-117.

Estrada, P., J. Kim, J. Coleman, L. Walker, B. Dunn, P. Takizawa, P. Novick, and S. Ferro-Novick. 2003. Myo4p and She3p are required for cortical ER inheritance in Saccharomyces cerevisiae. *J Cell Biol*. 163:1255-1266.

Fagarasanu, A., M. Fagarasanu, G.A. Eitzen, J.D. Aitchison, and R.A. Rachubinski. 2006. The peroxisomal membrane protein Inp2p is the peroxisome-specific receptor for the myosin V motor Myo2p of Saccharomyces cerevisiae. *Dev Cell*. 10:587-600.

Fagarasanu, A., M. Fagarasanu, and R.A. Rachubinski. 2007. Maintaining peroxisome populations: a story of division and inheritance. *Annu Rev Cell Dev Biol*. 23:321-344.

Fagarasanu, A., F.D. Mast, B. Knoblach, Y. Jin, M.J. Brunner, M.R. Logan, J.N. Glover, G.A. Eitzen, J.D. Aitchison, L.S. Weisman, and R.A. Rachubinski. 2009. Myosin-driven peroxisome partitioning in S. cerevisiae. *J Cell Biol*. 186:541-554.

Fagarasanu, M., A. Fagarasanu, Y.Y. Tam, J.D. Aitchison, and R.A. Rachubinski. 2005a. Inp1p is a peroxisomal membrane protein required for peroxisome inheritance in Saccharomyces cerevisiae. *J Cell Biol*. 169:765-775.

Fagarasanu, M., A. Fagarasanu, Y.Y. Tam, J.D. Aitchison, and R.A. Rachubinski. 2005b. Inp1p is a peroxisomal membrane protein required for peroxisome inheritance in Saccharomyces cerevisiae. *J Cell Biol*. 169:765-775.

Feldbrugge, M., J. Kamper, G. Steinberg, and R. Kahmann. 2004. Regulation of mating and pathogenic development in Ustilago maydis. *Current opinion in microbiology*. 7:666-672.

Fink, G., and G. Steinberg. 2006. Dynein-dependent motility of microtubules and nucleation sites supports polarization of the tubulin array in the fungus Ustilago maydis. *Mol Biol Cell*. 17:3242-3253.

Fischer, R., N. Zekert, and N. Takeshita. 2008. Polarized growth in fungi--interplay between the cytoskeleton, positional markers and membrane domains. *Molecular microbiology*. 68:813-826.

Fuchs, F., and B. Westermann. 2005. Role of Unc104/KIF1-related motor proteins in mitochondrial transport in Neurospora crassa. *Mol Biol Cell*. 16:153-161.

Fuchs, U., I. Manns, and G. Steinberg. 2005. Microtubules are dispensable for the initial pathogenic development but required for long-distance hyphal growth in the corn smut fungus Ustilago maydis. *Mol Biol Cell*. 16:2746-2758.

Fujihara, N., A. Sakaguchi, S. Tanaka, S. Fujii, G. Tsuji, T. Shiraishi, R. O'Connell, and Y. Kubo. 2010. Peroxisome biogenesis factor PEX13 is required for appressorium-mediated plant infection by the anthracnose fungus Colletotrichum orbiculare. *Mol Plant Microbe Interact*. 23:436-445.

Garrido, E., U. Voss, P. Muller, S. Castillo-Lluva, R. Kahmann, and J. Perez-Martin. 2004. The induction of sexual development and virulence in the smut fungus Ustilago maydis depends on Crk1, a novel MAPK protein. *Genes & development*. 18:3117-3130.

Geuze, H.J., J.L. Murk, A.K. Stroobants, J.M. Griffith, M.J. Kleijmeer, A.J. Koster, A.J. Verkleij, B. Distel, and H.F. Tabak. 2003. Involvement of the endoplasmic reticulum in peroxisome formation. *Mol Biol Cell*. 14:2900-2907.

Goldstein, L.S., and R.D. Vale. 1991. Motor proteins. A brave new world for dynein. *Nature*. 352:569-570.

Goodson, H.V., C. Valetti, and T.E. Kreis. 1997. Motors and membrane traffic. *Current opinion in cell biology*. 9:18-28.

Goto, Y., and T. Asada. 2007. Excessive expression of the plant kinesin TBK5 converts cortical and perinuclear microtubules into a radial array emanating from a single focus. *Plant Cell Physiol*. 48:753-761.

Gould, S.J., G.A. Keller, N. Hosken, J. Wilkinson, and S. Subramani. 1989. A conserved tripeptide sorts proteins to peroxisomes. *J Cell Biol*. 108:1657-1664.

Grant, B.D., and M. Sato. 2006. Intracellular trafficking. *WormBook : the online review of C. elegans biology*:1-9.

Gronemeyer, T., S. Wiese, S. Grinhagens, L. Schollenberger, A. Satyagraha, L.A. Huber, H.E. Meyer, B. Warscheid, and W.W. Just. 2013. Localization of Rab proteins to peroxisomes: a proteomics and immunofluorescence study. *FEBS Lett*. 587:328-338.

Haan, G.J., R.J. Baerends, A.M. Krikken, M. Otzen, M. Veenhuis, and I.J. van der Klei. 2006. Reassembly of peroxisomes in Hansenula polymorpha pex3 cells on reintroduction of Pex3p involves the nuclear envelope. *FEMS Yeast Res*. 6:186-194.

Hackney, D.D. 1996. The kinetic cycles of myosin, kinesin, and dynein. *Annual review of physiology*. 58:731-750.

Hammer, J.A., 3rd, and J.R. Sellers. 2012. Walking to work: roles for class V myosins as cargo transporters. *Nat Rev Mol Cell Biol*. 13:13-26.

Hanahan, D. 1983. Studies on transformation of Escherichia coli with plasmids. *Journal of molecular biology*. 166:557-580.

Harada, A., Y. Takei, Y. Kanai, Y. Tanaka, S. Nonaka, and N. Hirokawa. 1998. Golgi vesiculation and lysosome dispersion in cells lacking cytoplasmic dynein. *J Cell Biol*. 141:51-59.

Harrell, J.M., P.J. Murphy, Y. Morishima, H. Chen, J.F. Mansfield, M.D. Galigniana, and W.B. Pratt. 2004. Evidence for glucocorticoid receptor transport on microtubules by dynein. *J Biol Chem*. 279:54647-54654.

Hartmann, H.A., J. Kruger, F. Lottspeich, and R. Kahmann. 1999. Environmental signals controlling sexual development of the corn Smut fungus Ustilago maydis through the transcriptional regulator Prf1. *The Plant cell*. 11:1293-1306.

Heath, I.B. 1980. Variant mitoses in lower eukaryotes: indicators of the evolution of mitosis. *International review of cytology*. 64:1-80.
Heiland, I., and R. Erdmann. 2005. Biogenesis of peroxisomes. Topogenesis of the peroxisomal membrane and matrix proteins. *FEBS J*. 272:2362-2372.
Higaki, T., N. Kutsuna, E. Okubo, T. Sano, and S. Hasezawa. 2006. Actin microfilaments regulate vacuolar structures and dynamics: dual observation of actin microfilaments and vacuolar membrane in living tobacco BY-2 Cells. *Plant Cell Physiol*. 47:839-852.
Higuchi, Y., P. Ashwin, Y. Roger, and G. Steinberg. 2014. Early endosome motility spatially organizes polysome distribution. *J Cell Biol*. 204:343-357.
Hirokawa, N., Y. Noda, Y. Tanaka, and S. Niwa. 2009. Kinesin superfamily motor proteins and intracellular transport. *Nature Reviews Molecular Cell Biology* 10:682-696.
Hirokawa, N., and R. Takemura. 2005. Molecular motors and mechanisms of directional transport in neurons. *Nature reviews. Neuroscience*. 6:201-214.
Hirose, S., N. Yaginuma, and Y. Inada. 1974. Disruption of charge separation followed by that of the proton gradient in the mitochondrial membrane by CCCP. *Journal of biochemistry*. 76:213-216.
Hirotsune, S. 2008. [Molecular mechanism of lissencephaly--how LIS1 and NDEL1 regulate cytoplasmic dynein?]. *Brain and nerve = Shinkei kenkyu no shinpo*. 60:375-381.
Hoepfner, D., D. Schildknegt, I. Braakman, P. Philippsen, and H.F. Tabak. 2005. Contribution of the endoplasmic reticulum to peroxisome formation. *Cell*. 122:85-95.
Hoepfner, D., M. van den Berg, P. Philippsen, H.F. Tabak, and E.H. Hettema. 2001. A role for Vps1p, actin, and the Myo2p motor in peroxisome abundance and inheritance in Saccharomyces cerevisiae. *J Cell Biol*. 155:979-990.
Holleran, E.A., S. Karki, and E.L. Holzbaur. 1998. The role of the dynactin complex in intracellular motility. *Int Rev Cytol*. 182:69-109.
Holliday, R. 1974. Molecular aspects of genetic exchange and gene conversion. *Genetics*. 78:273-287.
Hoogenraad, C.C., A. Akhmanova, S.A. Howell, B.R. Dortland, C.I. De Zeeuw, R. Willemsen, P. Visser, F. Grosveld, and N. Galjart. 2001. Mammalian Golgi-associated Bicaudal-D2 functions in the dynein-dynactin pathway by interacting with these complexes. *Embo J*. 20:4041-4054.
Horst, R.J., G. Doehlemann, R. Wahl, J. Hofmann, A. Schmiedl, R. Kahmann, J. Kamper, and L.M. Voll. 2010. A model of Ustilago maydis leaf tumor metabolism. *Plant signaling & behavior*. 5:1446-1449.
Huber, C.M., R. Saffrich, W. Ansorge, and W.W. Just. 1999. Receptor-mediated regulation of peroxisomal motility in CHO and endothelial cells. *Embo J*. 18:5476-5485.
Hume, A.N., L.M. Collinson, A. Rapak, A.Q. Gomes, C.R. Hopkins, and M.C. Seabra. 2001. Rab27a regulates the peripheral distribution of melanosomes in melanocytes. *J Cell Biol*. 152:795-808.

Hynes, M.J., S.L. Murray, G.S. Khew, and M.A. Davis. 2008. Genetic analysis of the role of peroxisomes in the utilization of acetate and fatty acids in Aspergillus nidulans. *Genetics*. 178:1355-1369.

Islinger, M., S. Grille, H.D. Fahimi, and M. Schrader. 2012. The peroxisome: an update on mysteries. *Histochem Cell Biol*. 137:547-574.

Issemann, I., R. Prince, J. Tugwood, and S. Green. 1992. A role for fatty acids and liver fatty acid binding protein in peroxisome proliferation? *Biochem Soc Trans*. 20:824-827.

Jedd, G., and N.H. Chua. 2002. Visualization of peroxisomes in living plant cells reveals acto-myosin-dependent cytoplasmic streaming and peroxisome budding. *Plant Cell Physiol*. 43:384-392.

Jezek, P., and L. Hlavata. 2005. Mitochondria in homeostasis of reactive oxygen species in cell, tissues, and organism. *Int J Biochem Cell Biol*. 37:2478-2503.

Jourdain, I., D. Sontam, C. Johnson, C. Dillies, and J.S. Hyams. 2008. Dynamin-dependent biogenesis, cell cycle regulation and mitochondrial association of peroxisomes in fission yeast. *Traffic*. 9:353-365.

Jung, M.K., I.B. Wilder, and B.R. Oakley. 1992. Amino acid alterations in the benA (beta-tubulin) gene of Aspergillus nidulans that confer benomyl resistance. *Cell motility and the cytoskeleton*. 22:170-174.

Kahmann, R., T. Romeis, M. Bolker, and J. Kamper. 1995. Control of mating and development in Ustilago maydis. *Current opinion in genetics & development*. 5:559-564.

Kamper, J., R. Kahmann, M. Bolker, L.J. Ma, T. Brefort, B.J. Saville, F. Banuett, J.W. Kronstad, S.E. Gold, O. Muller, M.H. Perlin, H.A. Wosten, R. de Vries, J. Ruiz-Herrera, C.G. Reynaga-Pena, K. Snetselaar, M. McCann, J. Perez-Martin, M. Feldbrugge, C.W. Basse, G. Steinberg, J.I. Ibeas, W. Holloman, P. Guzman, M. Farman, J.E. Stajich, R. Sentandreu, J.M. Gonzalez-Prieto, J.C. Kennell, L. Molina, J. Schirawski, A. Mendoza-Mendoza, D. Greilinger, K. Munch, N. Rossel, M. Scherer, M. Vranes, O. Ladendorf, V. Vincon, U. Fuchs, B. Sandrock, S. Meng, E.C. Ho, M.J. Cahill, K.J. Boyce, J. Klose, S.J. Klosterman, H.J. Deelstra, L. Ortiz-Castellanos, W. Li, P. Sanchez-Alonso, P.H. Schreier, I. Hauser-Hahn, M. Vaupel, E. Koopmann, G. Friedrich, H. Voss, T. Schluter, J. Margolis, D. Platt, C. Swimmer, A. Gnirke, F. Chen, V. Vysotskaia, G. Mannhaupt, U. Guldener, M. Munsterkotter, D. Haase, M. Oesterheld, H.W. Mewes, E.W. Mauceli, D. DeCaprio, C.M. Wade, J. Butler, S. Young, D.B. Jaffe, S. Calvo, C. Nusbaum, J. Galagan, and B.W. Birren. 2006. Insights from the genome of the biotrophic fungal plant pathogen Ustilago maydis. *Nature*. 444:97-101.

Kanai, Y., N. Dohmae, and N. Hirokawa. 2004. Kinesin transports RNA: isolation and characterization of an RNA-transporting granule. *Neuron*. 43:513-525.

Kanai, Y., Y. Okada, Y. Tanaka, A. Harada, S. Terada, and N. Hirokawa. 2000. KIF5C, a novel neuronal kinesin enriched in motor neurons. *J Neurosci*. 20:6374-6384.

Kardon, J.R., and R.D. Vale. 2009. Regulators of the cytoplasmic dynein motor. *Nat Rev Mol Cell Biol*. 10:854-865.

Karki, S., and E.L. Holzbaur. 1999. Cytoplasmic dynein and dynactin in cell division and intracellular transport. *Curr Opin Cell Biol*. 11:45-53.
Keon, J.P., G.A. White, and J.A. Hargreaves. 1991. Isolation, characterization and sequence of a gene conferring resistance to the systemic fungicide carboxin from the maize smut pathogen, Ustilago maydis. *Current genetics*. 19:475-481.
Kern, J.V., Y.V. Zhang, S. Kramer, J.E. Brenman, and T.M. Rasse. 2013. The kinesin-3, unc-104 regulates dendrite morphogenesis and synaptic development in Drosophila. *Genetics*. 195:59-72.
Kim, P.K., R.T. Mullen, U. Schumann, and J. Lippincott-Schwartz. 2006. The origin and maintenance of mammalian peroxisomes involves a de novo PEX16-dependent pathway from the ER. *J Cell Biol*. 173:521-532.
Kimura, A., Y. Takano, I. Furusawa, and T. Okuno. 2001. Peroxisomal metabolic function is required for appressorium-mediated plant infection by Colletotrichum lagenarium. *Plant Cell*. 13:1945-1957.
King, S.M. 2002. Dyneins motor on in plants. *Traffic*. 3:930-931.
Kitazono, A.A. 2009. Improved gap-repair cloning method that uses oligonucleotides to target cognate sequences. *Yeast*. 26:497-505.
Klopfenstein, D.R., M. Tomishige, N. Stuurman, and R.D. Vale. 2002. Role of phosphatidylinositol(4,5)bisphosphate organization in membrane transport by the Unc104 kinesin motor. *Cell*. 109:347-358.
Klopfenstein, D.R., and R.D. Vale. 2004. The lipid binding pleckstrin homology domain in UNC-104 kinesin is necessary for synaptic vesicle transport in Caenorhabditis elegans. *Mol Biol Cell*. 15:3729-3739.
Klose, J., and J.W. Kronstad. 2006. The multifunctional beta-oxidation enzyme is required for full symptom development by the biotrophic maize pathogen Ustilago maydis. *Eukaryot Cell*. 5:2047-2061.
Koch, A., G. Schneider, G.H. Luers, and M. Schrader. 2004. Peroxisome elongation and constriction but not fission can occur independently of dynamin-like protein 1. *J Cell Sci*. 117:3995-4006.
Koch, A., Y. Yoon, N.A. Bonekamp, M.A. McNiven, and M. Schrader. 2005. A role for Fis1 in both mitochondrial and peroxisomal fission in mammalian cells. *Mol Biol Cell*. 16:5077-5086.
Krendel, M., and M.S. Mooseker. 2005. Myosins: tails (and heads) of functional diversity. *Physiology (Bethesda)*. 20:239-251.
Kress, W., H. Mutschler, and E. Weber-Ban. 2009. Both ATPase domains of ClpA are critical for processing of stable protein structures. *J Biol Chem*. 284:31441-31452.
Kretschmer, M., J. Klose, and J.W. Kronstad. 2012. Defects in mitochondrial and peroxisomal beta-oxidation influence virulence in the maize pathogen Ustilago maydis. *Eukaryot Cell*. 11:1055-1066.
Kulic, I.M., A.E. Brown, H. Kim, C. Kural, B. Blehm, P.R. Selvin, P.C. Nelson, and V.I. Gelfand. 2008. The role of microtubule movement in bidirectional organelle transport. *Proc Natl Acad Sci U S A*. 105:10011-10016.
Kunze, M., I. Pracharoenwattana, S.M. Smith, and A. Hartig. 2006. A central role for the peroxisomal membrane in glyoxylate cycle function. *Biochim Biophys Acta*. 1763:1441-1452.

Kural, C., H. Kim, S. Syed, G. Goshima, V.I. Gelfand, and P.R. Selvin. 2005. Kinesin and dynein move a peroxisome in vivo: a tug-of-war or coordinated movement? *Science*. 308:1469-1472.

Lalwani, N.D., M.K. Reddy, S. Ghosh, S.D. Barnard, J.A. Molello, and J.K. Reddy. 1985. Induction of fatty acid beta-oxidation and peroxisome proliferation in the liver of rhesus monkeys by DL-040, a new hypolipidemic agent. *Biochem Pharmacol*. 34:3473-3482.

Langford, G.M. 2002. Myosin-V, a versatile motor for short-range vesicle transport. *Traffic*. 3:859-865.

Lanver, D., P. Berndt, M. Tollot, V. Naik, M. Vranes, T. Warmann, K. Munch, N. Rossel, and R. Kahmann. 2014. Plant surface cues prime Ustilago maydis for biotrophic development. *PLoS pathogens*. 10:e1004272.

Larkin, M.A., G. Blackshields, N.P. Brown, R. Chenna, P.A. McGettigan, H. McWilliam, F. Valentin, I.M. Wallace, A. Wilm, R. Lopez, J.D. Thompson, T.J. Gibson, and D.G. Higgins. 2007. Clustal W and Clustal X version 2.0. *Bioinformatics*. 23:2947-2948.

Lazarow, P.B., and Y. Fujiki. 1985. Biogenesis of peroxisomes. *Annual review of cell biology*. 1:489-530.

Lee, Y.R., H.M. Giang, and B. Liu. 2001. A novel plant kinesin-related protein specifically associates with the phragmoplast organelles. *Plant Cell*. 13:2427-2439.

Lehmler, C., G. Steinberg, K.M. Snetselaar, M. Schliwa, R. Kahmann, and M. Bolker. 1997. Identification of a motor protein required for filamentous growth in Ustilago maydis. *Embo J*. 16:3464-3473.

Lenz, J.H., I. Schuchardt, A. Straube, and G. Steinberg. 2006. A dynein loading zone for retrograde endosome motility at microtubule plus-ends. *Embo J*. 25:2275-2286.

Letunic, I., T. Doerks, and P. Bork. 2012. SMART 7: recent updates to the protein domain annotation resource. *Nucleic acids research*. 40:D302-305.

Liebe, S., and D. Menzel. 1995. Actomyosin-based motility of endoplasmic reticulum and chloroplasts in Vallisneria mesophyll cells. *Biol Cell*. 85:207-222.

Ling, S.C., P.S. Fahrner, W.T. Greenough, and V.I. Gelfand. 2004. Transport of Drosophila fragile X mental retardation protein-containing ribonucleoprotein granules by kinesin-1 and cytoplasmic dynein. *Proc Natl Acad Sci U S A*. 101:17428-17433.

Liu, X., D. Weaver, O. Shirihai, and G. Hajnoczky. 2009. Mitochondrial 'kiss-and-run': interplay between mitochondrial motility and fusion-fission dynamics. *Embo J*. 28:3074-3089.

Loson, O.C., Z. Song, H. Chen, and D.C. Chan. 2013. Fis1, Mff, MiD49, and MiD51 mediate Drp1 recruitment in mitochondrial fission. *Molecular biology of the cell*. 24:659-667.

Lyons, S.E., M.E. Bruck, E.J. Bowie, and D. Ginsburg. 1992. Impaired intracellular transport produced by a subset of type IIA von Willebrand disease mutations. *J Biol Chem*. 267:4424-4430.

Maeda, M., and G.A. Thompson, Jr. 1986. On the mechanism of rapid plasma membrane and chloroplast envelope expansion in Dunaliella salina exposed to hypoosmotic shock. *J Cell Biol*. 102:289-297.

Mano, S., C. Nakamori, M. Hayashi, A. Kato, M. Kondo, and M. Nishimura. 2002. Distribution and Characterization of Peroxisomes in Arabidopsis by Visualization with GFP: Dynamic Morphology and Actin-dependent Movement *Plant Cell Physiology*. 43:331-341.

Marsh, L., and M.D. Rose. 1997. The pathway of cell and nuclear fusion during mating in S. cerevisiae. *In The Molecular and Cellular Biology of the Yeast Saccharomyces: Cell Cycle And Cell Biology*. 3:827-888.

Mast, F.D., J. Li, M.K. Virk, S.C. Hughes, A.J. Simmonds, and R.A. Rachubinski. 2011. A Drosophila model for the Zellweger spectrum of peroxisome biogenesis disorders. *Dis Model Mech*. 4:659-672.

Mateus, A.M., N. Gorfinkiel, S. Schamberg, and A. Martinez Arias. 2011. Endocytic and recycling endosomes modulate cell shape changes and tissue behaviour during morphogenesis in Drosophila. *PLoS One*. 6:e18729.

Mathur, J., N. Mathur, and M. Hulskamp. 2002. Simultaneous Visualization of Peroxisomes and Cytoskeletal Elements Reveals Actin and Not Microtubule-Based Peroxisome Motility in Plants. *Plant Physiol*. 128:1031–1045.

McCart, A.E., D. Mahony, and J.A. Rothnagel. 2003. Alternatively spliced products of the human kinesin light chain 1 (KNS2) gene. *Traffic*. 4:576-580.

McKenney, R.J., W. Huynh, M.E. Tanenbaum, G. Bhabha, and R.D. Vale. 2014. Activation of cytoplasmic dynein motility by dynactin-cargo adapter complexes. *Science*. 345:337-341.

Melkonian, K.A., K.C. Maier, J.E. Godfrey, M. Rodgers, and T.A. Schroer. 2007. Mechanism of dynamitin-mediated disruption of dynactin. *The Journal of biological chemistry*. 282:19355-19364.

Mendoza-Mendoza, A., P. Berndt, A. Djamei, C. Weise, U. Linne, M. Marahiel, M. Vranes, J. Kamper, and R. Kahmann. 2009. Physical-chemical plant-derived signals induce differentiation in Ustilago maydis. *Molecular microbiology*. 71:895-911.

Miki, F., K. Okazaki, M. Shimanuki, A. Yamamoto, Y. Hiraoka, and O. Niwa. 2002. The 14-kDa dynein light chain-family protein Dlc1 is required for regular oscillatory nuclear movement and efficient recombination during meiotic prophase in fission yeast. *Mol Biol Cell*. 13:930-946.

Miki, H., M. Setou, N. Hirokawa, R.G. Group, and G.S.L. Members. 2003. Kinesin superfamily proteins (KIFs) in the mouse transcriptome. *Genome research*. 13:1455-1465.

Mimori-Kiyosue, Y., and S. Tsukita. 2003. "Search-and-capture" of microtubules through plus-end-binding proteins (+TIPs). *Journal of biochemistry*. 134:321-326.

Moldovan, L., and N.I. Moldovan. 2004. Oxygen free radicals and redox biology of organelles. *Histochem Cell Biol*. 122:395-412.

Moore, J.K., J. Li, and J.A. Cooper. 2008. Dynactin function in mitotic spindle positioning. *Traffic*. 9:510-527.

Motley, A., E. Hettema, B. Distel, and H. Tabak. 1994. Differential protein import deficiencies in human peroxisome assembly disorders. *The Journal of cell biology*. 125:755-767.

Muench, D.G., and R.T. Mullen. 2003. Peroxisome dynamics in plant cells: a role for the cytoskeleton. *Plant Science*. 164:307-315.

Mukai, S., and Y. Fujiki. 2006. Molecular mechanisms of import of peroxisome-targeting signal type 2 (PTS2) proteins by PTS2 receptor Pex7p and PTS1 receptor Pex5pL. *J Biol Chem*. 281:37311-37320.

Mullen, R.T., C.S. Lisenbee, J.A. Miernyk, and R.N. Trelease. 1999. Peroxisomal membrane ascorbate peroxidase is sorted to a membranous network that resembles a subdomain of the endoplasmic reticulum. *Plant Cell*. 11:2167-2185.

Mullen, R.T., and R.N. Trelease. 2006. The ER-peroxisome connection in plants: development of the "ER semi-autonomous peroxisome maturation and replication" model for plant peroxisome biogenesis. *Biochim Biophys Acta*. 1763:1655-1668.

Muller, P., G. Weinzierl, A. Brachmann, M. Feldbrugge, and R. Kahmann. 2003. Mating and pathogenic development of the Smut fungus Ustilago maydis are regulated by one mitogen-activated protein kinase cascade. *Eukaryotic cell*. 2:1187-1199.

Müller, S., S. Han, and L.G. Smith. 2006. Two kinesins are involved in the spatial control of cytokinesis in Arabidopsis thaliana. *Curr Biol*. 16:888-894.

Münsterkötter, M., and G. Steinberg. 2007. The fungus Ustilago maydis and humans share disease-related proteins that are not found in Saccharomyces cerevisiae. *BMC Genomics*. 8:473.

Nguyen, T., J. Bjorkman, B.C. Paton, and D.I. Crane. 2005. Failure of microtubule-mediated peroxisome division and trafficking in disorders with reduced peroxisome abundance. *J Cell Sci*. 119:636-645.

Nielsen, E., F. Severin, J.M. Backer, A.A. Hyman, and M. Zerial. 1999. Rab5 regulates motility of early endosomes on microtubules. *Nat Cell Biol*. 1:376-382.

Niwa, S., Y. Tanaka, and N. Hirokawa. 2008. KIF1Bbeta- and KIF1A-mediated axonal transport of presynaptic regulator Rab3 occurs in a GTP-dependent manner through DENN/MADD. *Nat Cell Biol*. 10:1269-1279.

Nurse, P. 2002. The Nobel Prize and beyond: an interview with Sir Paul Nurse. Interview by Susan R. Owens. *EMBO reports*. 3:204-206.

Oberholzer, U., A. Marcil, E. Leberer, D.Y. Thomas, and M. Whiteway. 2002. Myosin I is required for hypha formation in Candida albicans. *Eukaryotic cell*. 1:213-228.

Ozaki, Y., H. Matsui, A. Nagamachi, H. Asou, D. Aki, and T. Inaba. 2011. The dynactin complex maintains the integrity of metaphasic centrosomes to ensure transition to anaphase. *The Journal of biological chemistry*. 286:5589-5598.

Pfister, K.K. 1999. Cytoplasmic dynein and microtubule transport in the axon: the action connection. *Mol Neurobiol*. 20:81-91.

Plamann, M., P.F. Minke, J.H. Tinsley, and K.S. Bruno. 1994. Cytoplasmic dynein and actin-related protein Arp1 are required for normal nuclear distribution in filamentous fungi. *The Journal of cell biology*. 127:139-149.

Preuss, M.L., D.P. Delmer, and B. Liu. 2003. The cotton kinesin-like calmodulin-binding protein associates with cortical microtubules in cotton fibers. *Plant Physiol*. 132:154-160.

Quadbeck-Seeger, C., G. Wanner, S. Huber, R. Kahmann, and J. Kamper. 2000. A protein with similarity to the human retinoblastoma binding protein 2 acts specifically as a repressor for genes regulated by the b mating type locus in Ustilago maydis. *Molecular microbiology*. 38:154-166.

Rabut, G., P. Lenart, and J. Ellenberg. 2004. Dynamics of nuclear pore complex organization through the cell cycle. *Current opinion in cell biology*. 16:314-321.

Rapp, S., R. Saffrich, M. Anton, U. Jakle, W. Ansorge, K. Gorgas, and W.W. Just. 1996. Microtubule-based peroxisome movement. *J Cell Sci*. 109 ( Pt 4):837-849.

Raymond, C., T. Pownder, and S. Sexson. 1999. General method for plasmid construction using homologous recombination. *Biotechniques*. 26:134-138.

Reck-Peterson, S.L., D.W. Provance, Jr., M.S. Mooseker, and J.A. Mercer. 2000. Class V myosins. *Biochim Biophys Acta*. 1496:36-51.

Reedy, M.K. 1993. Myosin-actin motors: the partnership goes atomic. *Structure*. 1:1-5.

Reid, E., M. Kloos, A. Ashley-Koch, L. Hughes, S. Bevan, I.K. Svenson, F.L. Graham, P.C. Gaskell, A. Dearlove, M.A. Pericak-Vance, D.C. Rubinsztein, and D.A. Marchuk. 2002. A kinesin heavy chain (KIF5A) mutation in hereditary spastic paraplegia (SPG10). *American journal of human genetics*. 71:1189-1194.

Requena, N., C. Alberti-Segui, E. Winzenburg, C. Horn, M. Schliwa, P. Philippsen, R. Liese, and R. Fischer. 2001. Genetic evidence for a microtubule-destabilizing effect of conventional kinesin and analysis of its consequences for the control of nuclear distribution in Aspergillus nidulans. *Mol Microbiol*. 42:121-132.

Reumann, S., and A.P. Weber. 2006. Plant peroxisomes respire in the light: some gaps of the photorespiratory C2 cycle have become filled--others remain. *Biochim Biophys Acta*. 1763:1496-1510.

Schlager, M.A., and C.C. Hoogenraad. 2009. Basic mechanisms for recognition and transport of synaptic cargos. *Molecular brain*. 2:25.

Schlesinger, R., R. Kahmann, and J. Kamper. 1997. The homeodomains of the heterodimeric bE and bW proteins of Ustilago maydis are both critical for function. *Molecular & general genetics : MGG*. 254:514-519.

Schnapp, B.J., and T.S. Reese. 1989. Dynein is the motor for retrograde axonal transport of organelles. *Proc Natl Acad Sci U S A*. 86:1548-1552.

Schrader, M. 2001. Tubulo-reticular clusters of peroxisomes in living COS-7 cells: dynamic behavior and association with lipid droplets. *J Histochem Cytochem*. 49:1421-1429.

Schrader, M., J.K. Burkhardt, E. Baumgart, G. Luers, H. Spring, A. Volkl, and H.D. Fahimi. 1996. Interaction of microtubules with peroxisomes. Tubular and spherical peroxisomes in HepG2 cells and their alterations induced by microtubule-active drugs. *Eur J Cell Biol*. 69:24-35.

Schrader, M., and H.D. Fahimi. 2006. Peroxisomes and oxidative stress. *Biochim Biophys Acta*. 1763:1755-1766.

Schrader, M., and H.D. Fahimi. 2008. The peroxisome: still a mysterious organelle. *Histochemistry and cell biology*. 129:421-440.

Schrader, M., S.J. King, T.A. Stroh, and T.A. Schroer. 2000. Real time imaging reveals a peroxisomal reticulum in living cells. *J Cell Sci*. 113 ( Pt 20):3663-3671.
Schrader, M., M. Thiemann, and H.D. Fahimi. 2003. Peroxisomal motility and interaction with microtubules. *Microsc Res Tech*. 61:171-178.
Schrader, M., and Y. Yoon. 2007. Mitochondria and peroxisomes: are the 'big brother' and the 'little sister' closer than assumed? *Bioessays*. 29:1105-1114.
Schroer, T.A. 2004. Dynactin. *Annu Rev Cell Dev Biol*. 20:759-779.
Schuchardt, I., D. Assmann, E. Thines, C. Schuberth, and G. Steinberg. 2005. Myosin-V, Kinesin-1, and Kinesin-3 cooperate in hyphal growth of the fungus Ustilago maydis. *Mol Biol Cell*. 16:5191-5201.
Schultz, J., F. Milpetz, P. Bork, and C.P. Ponting. 1998. SMART, a simple modular architecture research tool: identification of signaling domains. *Proc Natl Acad Sci U S A*. 95:5857-5864.
Schulz, B., F. Banuett, M. Dahl, R. Schlesinger, W. Schafer, T. Martin, I. Herskowitz, and R. Kahmann. 1990. The b alleles of U. maydis, whose combinations program pathogenic development, code for polypeptides containing a homeodomain-related motif. *Cell*. 60:295-306.
Schuster, M., S. Kilaru, P. Ashwin, C. Lin, N.J. Severs, and G. Steinberg. 2011a. Controlled and stochastic retention concentrates dynein at microtubule ends to keep endosomes on track. *Embo J*. 30:652-664.
Schuster, M., S. Kilaru, G. Fink, J. Collemare, Y. Roger, and G. Steinberg. 2011b. Kinesin-3 and dynein cooperate in long-range retrograde endosome motility along a nonuniform microtubule array. *Mol Biol Cell*. 22:3645-3657.
Schuster, M., R. Lipowsky, M.A. Assmann, P. Lenz, and G. Steinberg. 2011c. Transient binding of dynein controls bidirectional long-range motility of early endosomes. *Proc Natl Acad Sci U S A*. 108:3618-3623.
Schuster, M., S. Treitschke, S. Kilaru, J. Molloy, N.J. Harmer, and G. Steinberg. 2012. Myosin-5, kinesin-1 and myosin-17 cooperate in secretion of fungal chitin synthase. *Embo J*. 31:214-227.
Seidel, C., S.D. Moreno-Velasquez, M. Riquelme, and R. Fischer. 2013. Neurospora crassa NKIN2, a kinesin-3 motor, transports early endosomes and is required for polarized growth. *Eukaryot Cell*. 12:1020-1032.
Seiler, S., F.E. Nargang, G. Steinberg, and M. Schliwa. 1997. Kinesin is essential for cell morphogenesis and polarized secretion in Neurospora crassa. *Embo J*. 16:3025-3034.
Seiler, S., M. Plamann, and M. Schliwa. 1999. Kinesin and dynein mutants provide novel insights into the roles of vesicle traffic during cell morphogenesis in Neurospora. *Curr Biol*. 9:779-785.
Sheetz, M.P., R. Vale, B. Schnapp, T. Schroer, and T. Reese. 1986. Vesicle movements and microtubule-based motors. *Journal of cell science. Supplement*. 5:181-188.
Shimozawa, N., T. Nagase, Y. Takemoto, M. Funato, N. Kondo, and Y. Suzuki. 2005. Molecular and neurologic findings of peroxisome biogenesis disorders. *J Child Neurol*. 20:326-329.

Simmchen, J., A. Baeza, D. Ruiz, M.J. Esplandiu, and M. Vallet-Regi. 2012. Asymmetric hybrid silica nanomotors for capture and cargo transport: towards a novel motion-based DNA sensor. *Small*. 8:2053-2059.

Sivagurunathan, S., R.R. Schnittker, S. Nandini, M.D. Plamann, and S.J. King. 2012. A mouse neurodegenerative dynein heavy chain mutation alters dynein motility and localization in Neurospora crassa. *Cytoskeleton*. 69:613-624.

Skop, A.R., and J.G. White. 1998. The dynactin complex is required for cleavage plane specification in early Caenorhabditis elegans embryos. *Current biology : CB*. 8:1110-1116.

Smith, J.J., and J.D. Aitchison. 2009. Regulation of peroxisome dynamics. *Curr Opin Cell Biol*. 21:119-126.

Smith, J.J., and J.D. Aitchison. 2013. Peroxisomes take shape. *Nature reviews. Molecular cell biology*. 14:803-817.

Smith, J.J., T.W. Brown, G.A. Eitzen, and R.A. Rachubinski. 2000. Regulation of peroxisome size and number by fatty acid beta -oxidation in the yeast yarrowia lipolytica. *The Journal of biological chemistry*. 275:20168-20178.

Smith, J.J., M. Marelli, R.H. Christmas, F.J. Vizeacoumar, D.J. Dilworth, T. Ideker, T. Galitski, K. Dimitrov, R.A. Rachubinski, and J.D. Aitchison. 2002. Transcriptome profiling to identify genes involved in peroxisome assembly and function. *The Journal of cell biology*. 158:259-271.

Sparkes, I. 2011. Recent advances in understanding plant myosin function: life in the fast lane. *Molecular plant*. 4:805-812.

Sparkes, I., J. Runions, C. Hawes, and L. Griffing. 2009. Movement and remodeling of the endoplasmic reticulum in nondividing cells of tobacco leaves. *Plant Cell*. 21:3937-3949.

Spector, I., N.R. Shochet, D. Blasberger, and Y. Kashman. 1989. Latrunculins--novel marine macrolides that disrupt microfilament organization and affect cell growth: I. Comparison with cytochalasin D. *Cell motility and the cytoskeleton*. 13:127-144.

Spellig, T., M. Bolker, F. Lottspeich, R.W. Frank, and R. Kahmann. 1994. Pheromones trigger filamentous growth in Ustilago maydis. *The EMBO journal*. 13:1620-1627.

Spellig, T., A. Bottin, and R. Kahmann. 1996. Green fluorescent protein (GFP) as a new vital marker in the phytopathogenic fungus Ustilago maydis. *Molecular & general genetics : MGG*. 252:503-509.

Springer, T.A. 2006. Complement and the multifaceted functions of VWA and integrin I domains. *Structure*. 14:1611-1616.

Steinberg, G. 2000. The cellular roles of molecular motors in fungi. *Trends in microbiology*. 8:162-168.

Steinberg, G., and J. Perez-Martin. 2008. Ustilago maydis, a new fungal model system for cell biology. *Trends Cell Biol*. 18:61-67.

Steinberg, G., M. Schliwa, C. Lehmler, M. Bolker, R. Kahmann, and J.R. McIntosh. 1998. Kinesin from the plant pathogenic fungus Ustilago maydis is involved in vacuole formation and cytoplasmic migration. *Journal of cell science*. 111 ( Pt 15):2235-2246.

Steinberg, G., and M. Schuster. 2011. The dynamic fungal cell. *Fungal biology reviews*. 25:14-37.

Steinberg, G., M. Schuster, U. Theisen, S. Kilaru, A. Forge, and M. Martin-Urdiroz. 2012. Motor-driven motility of fungal nuclear pores organizes chromosomes and fosters nucleocytoplasmic transport. *J Cell Biol*. 198:343-355.

Steinberg, G., R. Wedlich-Soldner, M. Brill, and I. Schulz. 2001. Microtubules in the fungal pathogen Ustilago maydis are highly dynamic and determine cell polarity. *Journal of cell science*. 114:609-622.

Stenmark, H., A. Valencia, O. Martinez, O. Ullrich, B. Goud, and M. Zerial. 1994. Distinct structural elements of rab5 define its functional specificity. *Embo J*. 13:575-583.

Stojanovski, D., O.S. Koutsopoulos, K. Okamoto, and M.T. Ryan. 2004. Levels of human Fis1 at the mitochondrial outer membrane regulate mitochondrial morphology. *J Cell Sci*. 117:1201-1210.

Straube, A., W. Enard, A. Berner, R. Wedlich-Soldner, R. Kahmann, and G. Steinberg. 2001. A split motor domain in a cytoplasmic dynein. *Embo J*. 20:5091-5100.

Straube, A., G. Hause, G. Fink, and G. Steinberg. 2006. Conventional kinesin mediates microtubule-microtubule interactions in vivo. *Mol Biol Cell*. 17:907-916.

Strom, M., A.N. Hume, A.K. Tarafder, E. Barkagianni, and M.C. Seabra. 2002. A family of Rab27-binding proteins. Melanophilin links Rab27a and myosin Va function in melanosome transport. *J Biol Chem*. 277:25423-25430.

Su, Q., Q. Cai, C. Gerwin, C.L. Smith, and Z.H. Sheng. 2004. Syntabulin is a microtubule-associated protein implicated in syntaxin transport in neurons. *Nat Cell Biol*. 6:941-953.

Subramani, S. 1996. Protein translocation into peroxisomes. *The Journal of biological chemistry*. 271:32483-32486.

Suelmann, R., and R. Fischer. 2000. Nuclear migration in fungi--different motors at work. *Research in microbiology*. 151:247-254.

Suetsugu, N., N. Yamada, T. Kagawa, H. Yonekura, T.Q. Uyeda, A. Kadota, and M. Wada. 2010. Two kinesin-like proteins mediate actin-based chloroplast movement in Arabidopsis thaliana. *Proc Natl Acad Sci U S A*. 107:8860-8865.

Tabak, H.F., D. Hoepfner, A. Zand, H.J. Geuze, I. Braakman, and M.A. Huynen. 2006. Formation of peroxisomes: present and past. *Biochimica et biophysica acta*. 1763:1647-1654.

Tai, C.Y., D.L. Dujardin, N.E. Faulkner, and R.B. Vallee. 2002. Role of dynein, dynactin, and CLIP-170 interactions in LIS1 kinetochore function. *The Journal of cell biology*. 156:959-968.

Tanaka, M., J. Miyoshi, H. Ishizaki, A. Togawa, K. Ohnishi, K. Endo, K. Matsubara, A. Mizoguchi, T. Nagano, M. Sato, T. Sasaki, and Y. Takai. 2001. Role of Rab3 GDP/GTP exchange protein in synaptic vesicle trafficking at the mouse neuromuscular junction. *Mol Biol Cell*. 12:1421-1430.

Tanaka, Y., Y. Kanai, Y. Okada, S. Nonaka, S. Takeda, A. Harada, and N. Hirokawa. 1998. Targeted disruption of mouse conventional kinesin heavy chain, kif5B, results in abnormal perinuclear clustering of mitochondria. *Cell*. 93:1147-1158.

Tang, J., N. Abovich, and M. Rosbash. 1996. Identification and characterization of a yeast gene encoding the U2 small nuclear ribonucleoprotein particle B" protein. *Molecular and cellular biology*. 16:2787-2795.

Theisen, U., A. Straube, and G. Steinberg. 2008. Dynamic rearrangement of nucleoporins during fungal "open" mitosis. *Mol Biol Cell*. 19:1230-1240.

Thiemann, M., M. Schrader, A. Volkl, E. Baumgart, and H.D. Fahimi. 2000. Interaction of peroxisomes with microtubules. In vitro studies using a novel peroxisome-microtubule binding assay. *European journal of biochemistry / FEBS*. 267:6264-6275.

Thompson, J.D., D.G. Higgins, and T.J. Gibson. 1994. CLUSTAL W: improving the sensitivity of progressive multiple sequence alignment through sequence weighting, position-specific gap penalties and weight matrix choice. *Nucleic acids research*. 22:4673-4680.

Titorenko, V.I., H. Chan, and R.A. Rachubinski. 2000. Fusion of small peroxisomal vesicles in vitro reconstructs an early step in the in vivo multistep peroxisome assembly pathway of Yarrowia lipolytica. *J Cell Biol*. 148:29-44.

Titorenko, V.I., and R.T. Mullen. 2006. Peroxisome biogenesis: the peroxisomal endomembrane system and the role of the ER. *The Journal of cell biology*. 174:11-17.

Titorenko, V.I., D.M. Ogrydziak, and R.A. Rachubinski. 1997. Four distinct secretory pathways serve protein secretion, cell surface growth, and peroxisome biogenesis in the yeast Yarrowia lipolytica. *Mol Cell Biol*. 17:5210-5226.

Titorenko, V.I., and R.A. Rachubinski. 1998. Mutants of the yeast Yarrowia lipolytica defective in protein exit from the endoplasmic reticulum are also defective in peroxisome biogenesis. *Mol Cell Biol*. 18:2789-2803.

Titorenko, V.I., and R.A. Rachubinski. 2000. Peroxisomal membrane fusion requires two AAA family ATPases, Pex1p and Pex6p. *J Cell Biol*. 150:881-886.

Titorenko, V.I., and R.A. Rachubinski. 2001. The life cycle of the peroxisome. *Nature reviews. Molecular cell biology*. 2:357-368.

Titorenko, V.I., and R.A. Rachubinski. 2004. The peroxisome: orchestrating important developmental decisions from inside the cell. *The Journal of cell biology*. 164:641-645.

Tran, P.B., and R.J. Miller. 1999. Aggregates in neurodegenerative disease: crowds and power? *Trends in neurosciences*. 22:194-197.

Trautwein, M., J. Dengjel, M. Schirle, and A. Spang. 2004. Arf1p provides an unexpected link between COPI vesicles and mRNA in Saccharomyces cerevisiae. *Mol Biol Cell*. 15:5021-5037.

Urban, M., R. Kahmann, and M. Bolker. 1996a. The biallelic a mating type locus of Ustilago maydis: remnants of an additional pheromone gene indicate evolution from a multiallelic ancestor. *Molecular & general genetics : MGG*. 250:414-420.

Urban, M., R. Kahmann, and M. Bolker. 1996b. Identification of the pheromone response element in Ustilago maydis. *Molecular & general genetics : MGG*. 251:31-37.

Vale, R.D. 1992. Microtubule motors: many new models off the assembly line. *Trends in biochemical sciences*. 17:300-304.

Vale, R.D. 1999. Millennial musings on molecular motors. *Trends in cell biology*. 9:M38-42.
Vale, R.D. 2003. The molecular motor toolbox for intracellular transport. *Cell*. 112:467-480.
Valenciano, S., J.R. Lucas, A. Pedregosa, I.F. Monistrol, and F. Laborda. 1996. Induction of beta-oxidation enzymes and microbody proliferation in Aspergillus nidulans. *Archives of microbiology*. 166:336-341.
Valetti, C., D.M. Wetzel, M. Schrader, M.J. Hasbani, S.R. Gill, T.E. Kreis, and T.A. Schroer. 1999. Role of dynactin in endocytic traffic: effects of dynamitin overexpression and colocalization with CLIP-170. *Molecular biology of the cell*. 10:4107-4120.
Vallee, R.B., N.E. Faulkner, and C.Y. Tai. 2000. The role of cytoplasmic dynein in the human brain developmental disease lissencephaly. *Biochimica et biophysica acta*. 1496:89-98.
van der Klei, I.J., H. Yurimoto, Y. Sakai, and M. Veenhuis. 2006. The significance of peroxisomes in methanol metabolism in methylotrophic yeast. *Biochim Biophys Acta*. 1763:1453-1462.
van der Zand, A., I. Braakman, H.J. Geuze, and H.F. Tabak. 2006. The return of the peroxisome. *J Cell Sci*. 119:989-994.
Van Gestel, K., R.H. Kohler, and J.P. Verbelen. 2002. Plant mitochondria move on F-actin, but their positioning in the cortical cytoplasm depends on both F-actin and microtubules. *J Exp Bot*. 53:659-667.
Veenhuis, M., M. Mateblowski, W.H. Kunau, and W. Harder. 1987. Proliferation of microbodies in Saccharomyces cerevisiae. *Yeast*. 3:77-84.
Wada, M., T. Kagawa, and Y. Sato. 2003. Chloroplast movement. *Annual review of plant biology*. 54:455-468.
Wanders, R.J. 2014. Metabolic functions of peroxisomes in health and disease. *Biochimie*. 98:36-44.
Wang, J., J.J. Song, M.C. Franklin, S. Kamtekar, Y.J. Im, S.H. Rho, I.S. Seong, C.S. Lee, C.H. Chung, and S.H. Eom. 2001. Crystal structures of the HslVU peptidase-ATPase complex reveal an ATP-dependent proteolysis mechanism. *Structure*. 9:177-184.
Wang, J., Z. Zhang, Y. Wang, L. Li, R. Chai, X. Mao, H. Jiang, H. Qiu, X. Du, F. Lin, and G. Sun. 2013. PTS1 peroxisomal import pathway plays shared and distinct roles to PTS2 pathway in development and pathogenicity of Magnaporthe oryzae. *PLoS One*. 8:e55554.
Wang, Z.Y., D.M. Soanes, M.J. Kershaw, and N.J. Talbot. 2007. Functional analysis of lipid metabolism in Magnaporthe grisea reveals a requirement for peroxisomal fatty acid beta-oxidation during appressorium-mediated plant infection. *Mol Plant Microbe Interact*. 20:475-491.
Weber, I., C. Gruber, and G. Steinberg. 2003. A class-V myosin required for mating, hyphal growth, and pathogenicity in the dimorphic plant pathogen Ustilago maydis. *Plant Cell*. 15:2826-2842.
Wedlich-Söldner, R., M. Bolker, R. Kahmann, and G. Steinberg. 2000. A putative endosomal t-SNARE links exo- and endocytosis in the phytopathogenic fungus Ustilago maydis. *EMBO J*
. 19:1974-1986.

Wedlich-Söldner, R., I. Schulz, A. Straube, and G. Steinberg. 2002a. Dynein supports motility of endoplasmic reticulum in the fungus Ustilago maydis. *Mol Biol Cell*. 13:965-977.

Wedlich-Söldner, R., A. Straube, M.W. Friedrich, and G. Steinberg. 2002b. A balance of KIF1A-like kinesin and dynein organizes early endosomes in the fungus Ustilago maydis. *Embo J*. 21:2946-2957.

Wei, L., W. Zhang, Z. Liu, and Y. Li. 2009. AtKinesin-13A is located on Golgi-associated vesicle and involved in vesicle formation/budding in Arabidopsis root-cap peripheral cells. *BMC Plant Biol*. 9:138.

Wendler, P., S. Ciniawsky, M. Kock, and S. Kube. 2012. Structure and function of the AAA+ nucleotide binding pocket. *Biochim Biophys Acta*. 1823:2-14.

Whittaker, R.H. 1969. New concepts of kingdoms or organisms. Evolutionary relations are better represented by new classifications than by the traditional two kingdoms. *Science*. 163:150-160.

Wiemer, E.A., T. Wenzel, T.J. Deerinck, M.H. Ellisman, and S. Subramani. 1997. Visualization of the peroxisomal compartment in living mammalian cells: dynamic behavior and association with microtubules. *J Cell Biol*. 136:71-80.

Woo, M., K. Lee, and K. Song. 2003. MYO2 is not essential for viability, but is required for polarized growth and dimorphic switches in Candida albicans. *FEMS microbiology letters*. 218:195-202.

Wozniak, M.J., and V.J. Allan. 2006. Cargo selection by specific kinesin light chain 1 isoforms. *The EMBO journal*. 25:5457-5468.

Wu, X.S., K. Rao, H. Zhang, F. Wang, J.R. Sellers, L.E. Matesic, N.G. Copeland, N.A. Jenkins, and J.A. Hammer, 3rd. 2002. Identification of an organelle receptor for myosin-Va. *Nat Cell Biol*. 4:271-278.

Wynshaw-Boris, A. 2007. Lissencephaly and LIS1: insights into the molecular mechanisms of neuronal migration and development. *Clinical genetics*. 72:296-304.

Xiang, X. 2003. LIS1 at the microtubule plus end and its role in dynein-mediated nuclear migration. *The Journal of cell biology*. 160:289-290.

Xiang, X., and R. Fischer. 2004. Nuclear migration and positioning in filamentous fungi. *Fungal genetics and biology : FG & B*. 41:411-419.

Xiang, X., and M. Plamann. 2003. Cytoskeleton and motor proteins in filamentous fungi. *Current opinion in microbiology*. 6:628-633.

Xiang, X., C. Roghi, and N.R. Morris. 1995. Characterization and localization of the cytoplasmic dynein heavy chain in Aspergillus nidulans. *Proceedings of the National Academy of Sciences of the United States of America*. 92:9890-9894.

Yamada, M., S. Toba, Y. Yoshida, K. Haratani, D. Mori, Y. Yano, Y. Mimori-Kiyosue, T. Nakamura, K. Itoh, S. Fushiki, M. Setou, A. Wynshaw-Boris, T. Torisawa, Y.Y. Toyoshima, and S. Hirotsune. 2008. LIS1 and NDEL1 coordinate the plus-end-directed transport of cytoplasmic dynein. *Embo J*. 27:2471-2483.

Yamamoto, A., and Y. Hiraoka. 2003. Cytoplasmic dynein in fungi: insights from nuclear migration. *Journal of cell science*. 116:4501-4512.

Yamamoto, A., R.R. West, J.R. McIntosh, and Y. Hiraoka. 1999. A cytoplasmic dynein heavy chain is required for oscillatory nuclear

movement of meiotic prophase and efficient meiotic recombination in fission yeast. *J Cell Biol*. 145:1233-1249.

Yang, Y., T.L. Sage, Y. Liu, T.R. Ahmad, W.F. Marshall, S.H. Shiu, J.E. Froehlich, K.M. Imre, and K.W. Osteryoung. 2011. CLUMPED CHLOROPLASTS 1 is required for plastid separation in Arabidopsis. *Proc Natl Acad Sci U S A*. 108:18530-18535.

Yeh, E., C. Yang, E. Chin, P. Maddox, E.D. Salmon, D.J. Lew, and K. Bloom. 2000. Dynamic positioning of mitotic spindles in yeast: role of microtubule motors and cortical determinants. *Mol Biol Cell*. 11:3949-3961.

Yoon, Y., E.W. Krueger, B.J. Oswald, and M.A. McNiven. 2003. The mitochondrial protein hFis1 regulates mitochondrial fission in mammalian cells through an interaction with the dynamin-like protein DLP1. *Mol Cell Biol*. 23:5409-5420.

Zekert, N., and R. Fischer. 2009. The Aspergillus nidulans kinesin-3 UncA motor moves vesicles along a subpopulation of microtubules. *Mol Biol Cell*. 20:673-684.

Zhang, J., L. Zhuang, Y. Lee, J.F. Abenza, M.A. Penalva, and X. Xiang. 2010. The microtubule plus-end localization of Aspergillus dynein is important for dynein-early-endosome interaction but not for dynein ATPase activation. *Journal of cell science*. 123:3596-3604.

Zhao, C., J. Takita, Y. Tanaka, M. Setou, T. Nakagawa, S. Takeda, H.W. Yang, S. Terada, T. Nakata, Y. Takei, M. Saito, S. Tsuji, Y. Hayashi, and N. Hirokawa. 2001. Charcot-Marie-Tooth disease type 2A caused by mutation in a microtubule motor KIF1Bbeta. *Cell*. 105:587-597.